



THE HONG KONG
POLYTECHNIC UNIVERSITY

香港理工大學

Pao Yue-kong Library

包玉剛圖書館

Copyright Undertaking

This thesis is protected by copyright, with all rights reserved.

By reading and using the thesis, the reader understands and agrees to the following terms:

1. The reader will abide by the rules and legal ordinances governing copyright regarding the use of the thesis.
2. The reader will use the thesis for the purpose of research or private study only and not for distribution or further reproduction or any other purpose.
3. The reader agrees to indemnify and hold the University harmless from and against any loss, damage, cost, liability or expenses arising from copyright infringement or unauthorized usage.

IMPORTANT

If you have reasons to believe that any materials in this thesis are deemed not suitable to be distributed in this form, or a copyright owner having difficulty with the material being included in our database, please contact lbsys@polyu.edu.hk providing details. The Library will look into your claim and consider taking remedial action upon receipt of the written requests.

The Hong Kong Polytechnic University

Department of Industrial and Systems Engineering

**CARBON NANOTUBE
MICROWAVE-ASSISTED THERMAL
BONDING OF PLASTIC MICRO BIOCHIP**

By

Wong Lai Pik, Jolie

A thesis submitted

in partial fulfillment of the requirements for the degree of

Master of Philosophy

February 2010

CERTIFICATE OF ORIGINALITY

I hereby declare that this thesis is my own work and that, to the best of my knowledge and belief, it reproduces no material previously published or written, nor material that has been accepted for the award of any other degree or diploma, except where due acknowledgement has been made in the text.

_____ (Signed)

WONG LAI PIK _____ (Name of student)

ABSTRACT

Microfluidic device has been an emerging field in the past decades. The mounting demand of biochips in the health care area has shifted the manufacturing markets from silicon and glass to polymer. In order to fabricate a plastic biochip, bonding is a critical issue to be addressed to provide a reliable performance. Various bonding methods have been developed such as thermal bonding using low pressure strategy, holed pressure equalizing plates, and hybrid assembly; adhesive bonding using PDMS; solvent bonding using DMSO and methanol; and microwave bonding using a gold thin film. Although there are plenty of methods for plastic chip bonding, thermal bonding is still the preferential method to be used because it can provide a contamination-free homogenous assembly of the final products. Thermal bonding requires heating up of two polymeric substrates to their glass transition state (T_g) and the substrates are sealed under the ultimate contact by applied pressure. However, it always results in an immense energy loss and a microstructural deformation on the bonded biochip, due to the heating of bulky bonding machine and the prolonged waiting time for heat sink during bonding respectively.

In this work, a new thermal bonding method assisted by microwave irradiation with the advantages of material homogeneity, leakage-free and negligible deformation has been developed. Given the promising microwave absorption properties, gold nanoparticles (GNPs) and carbon nanotubes (CNTs)

have been used as the microwave absorbers to examine the feasibility on sealing plastic biochips in this study. It was found that CNTs were capable to release tremendous amount of heat energy to seal plastic biochip in an extremely short exposure time of microwave irradiation. The key microstructures on the plastic biochip were the microchannels with dimensions of 50 μm in depth and 100 μm in width. Unlike the previously developed method that CNTs were casted at the bonding interface, they were spray-coated on the non-bonding side of a planar substrate. With this, the bonding interface was homogeneous. The parameters including CNT thickness and exposure time of the proposed bonding method were further optimized to seal the plastic biochips. The microstructures were completely sealed and their integrity was found to be well-maintained through the cross-sectional images observed under microscope. Leakage test was conducted and an injected dye successfully passed through the sealed microchannels without leakage. The bonded biochip was able to withstand a pressure of 2 MPa as found in the tensile test.

The bonding method developed in this study possesses the criteria in material homogeneity on bonded assembly, leakage-free on sealing and negligible deformation on prime structures. This bonding method is able to be conducted with short processing time and high bonding efficiency, and to be potentially developed as a high throughput process. CNT–microwave-assisted thermal bonding featuring with these criteria has been developed as a promising alternative for bonding plastic biochips in industrial scale production.

ACKNOWLEDGEMENTS

I would like to express my sincere thank to my supervisor, Professor K.L. Yung, for giving me the opportunity to join his research team and the valuable time he spent on advising me, and also for his support and understanding throughout the years of my study.

I would also like to acknowledge my co-supervisor, Dr. Thomas M.H. Lee for his precious guidance and frequent discussion on my research direction, and also his patience on sharing my opinions.

Thanks also expressed to my colleagues in Prof. Yung's group and in Dr. Lee's group to provide me with the technical supports and experimental assistance. The technical supports from the technicians, Rico and Mr. Lau in CD 003 and CD 004 respectively, are highly appreciated.

Last but not least, I would like to thank my family for their love, their greatest support and touching understanding throughout the years of my study.

TABLE OF CONTENTS

ABSTRACT	III
ACKNOWLEDGEMENTS	V
TABLE OF CONTENTS	VI
LIST OF FIGURES AND TABLES	X
ABBREVIATIONS	XVI
.....	

Chapter 1: Introduction

1.1 Background	1
1.1.1 Idea behind biochips	1
1.1.2 Advanced developments in biochips.....	2
1.1.2.1 Polymerase chain reaction (PCR).....	4
1.1.2.2 Capillary electrophoresis (CE)	6
1.1.2.3 Biochips for bioanalytical applications	9
1.1.3 New trend in biochip industry	9
1.2 Rationale, scope of study and objectives	10

Chapter 2: Literature Review

2.1 Polymer materials	13
2.2 Types of bonding methods for sealing polymers	18
2.2.1 Thermal bonding.....	19
2.2.2 Microwave bonding	21
2.2.3 Adhesive bonding	24
2.2.4 Solvent bonding	26

2.2.5 Ultrasonic bonding.....	27
2.2.6 Others.....	29
2.3 Summary.....	29
Chapter 3: Microwave Bonding	
3.1 Development from literature review.....	30
3.2 Proposed method I – gold nanoparticles (GNPs).....	33
3.2.1 Microwave absorption properties of metals and significance of GNPs.....	33
3.2.2 Microwave bonding model for GNPs.....	35
3.3 Proposed method II – carbon nanotubes (CNTs).....	38
3.3.1 Dielectric properties and significance of CNTs.....	38
3.3.2 Microwave bonding model for CNTs.....	40
3.4 Summary.....	41
Chapter 4: Experimental Preparations	
4.1 Overview of experimental preparations.....	42
4.2 Fabrication of moulds.....	43
4.2.1 Photolithography and deep reactive ion etching (DRIE).....	43
4.2.2 Electroforming.....	49
4.3 Fabrication of plastic biochips.....	52
4.3.1 Hot embossing.....	53
4.3.2 Microinjection moulding.....	55
4.4 Materials and equipments for microwave bonding.....	57
4.4.1 Materials.....	58
4.4.1.1 Gold nanoparticles (GNPs).....	58

4.4.1.2 Carbon nanotubes (CNTs)	60
4.4.2 Equipments	61
4.5 Summary	65
Chapter 5: Responses of Gold Nanoparticles and Carbon Nanotubes towards Microwave Irradiation	
5.1 Gold nanoparticles (GNPs)	66
5.1.1 Deposition of GNPs	66
5.1.1.1 Droplet-based coating of GNPs.....	67
5.1.1.2 Dip-coating of GNPs	68
5.1.2 Response towards microwave irradiation	69
5.2 Carbon nanotubes (CNTs).....	74
5.2.1 Deposition of CNTs	74
5.2.1.1 Droplet-based coating of CNTs	74
5.2.1.2 Spray-coating of CNTs	75
5.2.2 Response towards microwave irradiation	79
5.3 Summary	81
Chapter 6: Carbon Nanotube–Microwave-Assisted Thermal Bonding	
6.1 Redevelopment of microwave bonding model for carbon nanotubes (CNTs) – CNT–microwave-assisted thermal bonding.....	82
6.2 Experimental setup.....	88
6.3 Effective thickness of CNT layers	90
6.4 Performance of different CNT thicknesses under optimal exposure time	92
6.4.1 Time optimization	93

6.4.2 Comparison on appearance	94
6.4.3 Evaluation test on leakage	97
6.5 Comparison between CNT–microwave–assisted thermal bonding and conventional thermal bonding.....	99
6.5.1 Conventional thermal bonding of plastic biochips	99
6.5.2 Cross-sectional images observed under microscope	101
6.5.3 Tensile test of the bonded biochips	103
6.5.4 Analysis of CNT–microwave–assisted thermal bonding performance	106
6.6 Summary	109
Chapter 7: Conclusions	
7.1 Contribution to knowledge	111
7.2 Limitations	112
7.3 Suggestions for future investigation	113
.....	
APPENDICES	115
REFERENCES.....	118

LIST OF FIGURES AND TABLES

List of Figures

Figure 1.1 Principle of polymerase chain reaction.	4
Figure 1.2 Multiplication of DNA segment of interest versus number of thermal cycles.	5
Figure 1.3. Working principle of gel electrophoresis.....	7
Figure 1.4. Charge distribution during electroosmotic flow in CE.....	8
Figure 2.1. Autofluorescence intensity of polymers relative to BoroFloat glass, where the absolute intensity is shown in top right, after 60 s illumination of 1 mW laser [59].....	16
Figure 2.2. Healing models of polymers [64, 65]: a) distribution of polymer chains before contact; b) two polymer surfaces in ultimate contact; c) diffusion and intercalation of polymer chains.....	19
Figure 2.3. Schematic drawing of a hot embossing machine.	21
Figure 2.4. Bonded PMMA using gold film..	23
Figure 2.5. Peel test for a PC/CNTs/PC junction. A) Setup of the test; B) cracking of the joint during the test [82].....	24
Figure 2.6. Schematic diagram of an ultrasonic welding device.	28
Figure 3.1. Cracks observed on a gold thin film resulted from arcing after the exposure to microwave irradiation.	34
Figure 3.2. Model setup for microwave bonding using GNPs.	35

Figure 3.3. An illustration of the heating effect generated by eddy current on the GNP surfaces.	36
Figure 3.4. Model setup for microwave bonding using CNTs.....	40
Figure 4.1. Chromium-patterned glass masks for photolithography.....	44
Figure 4.2. Schematic diagrams of photolithography procedures. (a) Oxide growth; (b) photoresist coating; (c) UV exposure through a mask; (d) UV exposure without a mask; (e) photoresist development; (f) oxide etching.	45
Figure 4.3. Working principle of deep reactive ion etching (DRIE).....	46
Figure 4.4. Silicon master mould fabricated using DRIE. Left top: silicon master mould; left bottom, right top: microchannels on silicon master mould; right bottom: microvalves on silicon master mould.	47
Figure 4.5. Cross-sectional image of a series of microchannels in silicon mould.	48
Figure 4.6. Enlarged cross-sectional image of several microchannels in silicon mould.....	48
Figure 4.7. Simplified working diagram for electroforming.	49
Figure 4.8. Electroforming machine.	50
Figure 4.9. Back side view of the nickel mould electroformed from a silicon master mould.....	51
Figure 4.10. Electroformed nickel mould.	51
Figure 4.11. Cross-sectional image of microchannels in nickel mould.	52

Figure 4.12. Hot embossing machine.	54
Figure 4.13. Fabricated PC biochip using hot embossing machine.	54
Figure 4.14. Cross-sectional image of a series of microchannels of the embossed PC biochip.	55
Figure 4.15. Microinjection moulding machine in Microsystems Technology Center in the Hong Kong Polytechnic University.	56
Figure 4.16. Fabricated PC biochip using microinjection moulding machine.	56
Figure 4.17. Cross-sectional image of a series of microchannels of the microinjection moulded PC biochip.	57
Figure 4.18. Experimental setup for GNPs synthesis	59
Figure 4.19. Vigorous stirring of solution in the flask	59
Figure 4.20. Burgundy color given by GNPs with 13 nm in diameters.	60
Figure 4.21. SEM image of the purchased CNTs.	61
Figure 4.22. Equipments for microwave thermal bonding. Left: a domestic microwave oven; right: a stack of glasses.	61
Figure 4.23. Equipments for sample preparation. Left: a mortar and pestle; right: a spray gun.	62
Figure 5.1. Aggregated GNPs upon evaporation of propanol.	67
Figure 5.2. SEM image of GNP-coated PC substrate using dip-coating method.	69
Figure 5.3. Positive control: dip-coating.	70
Figure 5.4. Negative control: dip-coating and washing.	71

Figure 5.5. Sample: dip-coating, microwave irradiation and washing.	71
Figure 5.6. Homemade plastic holder made of PC.	73
Figure 5.7. Coating of CNTs upon evaporation of propanol.	75
Figure 5.8. Mortar and pestle for grinding CNTs.	76
Figure 5.9. CNTs in propanol: (A) before grinding; (B) after grinding.	77
Figure 5.10. Microscopic images of well-sprayed (left) and poor-sprayed (right) of CNTs.....	77
Figure 5.11. Setup of the thickness measurement of CNTs on the spray-coated PC plates.....	78
Figure 5.12. CNT-coated PC plate using spray coating.....	78
Figure 5.13. Bonded assembly after microwave irradiation for 30 sec under 307 W. (a) Bonded CNT-coated PC and plastic holder; (b) tore part of the assembly.	80
Figure 6.1. Redeveloped bonding model for CNT–microwave-assisted thermal bonding.	83
Figure 6.2. Elemental diagram for heat conduction analysis inside the cover plate.....	85
Figure 6.3. Dimensions of cover plate.....	88
Figure 6.4. (a) Embossed biochip and (b) CNT-coated cover plate.....	89
Figure 6.5. Bonding equipments. Left: microwave oven; right: bonding setup inside microwave oven with water loading.....	90

Figure 6.6. Bonding time for over 90% sealed varies with thickness of CNTs.....	91
Figure 6.7. Optimal exposure time corresponding to three CNT thicknesses.....	93
Figure 6.8. Bonded plastic biochip (a) before and (b) after removal of the loosely adhered CNTs.....	95
Figure 6.9. Backside views of the bonded biochips with decreasing CNT thickness from left to right: (a) 74.6 μm , (b) 61.7 μm , and (c) 37.5 μm	95
Figure 6.10. Microscopic images of microchannels (left top, right top and right bottom) and microchamber (left bottom) filled with blue dye.....	97
Figure 6.11. Microscopic image of microvalve (the left horizontal blue line) filled with blue dye.....	98
Figure 6.12. Cross-sectional images of the microstructures before bonding.....	101
Figure 6.13. Cross-sectional images of the bonded biochip using CNT–microwave-assisted thermal bonding.....	102
Figure 6.14. Cross-sectional images of the bonded biochip using conventional thermal bonding.....	102
Figure 6.15. Setup of the pulling system for the tensile test.....	104
Figure 6.16. Load–Extension graph of the CNT–microwave-assisted thermal bonded biochip.....	104

Figure 6.17. Load–Extension graph of the conventional thermal bonded biochip.	105
Figure 6.18. Schematic diagram of the heating model of CNT–microwave-assisted thermal bonding.....	107
Figure 6.19. Schematic diagram of the heating model of conventional thermal bonding.	107

List of Tables

Table 1. Physical and chemical properties of thermoplastics that are frequently used as biochip substrates.....	14
Table 2. Measurement of water temperature before and after microwave irradiation under different power levels.....	63
Table 3. Estimated power outputs of the three power level options.	64
Table 4. Bonding results of PC biochips using different bonding temperature under 2.5 MPa.....	100

ABBREVIATIONS

APTES	3-aminopropyltriethoxysilane
BOE	Buffer oxide etch
CE	Capillary electrophoresis
CNTs	Carbon nanotubes
COC	Cyclic olefin copolymer
DNA	Deoxyribonucleic acid
dNTP	Deoxynucleotide triphosphates
DRIE	Deep reactive ion etching
FTIR	Fourier transform infrared
GNPs	Gold nanoparticles
HDPE	High density polyethylene
HKUST	Hong Kong University of Science and Technology
IR	Infrared
LIF	Laser-induced fluorescence
LOC	Lab-on-a-chip
MEMS	Microelectromechanical systems
MWNTs	Multi-walled carbon nanotubes
NFF	Nanoelectronic Fabrication Facility
NTP	Nanotech Port
OGP	Optical Gaging Products
PMMA	Poly(methyl methacrylate)
PC	Polycarbonate
PCR	Polymerase chain reaction
POC	Point-of-care
PP	Polypropylene
PS	Polystyrene
SEM	Scanning electron microscope
SERS	Surface enhanced raman scattering
SWNTs	Single-walled carbon nanotubes
T_g	Glass transition temperature
UV	Ultraviolet
μTAS	Miniaturized total chemical analysis systems

Chapter 1: Introduction

This chapter will first introduce the project background including the idea behind biochips, advanced developments in biochips and the trend in biochip industry. At the end of this chapter, rationale, scope of study and objectives of this dissertation will be stated.

1.1 Background

Accompanying with the breakthroughs on the discovery of different biomarkers to specific diseases, the invention of advanced detection methods on various viruses or biomolecules, the evolution of sophisticated analysis technologies and the new drugs development in the past years, attention has been shifting to stronger tools to satisfy the imperative needs in the extensive science developments and the blooming medical care fields. Biochips are regarded as the promising solution towards these issues.

1.1.1 Idea behind biochips

Biochip is also called lab-on-a-chip (LOC) which is a device with at least one laboratory process performed on the chip-based platform sized in millimeters to centimeters. A significant concept of miniaturized total chemical analysis systems (μ TAS) was first introduced to biochip by Manz in 1990 [1]. μ TAS is a miniaturized self-contained device that integrates the whole laboratory processes of analysis including sampling, sample pre-treatment, chemical reactions,

analytical separations, analyte detection and data analysis [2]. The miniaturized sizes of biochips offer the advantages of drastic decrease in sample and reagent consumption, and waste generation; superior operation speed due to smaller thermal mass and shorter diffusion distance; incredibly high sensitivity and reliability because of high surface to volume ratios and automation; massive parallelization of analysis; and also enhanced portability as a result of miniaturization. The idea of μ TAS was originated from the trend that smaller inner diameter of channel enables better separation performance and shorter channel length reduces transport time, which means higher sensitivity and higher efficiency resulted upon miniaturization [1]. This novel concept dedicates scientists from multi-disciplines to work together towards miniaturization and integration.

1.1.2 Advanced developments in biochips

As mentioned previously, different types of laboratory functions are performed on a miniaturized self-contained analysis device. Fluid manipulations, such as reagent mixing and fluid pumping, are indispensable constituent to link different units together in the μ TAS. Fabrication of the microfeatures, hence, is the fundamental step to the μ TAS development. The microfeatures include, for examples, microchannels for fluid flowing, micropumps for fluid pumping and micromixers for reagent mixing.

Researchers have then started working on fabricating the microfeatures on silicon wafers by the sophisticated fabrication technologies developed in microelectronics industries, named MEMS (Microelectromechanical systems)

technology [3]. This technology focuses on the fabrication techniques of silicon including bulk and surface machining with precision in micrometers [4]. Other popular substrate materials for fabricating biochips are glass and quartz. They are used because of their standard photolithography and wet etching techniques that were capable for developing microfeatures in biochips.

In the μ TAS development, biological species including metabolites, proteins, nucleic acids and cells have been employed as analytes, recognition molecules or signal transducers. Amongst them, nucleic acids have been extensively investigated for the μ TAS because of its thriving development in bioanalytical technologies, and its specificity and uniqueness in providing the information of the identities of the biological species. Herein, two key technologies which are especially important for the miniaturized nucleic acid-based analysis systems development are introduced. They are polymerase chain reaction (PCR) and capillary electrophoresis (CE).

The development of these two advanced technologies has established the foundation of miniaturized nucleic acid-based analysis systems [5-10] and other electrophoresis-based studies, for examples single neuron [11] and cell [12, 13] analysis, binding chemistry in aptamers [14], and carbohydrates analysis [15]. The principles and developments of these two advanced technologies are introduced in the following subsections.

1.1.2.1 Polymerase chain reaction (PCR)

Polymerase chain reaction (PCR) is a sophisticated technique to amplify an interested target segment of DNA from trace amount of DNA to thousands of millions copies in a few hours. This groundbreaking invention was first introduced by Mullis in 1986 [16] and immediately become the fundamental technology in genomics. The principle of PCR is shown in Figure 1.1.

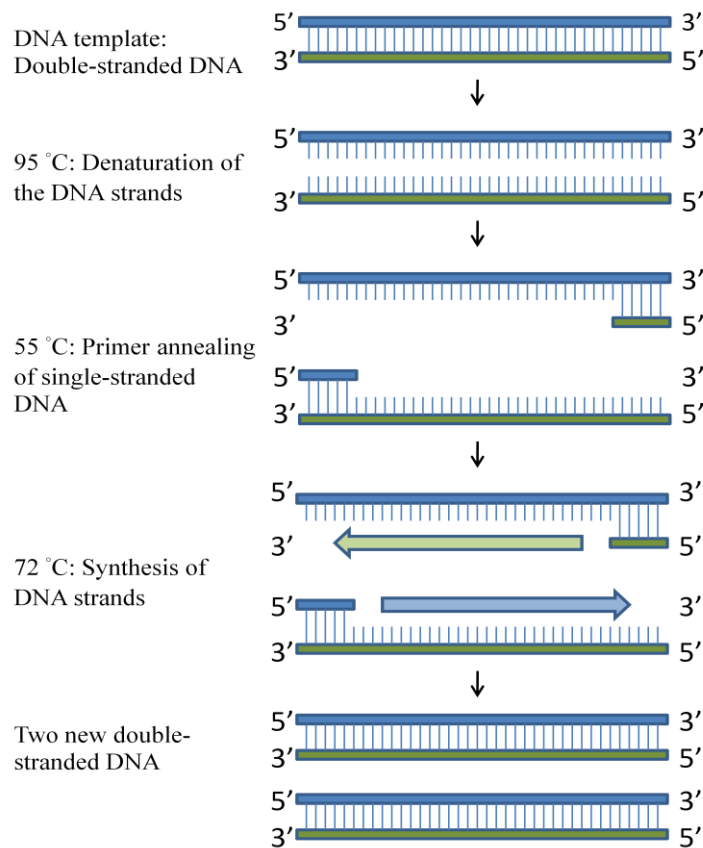
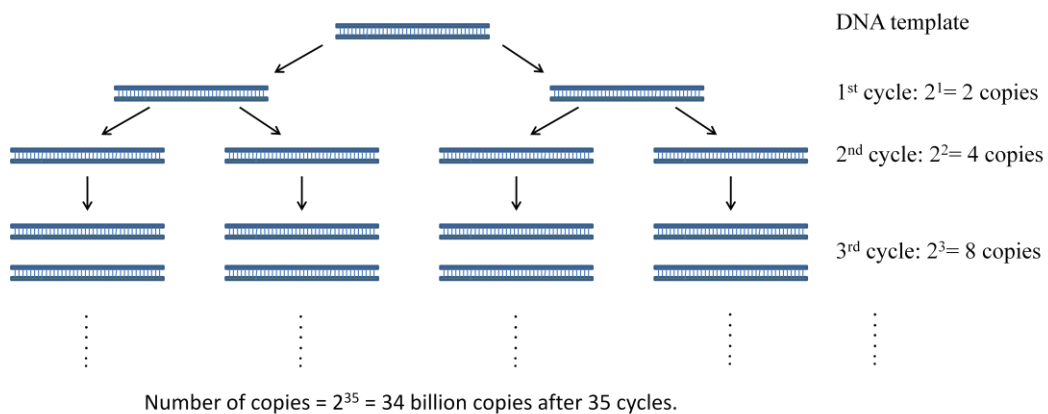


Figure 1.1 Principle of polymerase chain reaction.

PCR is a thermocycle process with three operation temperatures. The reaction starts with denaturing the double-stranded DNA, which is the DNA template, around 95 °C. Temperature then lessens to around 55 °C allowing primer annealing. Primers which are short segments of gene in 18–22 bases bind

to their target sites on the DNA template specifically. When the temperature is at 72 °C, a thermostable DNA polymerase called Taq polymerase extends the primers from 5' to 3' direction by assembling the deoxynucleotide triphosphates (dNTP, basic units of DNA) in specific orders. The synthesis cycle continues when the reaction mixture is subjected to the temperature cycle again. The number of copies of the target gene from one DNA template is 2^n , where n is the number of thermal cycle. A schematic representation of the amplification cycle is shown in Figure 1.2. A thermocycler is responsible for heating and cooling, temperature and time control in PCR. Since the thermocycler is bulky and the preparation process requires high level of skills, PCR is usually performed in laboratory by highly trained personnel. The introduction of miniaturization, however, has changed this perception.



Exponential amplification

Figure 1.2 Multiplication of DNA segment of interest versus number of thermal cycles.

PCR has been advancing the development in molecular biology, evolutionary biology, forensic analysis and medical diagnostics. Owing to its importance in genomics development and the idea of μ TAS, the first successful

miniaturized stationary PCR on a micromachined silicon wafer was reported by Northrup et al in 1993 [17]. The miniaturized PCR benefited from the small reaction volume (small thermal mass) of 20 nL which greatly reduced the processing time of conventional PCR process from hours to less than 7 minutes [18]. The other type of miniaturized PCR is called continuous-flow PCR introduced by Kopp et al in 1998 [19]. In continuous PCR, reaction mixture flows through three temperature zones continuously and repeatedly following the microchannels instead of confining in a reaction chamber for heating and cooling. On-chip continuous PCR reported by Kopp demonstrated an impressive improvement in lessening the amplification time to 1.5 min [19], which leaps forward to the realization of μ TAS. In a fully automated nucleic acid analysis system, genetic diagnostics are not limited to well-trained personnel anymore but are open to the public.

1.1.2.2 Capillary electrophoresis (CE)

Electrophoresis is a ubiquitous technique in genomics studies. Its fundamental principle is to separate the charged molecules, such as negatively charged DNA fragments, from a mixture under an applied electric field based on their differential mobilities which are proportional to their charge to mass ratios. Gel electrophoresis is a typical example of the electrophoresis family. In gel electrophoresis, DNA samples are loaded into the wells and an electric field is applied, negatively charged DNA molecules drift along the electric field with different velocities according to their sizes and charges. The working principle of gel electrophoresis is shown in Figure 1.3.

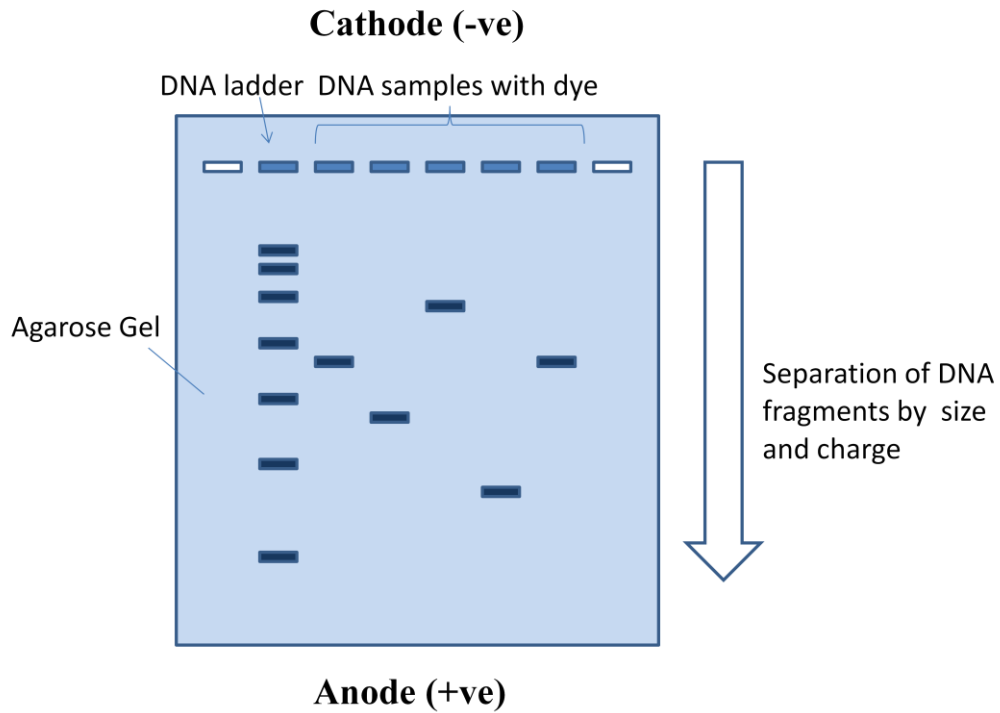


Figure 1.3. Working principle of gel electrophoresis.

Analogous to electrophoresis, capillary electrophoresis (CE) enables separation taking place inside a fused-silica capillary containing a polymer solution drawing the DNA samples by electrokinetic injection [20]. The first miniaturized CE chip was fabricated by Manz and Harrison using glass applying the idea of electroosmotic flow, where the bulk solution is driven along the capillary due to the electroosmotic motion of the solution and the driving force exerting on the charged samples by the electric field [21, 22]. The schematic diagram of electroosmotic flow is shown in Figure 1.4.

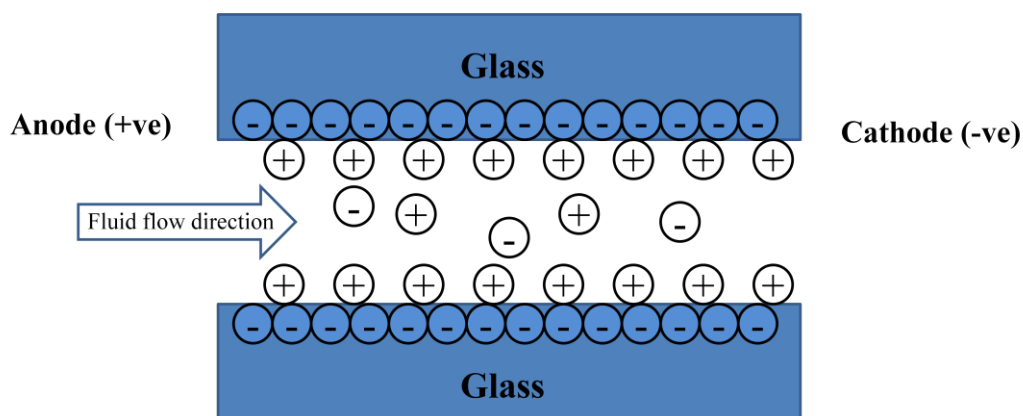


Figure 1.4. Charge distribution during electroosmotic flow in CE.

During electroosmotic flow, interior capillary surface is ionized which is usually negatively charged owing to reactive surface groups. Oppositely charged (+ve) ions adsorb to the interior surface while like charged (-ve) ions are repulsed from the interior surface. The positively charged ions hence form a shielding layer for the negatively charged ions against the interior capillary surface. The bulk solution, as a result, migrates towards the cathode (-ve). Since the electroosmotic flow is benefited from the surface charges of the substrate, it is important to ensure the substrate surface possesses high enough zeta potential ζ during material selection because ζ is proportional to the electroosmotic mobility μ_{EO} ($\mu_{EO} = -\frac{\epsilon\zeta}{\eta}$ where ϵ is the electrical permittivity of the medium and η is the fluid viscosity) [23, 24].

Miniaturization not only decreases the material cost of CE, but also leads to the emergence of an expeditious tool for molecular biology studies, i.e. chip-based CE (miniaturized CE) performs 100 times faster separation process than the conventional electrophoresis and 10 times faster than the capillary-based CE [25, 26]. Miniaturized CE is a remarkable technology to provide a rapid,

sensitive and reliable analysis information on DNA sizing, DNA sequencing and genotyping with high resolution to single base difference [27].

1.1.2.3 Biochips for bioanalytical applications

The applications of biochips are highly diversified including forensic analysis [28-30], medical diagnostics [31-33], drug discovery [34], biological warfare agent detection [35-37], and environmental monitoring [38, 39]. For example, CE-based DNA analysis microchips enable speedy screening of hereditary diseases [33] and rapid detection of contamination of yeast strains in blood culture bottles by genotyping [29]; CE microsystem enables detection and separation of explosives residues within 3 minutes [36, 37]; and microchip performs drug detection by immunoassay using just 1 min [30]. Miniaturization has largely reduced the processing time of the bioanalytical processes from more than an hour to several minutes.

Miniaturization has brought a wide range of advantages not limited to time-saving and reagent-saving, but also the enhancement in accuracy, sensitivity and automation.

1.1.3 New trend in biochip industry

In spite of the satisfactory performance of silicon, glass and quartz-based microfluidic devices provided, their costs are too expensive in terms of raw material costs and fabrication costs. The fabrication processes are conducted in clean rooms which require extremely expensive installment costs. The lengthy

fabrication time further increases its costs and also curbs the widespread use of the point-of-care (POC) diagnostic devices in the public. Due to its high fabrication and raw material costs, the microfluidic devices have to be reused which means to increase the chance of cross-contamination of biological samples.

Owing to the extensively developed applications and the huge biochip markets, the biochip industry is attempting to minimize the raw material and the fabrication costs of the microfluidic devices, and the installment and operation costs of the plant, so that the biochips can be in widespread use by the public. Under this situation, polymers have been chosen as the suitable candidate in biochip fabrication in recent years because of their prominence in low material cost, ease of fabrication and wide varieties of physical and chemical properties. Researchers have promptly studied the surface chemistry of polymers for their suitability on biological related applications [40-43], and numerous methods have been developed for passivating and modifying the polymer surfaces to be compatible with different biological tests [44-46]. However, establishment of polymer microfabrication and bonding technologies, corresponding to MEMS technology and bonding technologies in silicon and glass, are in order to realize the industrial scale production of plastic biochips.

1.2 Rationale, scope of study and objectives

In microfluidic chips, a sealed chip is essential to provide a contamination-free environment and to form functional parts for reliable biological analysis. The conventional method for sealing polymers is thermal

bonding which heats up the bulk polymers to its glass transition temperature (T_g) under pressure. Active polymer chains hence intercalate with each other in the bonding interface leading to bonding. This method, however, is easy to cause deformation or collapse of the microstructures on the microfluidic chip because of the elevated temperature and the increased pressure. Deformation becomes significant and has great influence on the integrity of the microstructures.

A desirable bonding should be able to offer the following characteristics:

- Material homogeneity
- Negligible deformation on prime structures
- Absence of leakage
- Sufficiently high bond strength

Material homogeneity is crucial for an accurate analysis when electroosmotic pumping is applied in the downstream applications like capillary electrophoresis [47], since different material surfaces may possess different zeta potentials where its values are proportional to the electroosmotic flow velocities [48]. Thus, in a hybrid microchannel, electroosmotic pumping would result in peak broadening and the separation accuracy would be affected. Material heterogeneity, as a result, should be avoided. Furthermore, intact prime structures and complete sealing are important for accurate manipulation of microfluidic flow, and sufficiently high bond strength should be guaranteed depending on the downstream applications.

A novel bonding method using carbon nanotubes (CNTs) for microwave bonding has been developed to fulfill the bonding requirements in this study. At

the beginning of the study, potential auxiliary materials, acting as microwave absorbers to generate heat for bonding, including gold nanoparticles (GNPs) and carbon nanotubes (CNTs) were compared and investigated for their bonding efficiency in sealing plastic biochips upon the microwave irradiation. CNTs were later chosen as the suitable candidate for further development owing to its vigorous response towards the microwave irradiation. Microwave bonding using CNTs developed in this study enables microstructures bonded with homogeneity, leakage-free and negligible deformation by short processing time and high fusion efficiency which, as a result, potentially lower the operation cost and facilitate the industrial scale production.

The objectives of this study are:

- (i) to compare and investigate the responses of GNPs and CNTs towards microwave irradiation in order to predict the bonding efficiency for sealing plastic biochips;
- (ii) to design a bonding model for the suitable microwave absorber(s);
- (iii) to study the relationship between bonding parameters such as the thickness of microwave absorber(s) and the duration of microwave exposure;
- (iv) to evaluate the bonding performance through the examination of microstructure integrity, leakage test and tensile test on the bonded plastic biochip.

Chapter 2: Literature Review

This chapter will first introduce some polymers that are frequently used for producing plastic biochips, in terms of their physical and chemical properties, and some basic criteria and concerns during material selection of biochips in section 2.1. Next, an extensive overview on the bonding methods for sealing polymer substrates and their recent development will be given in section 2.2. This chapter will be finished with a summary in section 2.3.

2.1 Polymer materials

In the fabrication of plastic biochips, the polymer materials commonly used are thermoplastics. Since thermoplastics can be softened and melted at an elevated temperature, the plastic biochips can be replicated from the fabricated moulds by heating. Thermoplastics offer various choices in fabrication methods including hot embossing [49], injection moulding [50], thermoforming [51] and laser ablation [52, 53]. They also offer wide varieties of physical and chemical properties that can fulfill different requirements of the downstream applications. The physical and chemical properties of some thermoplastics that are frequently used as biochip substrates are summarized in Table 1.

Table 1. Physical and chemical properties of thermoplastics that are frequently used as biochip substrates.

Name*	Tg(°C)	Heat distortion T (°C)	Water absorption (%)	Thermal expansion coefficient (10 ⁻⁶ /K)	Young's modulus (MPa)	Transparency	Compatible chemicals	Incompatible chemicals
COC	138	130	0.01	60	2400	Clear	Acids, alkalis, alcohols, ketones, esters.	Chlorinated and aromatic solvents, gasoline, oils.
PMMA	110	100	2	80	3200	Clear	Acids, alkalis, alcohols, gasoline, oils.	Ketones, esters, chlorinated and aromatic solvents.
PC	148	138	0.3	70	2400	Clear	Acids, alcohols, gasoline, oils.	Alkalis, ketones, esters, chlorinated and aromatic solvents.
PP	163	85	<0.1	100–200	1450	Translucent	Acids, alkalis, alcohols, organic solvent.	Ketones, esters, hydrocarbons.
PS	100	98	<0.1	80	3200	Clear	Acids, alkalis, alcohols.	Ketones, esters, chlorinated and aromatic solvent, gasoline, oils.
HDPE	135	86	<0.1	120–150	1350	Translucent	Acids, alkalis, alcohols.	Hydrocarbons.

*Abbreviations: COC (cyclic olefin copolymer); PMMA (poly(methyl methacrylate)); PC (polycarbonate); PP (polypropylene); PS (polystyrene); HDPE (high density polyethylene).

Physical properties of all materials are from an online resource [54] except that of COC are from product information provided by company [55-57]. Chemical properties of all materials are from the CHEMnetBASE database [58].

Though the listed polymers are all commonly used for making biochips, four basic criteria are setup for ensuring that the selected materials are suitable for any sensitive downstream application and detection of biochips. The four basic criteria are introduced in the following paragraphs as guidelines. Further requirements on material selection focusing on particular downstream applications, PCR and CE, are also addressed.

I Manufacturability

In order to attain mass production, injection moulding is one of the best fabrication tools to provide high throughput and low fabrication cost (in terms of large scale production). The fabrication materials, thereby, must be thermoplastics so that it can be melted and injected into the mould through the runner.

II Biocompatibility

The polymer surface should be compatible with biological species and shows no inhibition on the biological assays or no interaction with any reaction species, or it can be passivated to show no harm on the biological testing.

III Transparency

Optical detection is the most popular and direct method for detecting the final products. Transparency is thus the prime requirement for the fabrication materials. Nevertheless, owing to the advance development in the detection

methods, for instance electrochemical detection, transparency is no longer a necessary requirement for the biochip material; however, it is still preferential for the ease of observation.

IV Low autofluorescence

Laser-induced fluorescence (LIF) is a common optical detection method for DNA detection because of its high sensitivity. High background noise resulted from the autofluorescence of polymers would limit the sensitivity of the detection [27]. Polymers with low autofluorescence are thus preferential for being the fabrication materials.

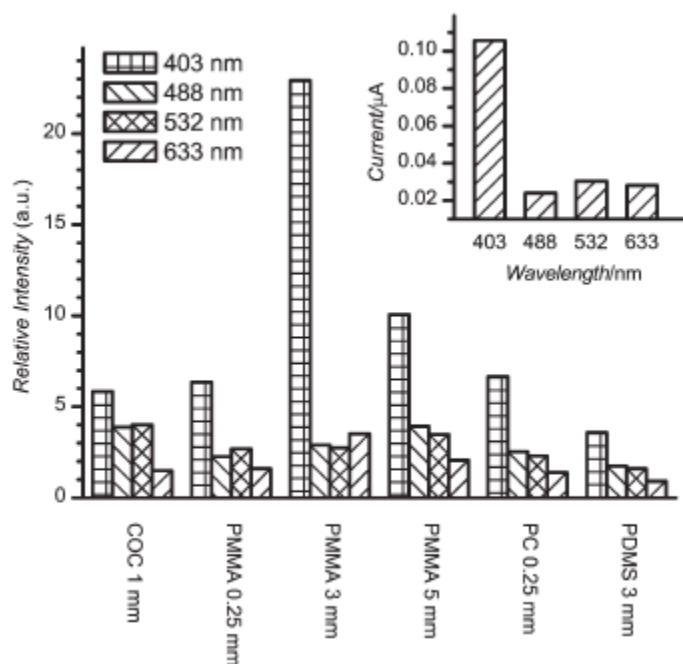


Figure 2.1. Autofluorescence intensity of polymers relative to BoroFloat glass, where the absolute intensity is shown in top right, after 60 s illumination of 1 mW laser [59].

Apart from the basic criteria, downstream applications also contribute to the predetermined requirements on the substrate materials. The material compatibilities towards the two advanced technologies (PCR and CE), which have been mentioned earlier in chapter 1, are common consideration factors owing to their ubiquitousness in genomics analysis in microfluidic devices, and their strict operation conditions and polymer surface requirements. PCR involves a high denaturation temperature at 95 °C, which is not a sustainable temperature for some polymeric materials with T_g close to this temperature. Polymers with distortion temperature below 95 °C, like PP, PS and HDPE, are considered to be unsuitable. PMMA is also not recommended to act as the substrate material for the reason of preventing potential distortion caused by the heat source.

Additionally, in order to perform a successful electrophoresis, the polymer substrates should have sufficient dielectric strength to prevent arcing across the substrate materials, adequate thermal conductivity to dissipate Joule heat and ample surface charges to aid electroosmotic flow [60]. Amongst the polymers shown in Table 1, polymers like PMMA, PC and COC have been successfully demonstrated in the applications of CE [61-63].

In order to fulfill the requirements of these two advanced technologies, PC and COC are found to be the suitable materials. However, reviewing the four basic criteria, PC demonstrated a lower autofluorescence than COC in the overall performance. PC would therefore be suggested as the most suitable substrate material for fabricating biochip.

2.2 Types of bonding methods for sealing polymers

In microfluidic systems, cover plates are essential to seal the microstructured substrates in order to enable reagent storage and to protect the experimental platforms from any contamination and interference of the environments. It is also important to form functional parts such as microchannels (for fluid transportation) and microchambers (for chemical reaction or incubation) for analyte processing. Accompanying with the advancement in fabrication technology and biotechnology, the dimensions of the biochip microstructures are continuously reducing which makes bonding in polymers more challenging. Bonding in polymer and in silicon/glass has totally different concerns owing to the ease of deformation of polymer microstructures under high temperature and exerted pressure, which are the basic conditions for thermal bonding. The extent of deformation is becoming dominant in miniaturized systems, which may significantly affect the actual volume flow and the performance of the devices. A vast number of bonding methods for sealing plastic biochips have been developed with the aim to alleviate these issues.

There are mainly five types of bonding methods for sealing polymers which include thermal bonding, microwave bonding, adhesive bonding, solvent bonding and ultrasonic bonding. General principles of these bonding methods and their merits and shortcomings will be reviewed in this section.

2.2.1 Thermal bonding

In thermal bonding, two polymer substrates are brought to their T_g , where polymers soften and become rubbery, under pressure. Polymer chains gain higher mobility at T_g and intercalate with neighboring polymer chains on the other substrate surface. The distinct interface, finally, disappears. After cooling to room temperature, the bonded assembly can be relieved from pressure [64]. A healing model of polymer surfaces is shown in Figure 2.2.

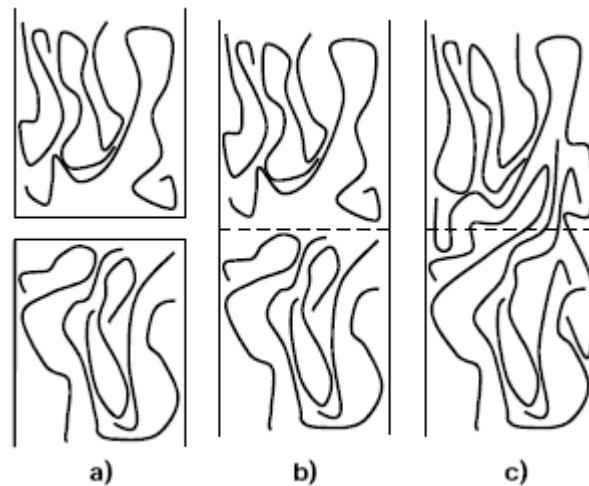


Figure 2.2. Healing models of polymers [64, 65]: a) distribution of polymer chains before contact; b) two polymer surfaces in ultimate contact; c) diffusion and intercalation of polymer chains.

During the bonding process, heat is directly transferred from the hotplate to polymer substrates from outside surface to the bonding interface through heat conduction. Under the circumstance of high temperature and pressure, deformation on the bonded microchannels is easy to happen. Attempts have been made by various groups to eliminate this issue by lessening the pressure; for

example, Sun et al. used a relatively low pressure but a temperature much higher than T_g for bonding [66]; Kim et al. developed a holed pressure equalizing plate to avoid the pressure acting on the microchambers directly [67]. Other groups have also attempted to reduce the surface T_g in the bonding interface by plasma treatment [68-72], corona discharge [73], UV irradiation [74], X-ray irradiation [75] and use of low molecular weight PMMA [76, 77]. The results are satisfactory especially for the plasma treatment using vacuum ultraviolet / ozone, which was able to reduce the bonding temperature of PMMA from 95 °C to 50 °C where PMMA still behaves as glass [70]. Other innovative thermal bonding methods, like PC/PMMA hybrid assembly with improved heat tolerance [78], boiling water for PMMA bonding [79], clamp-free bonding using vacuum oven [80] and thermal bond under ultrasonic field [81] have also been demonstrated.

The most common equipment utilized in thermal bonding is hot embossing machine, which consists of a large thermal mass (hotplate) that usually results in prolonged waiting time during heat sinks and hence aggravates the microstructure deformation. The involvement of heating and cooling of the thermal mass lead to an inefficiency of energy transmission because of heat loss and results in an enormous operating cost. Figure 2.3 shows the schematic drawing of a hot embossing machine. Though the processing time in thermal bonding is comparatively long (e.g. 30 – 45 min), it offers the advantages of material homogeneity and the ease of operation.

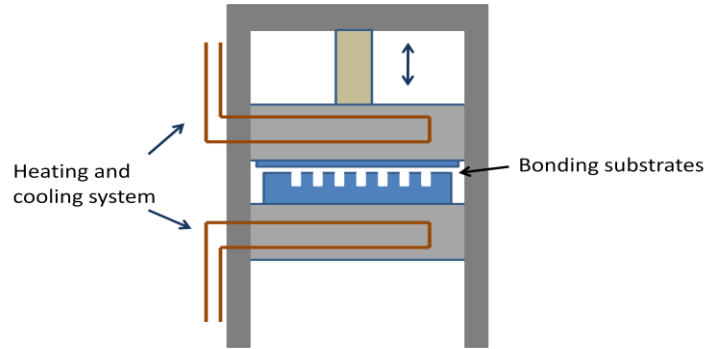


Figure 2.3. Schematic drawing of a hot embossing machine.

To summarize, homogeneity is one of the important features that thermal bonding provides. The involvement of the bulky thermal mass, however, limits its application in a high throughput production industry and the immense thermal energy loss also increases its operation cost. Nevertheless, it is still the most common and popular method for sealing plastic substrates because of its high reliability, high simplicity and ease of operation.

2.2.2 Microwave bonding

In microwave bonding, an auxiliary material, which possesses strong microwave absorption properties, is incorporated in the bonding interface of the two polymer substrates to act as a microwave absorber. The absorbed microwave energy instantly dissipates as heat to the adjacent polymer surfaces. Polymers in the bonding interface are hence softened or melted and followed by wetting the auxiliary material [82]. The molecules in both polymers and auxiliary material maintain the state of intercalation after cooling. The polymer substrates are eventually bonded through the auxiliary material. Polymer substrates used in microwave bonding should be optically transparent to the microwave or having

only small permanent dipole moment in the molecular structures [83] so that it would not absorb the microwave energy nor raise in temperature upon the microwave irradiation. The temperature of the global substrates is hence relatively low that would not deform the polymer microstructures. Heating is thus confined in the bonding interface induced by the auxiliary material which also serves to produce localized heating.

The auxiliary materials can be metals, electrically conducting polymers, ceramics, ferrites and carbons [83]. Its rate of heating under the electric field was derived by Metaxas and Meredith [84]:

$$\rho C_p \frac{dT}{dt} = 2\pi\epsilon_0\epsilon'' f E^2$$

where rate of heating $\frac{dT}{dt}$ is directly proportional to the permittivity of free space ϵ_0 , the loss factor ϵ'' of the material, the frequency f of the electric field and the square of the electric field E ; and is inversely proportional to the density ρ and the specific heat C_p of the material. Microwave heating of the auxiliary materials can happen through polarization heating, electrical resistance heating, Maxwell–Wanger effect, ion polarization and electron polarization (in decreasing efficiency order) [83, 85].

Auxiliary materials such as gold and polyaniline have been successfully demonstrated for their microwave absorption abilities in sealing microfluidic devices in the previous works. Lei et al. employed two layers of 0.1 μm gold thin film to seal an embossed polymer substrate and a polymer cover plate for potential applications in microfluidic devices [86]. The substrates were successfully bonded with satisfactory bond strength while, however, the image of

the bonded microchannel was vague as shown in Figure 2.4. The microchannel integrity after bonding thereby was able to be estimated. Attempt has also been made on patterning solvent-based polyaniline (a conductive polymer) alongside the microchannel for microwave bonding [87]. The bonded assembly possessed high bond strength; however the screen-printing technique raised a limitation on sealing more complex microfeatures smaller than 100 μm .

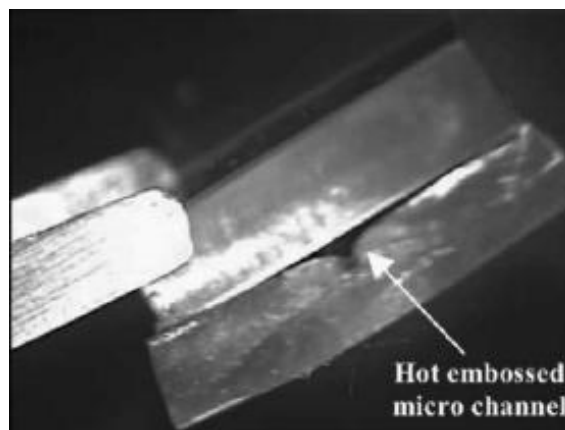


Figure 2.4. Bonded PMMA using gold film.

Another microwave bonding method using carbon nanotubes (CNTs) has also been reported by Wang et al. [82]. In this work, multi-walled carbon nanotubes (MWNTs) with diameters ranged 30 – 40 nm were dispersed in ethanol and sprayed on two bare polymer plates. The assembly was welded in a multimode microwave oven with power of 200 W for 10 s and resulted in an indivisible bonding as shown in Figure 2.5. Wang suggested that the welding between CNTs and polymers involves solely physical intercalation (no chemical reactions) judging from the results of Fourier transform infrared (FTIR). Owing to the vigorous response of CNTs to microwave irradiation, the time for welding is just within seconds.

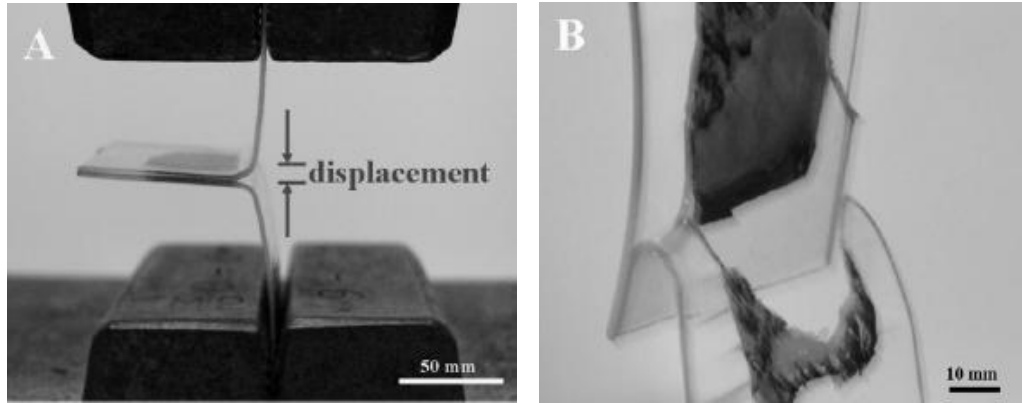


Figure 2.5. Peel test for a PC/CNTs/PC junction. A) Setup of the test; B) cracking of the joint during the test [82].

Microwave bonding offers an efficient bonding process, which largely reduces the time of conventional thermal bonding from almost an hour down to several seconds. It also enables the production in large scale and an efficient energy transfer that can minimize the unnecessary energy loss during bonding and hence the operation cost. The auxiliary material, however, may have adverse effects on the downstream bioanalytical processes. Chemistry between the auxiliary materials and the specific reagents involved should be studied in advance in order to ensure the biocompatibility of the auxiliary materials. Issue such as construction of the shielding layers in a production plant is important to be considered beforehand.

2.2.3 Adhesive bonding

In adhesive bonding, an adhesive layer is incorporated between the polymer substrate and the cover plate, or the adhesive layer itself acts as a cover plate. Adhesive bonding occurs when the attractive forces formed between the adhesive surfaces and the substrate surfaces are stronger than the cohesive forces on the

materials alone during the intimate contact [88]. The polymer substrates thereby are bonded through the adhesive layer.

Adhesives can be categorized into two groups; liquid adhesives (i.e. viscous mixtures) and solid adhesives (i.e. lamination films). When liquid adhesives apply, liquids with high viscosity are spin-coated or components with low viscosity are injected to the bonding surfaces. Most of the liquid adhesives contain photo initiators that undergo curing by UV exposure to crosslink resin [89-92]. There are also examples using laser [93] and heat [94] to perform curing of adhesives. In solid adhesives, lamination films are placed at the top of the polymer substrates. The films wet the bonding surfaces and then seal the polymer substrates under specific conditions, for instance, pressure exertion [95-97], temperature activation [98-102] and ultraviolet light exposure [103, 104].

In both liquid and dry adhesives approaches, foreign substances are incorporated. The involvement of foreign substances is not recommended especially for bioanalytical devices because the foreign substances may not be compatible or even toxic to the biological samples. Furthermore, squeezing and clogging of liquid adhesives in microchannels are easily happened because of the fluidity of the liquid adhesives, though it has been improved by researchers using method like capillary force action [92]. It is, however, still challenging to eliminate the adhesives invasion to guarantee the device reliability. Compared to liquid adhesives, dry lamination films are more direct and less complicated in terms of the procedures. It offers high simplicity in operation and efficient sealing which are parts of the reasons for making it still popular for being used in bonding microfluidic devices.

2.2.4 Solvent bonding

Solvent bonding is regarded as the strongest bonding method that provides the highest bond strength amongst various bonding methods of polymers. Generally, in solvent bonding, solvent with solubility parameter similar, but not the same, to that of the polymer substrates is added to the bonding surfaces of the polymers with or without washing before bonding. Polymer surfaces undergo swelling and softening because of the intertwining of solvent molecules into the surface polymer chains [105]. The intertwined solvent molecules loosen the bonding between surface polymer chains that result in a reduction of the polymer surface T_g. The polymer substrates, thereby, can be bonded with a temperature much lower than T_g under pressure.

Solvent bonding in PMMA is well-developed [99, 106-114] and some in COC are also reported [115-117]. The extent of solvation can be controlled by manipulating temperature [113], duration of solvation [108], amount of solvents (controlled by stamping [118] and vapor deposition [115, 116]) and solvent composition [107, 110]. Investigation on protecting the microchannels by sacrificial materials [106, 112], enhancing the bond strength by UV exposure [119] and shortening the bonding duration by microwave [120] have also been conducted.

As mentioned at the beginning of this section, solvent bonding features in offering the high bond strength of the bonded assembly, where the bonded device is capable to operate under a high pressure environment. The solvent bonding, however, has a limitation on the polymer materials. Since the degree of solvation

depends mainly on the solubility parameters of both solvents and polymer substrates, polymers have no suitable solvents with similar solubility parameters are not able to be bonded through this method. Furthermore, solvent residues trapped in the microfluidic channels would lead to contamination in the systems, which are still the main concern for applying solvent bonding in the downstream sensitive bioanalytical testing.

2.2.5 Ultrasonic bonding

Special equipment, an ultrasonic welding machine as shown in Figure 2.6, is required for ultrasonic bonding. Frequency generated from the generator transmits through the horn to the substrates on leveling anvil in form of structure-borne sound, which means the sound propagates through structures as vibration. Some quasi point- or line-shaped structures (also called asperities or energy director) are usually fabricated on the bonding surface to assist localizing the vibration energy. Localized energy on the energy director causes itself heating and melting as a result of intermolecular and interfacial friction [121]. The melted energy director, with the same material as the polymer substrates, acts as an adhesive to seal the bonding substrates.

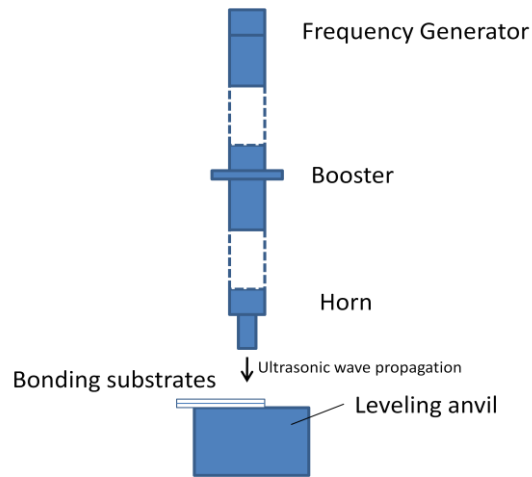


Figure 2.6. Schematic diagram of an ultrasonic welding device.

In microfluidic devices, dimensions of microstructures are usually within microns and thereby the fabricated energy directors have to be miniaturized so as not to flow into the microstructures during melting. Successful attempts have been made on sealing single microchannel sized $500\ \mu\text{m}$ in width and depth [122], and single microchannel sized $70\ \mu\text{m}$ in width and $40\ \mu\text{m}$ in depth [121]. Another ultrasonic bonding method assisted by preheating the polymer substrates to $20 - 30\ ^\circ\text{C}$ lower than the T_g of the polymers without the use of energy director has also been reported [123]. The reported method showed little deformation in the sealed microstructures.

Ultrasonic bonding offers the features of localized heating and homogeneity in the bonded devices, which raise the researchers' interest in investigating the use of ultrasonic bonding in microfluidic devices in recent years. Though successful attempts have been made on sealing single microchannel, sealing microstructures with more complex and dense patterns, which are the current trend in microfluidic devices, is still challenging. In more complicated and dense micropatterns, the requirements on size, distribution and alignment of the

miniaturized energy director are extremely stern in terms of the accuracy. All these issues cause the application of ultrasonic bonding in bonding microfluidic devices challenging.

2.2.6 Others

Some other bonding methods not belonging to the above dominant categories are included in this section. They include chemical modification by a silane solution (3-aminopropyltriethoxysilane, APTES) on PMMA surface [124], infrared laser welding [125] and laser welding using colorless dye to localize heating [126]. These bonding methods provide additional alternatives to seal polymers depending on the bonding requirements and production scale.

2.3 Summary

Various bonding methods for sealing polymers together with their merits and shortcomings have been reviewed in this chapter. There is, however, still room for improvement to integrate the features of homogeneity, free of deformation, high throughput and low cost into a single bonding method which is suitable for mass production. A potential bonding method possessing the features mentioned above will be developed and proposed in the following chapter.

Chapter 3: Microwave bonding

In this chapter, two bonding methods, microwave bonding using gold nanoparticles (GNPs) and carbon nanotubes (CNTs), will be developed from the literature review. The microwave absorption properties of these two auxiliary materials will be overviewed and the microwave bonding model will be proposed.

3.1 Development from literature review

In the previous chapter, numerous bonding methods have been overviewed. There is, however, no suitable general bonding method for sealing all kinds of polymers with homogeneity, negligible deformation, short processing time and high bonding efficiency which can potentially be developed into industrial scale production. In this section, different bonding methods will be commented on their suitabilities based on the stated requirements and a bonding method containing all these features will be developed.

There are five types of bonding methods reviewed in the last chapter including thermal bonding, microwave bonding, adhesive bonding, solvent bonding and ultrasonic bonding. Amongst these, thermal bonding and ultrasonic bonding can satisfy the requirement on homogeneity; while the use of adhesives in adhesive bonding, the use of auxiliary materials in microwave bonding and the use of solvents in solvent bonding incorporate foreign substances may leave residues inside the microchannels that may contaminate the downstream

bioanalytical testing, and hence are not preferable. On the other hand, concerning the requirement of short processing time, the involvement of hot embossing machine in thermal bonding and ultrasonic machine in ultrasonic bonding restricts a high throughput production because of their long processing time and primary fixation design respectively. The use of microwave, in this case, has the greatest potential to enable industrial scale production of bonding because of the effective transfer of energy.

Conventional microwave bonding requires an auxiliary material to absorb and generate heat energy. This auxiliary material is usually regarded as a foreign substance that contaminates the microfluidic device or has negative impact on the downstream application. In this study, two auxiliary materials which are potentially beneficial to the downstream bioanalytical testing are proposed. These auxiliary materials are developed from the literature review as follows.

In the previous work in microwave bonding, the use of gold thin film has been demonstrated successfully in sealing polymer substrates [86]. The bonding image, however, is vague and the use of a large area of conductive surface may lead to electric breakdown in the applications involving the electric field. Gold nanoparticles (GNPs), thereby, are proposed to be the auxiliary material for microwave absorber. There are several reasons why GNPs are proposed and what overwhelming features it has over the gold thin film. GNPs which are nanometers in size can greatly reduce the potentially adverse effect regarding the conductivity that gold thin film may cause. GNPs also have the advantage that GNP itself is biocompatible even in the sensitive and sophisticated biochemical reaction, PCR. GNPs have been proved as no harm and have positive effects

towards the PCR efficiency and specificity [127, 128]. The involvement of GNPs on microfluidic platform has great potential in developing more innovative applications. Microwave bonding using GNPs is expected to provide rapid bonding with localized heating of biochips.

In another reported work, carbon nanotubes (CNTs) have demonstrated a strong ability in absorbing microwave energy and converting it into heat energy through the indivisible bonding of polymer plates [82]. The heating process is amazingly fast. The whole bonding process is expected to be very short because of the nature properties of CNTs in rapid conversion of heat and the small thermal mass involved in the heating system. In the reported work, however, bonding has only been done on sealing bare polymer plates. Its result is encouraging in applying CNTs in bonding biochips. CNTs have also been demonstrated for its biocompatibility with PCR in a previous work [129]. The result showed the addition of CNTs is able to enhance the specificity of long PCR. The incorporation of CNTs in microfluidic devices may potentially benefit the future investigation in PCR-based biochips.

The two options proposed above will be considered as the potential investigation. Brief reviews on GNPs and CNTs will be carried out respectively, followed by the bonding models.

3.2 Proposed method I – gold nanoparticles (GNPs)

In this section, microwave bonding assisted by gold nanoparticles is introduced. Microwave absorption properties in metal and GNPs are evaluated, and followed by the design setup of microwave bonding of GNPs.

3.2.1 Microwave absorption properties of metals and significance of GNPs

Gold nanoparticles are colloid suspension of spherical-shaped gold in nanometers. Metals generally respond to microwave irradiation in two ways. Metals are conductive materials containing seas of free charges. Free charges in metal will concentrate on the sharp edges when the metal is exposed to microwave irradiation. The charged particles move rapidly in the edges because of the changing electric field and when its electric field strength reaches certain threshold, air near the edges will break down. A vast amount of released energy causes arcing happened as shown in Figure 3.1. Since the energy involved is huge and the heat generated is not easy to control, some researchers would use controlled microwave to make it for practical uses. Another way for metal reacting to microwave is the generation of eddy current. Eddy current is induced inside or on the surface of a conductor, depending on its conductivity, under the magnetic field. Owing to the resistive nature of the conductor, electric current is lost in the form of heat which is called Joule heating. The generated heat can be sufficiently large to melt the polymer surrounded and results in welding [83].

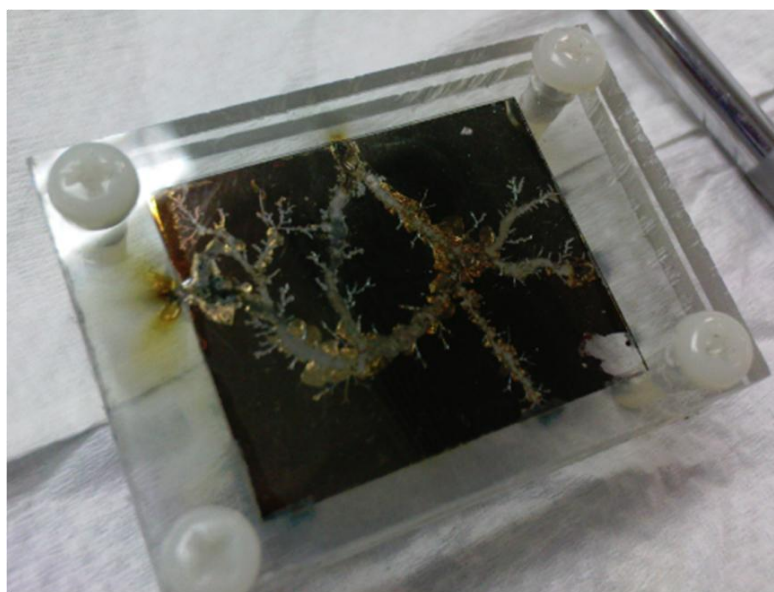


Figure 3.1. Cracks observed on a gold thin film resulted from arcing after the exposure to microwave irradiation.

The interested wavelength for investigating the electromagnetic wave absorption properties of GNPs is usually around 300 – 1500 nm which is the visible light region [130, 131]. Visible light on GNPs is of particular interest because GNPs usually have distinct absorption peaks according to their sizes. Though there is no direct investigation on microwave effect to GNPs, where the wavelength of microwave is around 12 cm for 2.45 GHz microwave oven, it is still worthwhile to examine the feasibility of using GNPs to weld polymers under microwave irradiation, based on the facts that eddy current generated in metals is able to weld polymers. Investigation on estimating these physical properties of GNPs in a microscopic world is fascinating.

GNPs have been widely developed for medical diagnostic applications, for examples, detection of cancer cells to forming GNP clusters followed by laser pulse to cause cell damage [132], selective targeting and imaging Chronic

Lymphocytic Leukemia cells by using Surface Enhanced Raman Scattering (SERS) GNPs [133], and drug delivery of insulin using chitosan reduced GNPs [134]. It has also been developed as nanoprobe in microfluidic devices, e.g. detection of tumor markers by GNP-labelled antibodies [135], detection of single-base polymorphism using oligonucleotide-modified GNP for single-base mismatch [136], and DNA extraction by cell spearing [137]. Important findings have also been reported in the enhancement of the PCR efficiency [127] and specificity [128] upon the addition of GNPs. Most of these reported researches in microfluidic devices have been using GNPs ranged from 10 – 15 nm

3.2.2 Microwave bonding model for GNPs

Below in Figure 3.2 shows the model for microwave bonding of plastic biochips using GNPs. GNPs are distributed in the bonding interface between the patterned substrate and the cover plate.

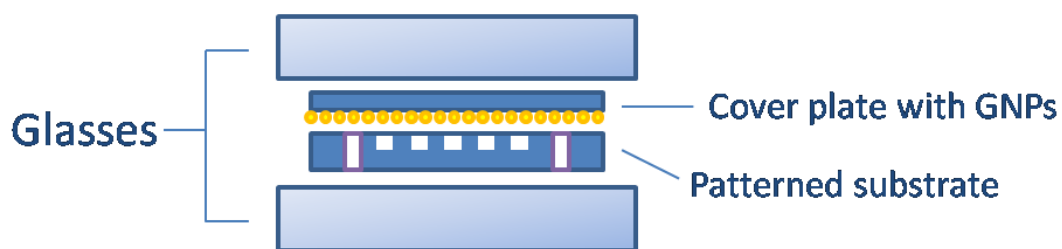


Figure 3.2. Model setup for microwave bonding using GNPs.

In the patterned substrate, holes are drilled for fluid access as shown. Two glasses are applied to equalize the exerted pressure and to provide leveled surfaces for bonding. The whole assembly is later exposed to the microwave irradiation.

Since GNPs are very small and have no sharp edge, arcing is not supposed to be happened in GNPs. Instead, upon the microwave irradiation, eddy current is induced on the GNP surfaces under the influence of magnetic field. The induced eddy current dissipates as heat on GNP surfaces owing to the resistive nature of conductors. The heating effect generated by the eddy current raises the temperature of GNPs and is transferred to the contacting polymers through heat conduction. The heating effect is illustrated in Figure 3.3.

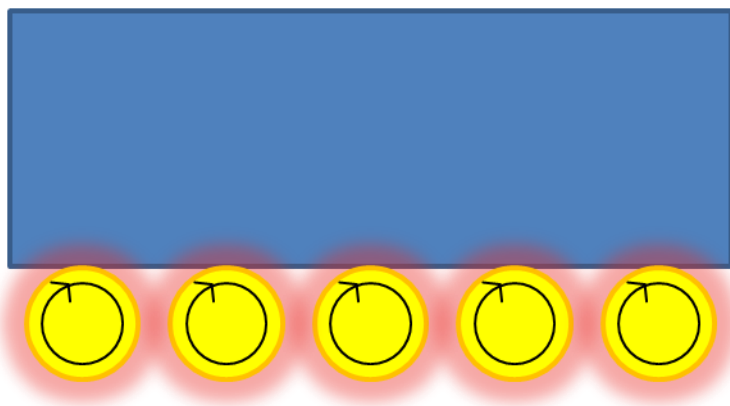


Figure 3.3. An illustration of the heating effect generated by eddy current on the GNP surfaces.

The surface polymer chains are “activated” with increased mobilities and intercalate with the polymer chains on the neighboring surface. GNPs in the bonding interface are wetted by the melted polymers and are immersed into the polymers. Since the heat sources are in nanometers and polymers are not good thermal conductors, the heat-affected region is expected to be confined in nanometer thickness. When the microwave irradiation terminates, GNPs cease generating heat and the thermal energy in the bonding interface rapidly loses to the bulk polymer substrates which are in a relatively low temperature and to the surrounding through heat convection. The whole bonding process, hence, is in

high efficiency with short processing time owing to the small thermal mass involved.

Since the bonding process is conducted by localized heating, integrity of the global microstructures of the bonded substrates is thus expected to be maintained without alteration by the heat. Deposition density of GNPs and exposure time would be the important parameters in the investigation. In the following section, an alternative bonding method will be developed.

3.3 Proposed method II – carbon nanotubes (CNTs)

The second proposed bonding method for sealing plastic biochips is the microwave bonding assisted by CNTs. Brief introduction on the dielectric properties of CNTs and the significance of CNTs in bioapplications will be addressed. The model setup of microwave bonding using CNTs will come up at the end of this section.

3.3.1 Dielectric properties and significance of CNTs

Carbon nanotubes are entirely composed of carbon atoms forming hexagonal array by the sp^2 hybridization orbits. Its shape is like a hollow tube which can be conceptualized as wrapping up of graphene sheet [138]. It can be categorized into single-walled carbon nanotubes (SWNTs) and multi-walled carbon nanotubes (MWNTs) depending on the number of the wrapped graphene(s).

In recent years, the notable dielectric properties of CNTs have fascinated researchers' extensive investigation on it [139-142]. Dielectric properties are generally described as the properties of materials undergoing polarization under alternative electric field, and also defined as the abilities of materials to store and release electrical energies. The ability of material to convert stored energy into heat is generally represented by the loss tangent, $\tan \delta$ where

$$\tan \delta = \frac{\epsilon_r''}{\epsilon_r'}$$

herein, ϵ_r'' is the relative loss factor indicating the ability of a material to absorb

electrical energy, and ϵ_r' is the relative dielectric constant indicating the ability to store electrical energy [143]. Hence, the values of $\tan \delta$ and ϵ_r'' should be higher in materials possessing stronger dielectric properties. It has been found that in CNTs, both $\tan \delta$ and ϵ_r'' are in a proportional relationship with temperature [144], which means the ability for CNTs converting electrical energy into heat is stronger in a higher temperature. Scientists have accounted the superior abilities of microwave energy absorption in CNTs for the dispersion of polarization of the hybridization orbit sp^2 , and the high speed motion of π bond electrons causing friction and heat in the changing electric field [142, 145].

In addition to strong dielectric properties, CNTs also possess superior thermal conductivity. Previous investigation on the thermal conductivity in a single multi-walled CNT was found to be above $3000 \text{ Wm}^{-1}\text{K}^{-1}$ at room temperature [146], which is much greater than that in diamond.

CNTs have also been applied in biotechnological science, for examples, forming nanofilters to remove virus from water [147]; assisting the plasmid transfer into *Escherichia coli* cells [148, 149]; and acting as vesicles to deliver therapeutic drugs to the target cells [150]. Owing to the mounting importance of CNTs in bioapplications, more investigations on the biocompatibility of CNTs were conducted. Until now, there is still no evidence showing CNTs is harmful or toxic to biological species [151-153]. On the contrary, CNTs have been found to possess significantly positive effect on PCR which is the enhancement on specificity of long DNA amplification [129]. The incorporation of CNTs in the microfluidic devices broadens the functionalities of the devices and opens it to more undiscovered applications.

3.3.2 Microwave bonding model for CNTs

The model for microwave bonding of plastic biochips using CNTs is setup as below in Figure 3.4. CNTs are positioned in the bonding interface between the patterned substrate and the cover plate.

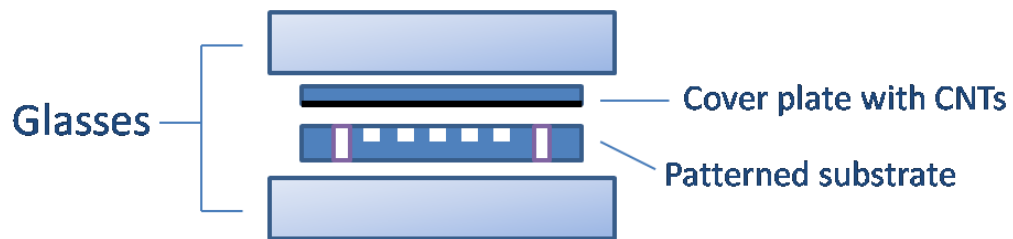


Figure 3.4. Model setup for microwave bonding using CNTs.

The entire model for CNTs is the same as that for GNPs except the type of auxiliary material used. The whole assembly is later exposed to microwave irradiation for microwave bonding.

During microwave irradiation, CNTs generate heat owing to the dispersion of polarization of the hybridization orbit sp^2 and the high speed motion of the π bond electrons. The heat generated by CNTs transfers to the surrounding polymers mainly through heat conduction and thermal radiation. Polymers in the bonding interface gain in energy and start softening or melting, followed by wetting the CNTs. CNTs then subside into the softened polymers where at the same time, polymer chains with enhanced mobilities intercalate with polymer chains on the neighboring surfaces. As the polymers are not good thermal conductors, the heating region is expected to be confined in nanometer thickness resulting in localized heating on the bonding interface. When the microwave

irradiation terminates, CNTs cease generating heat. Thermal energy in the bonding interface rapidly loses to the bulk polymer substrates which are in relatively low temperature and to the surrounding through heat convection. The bonding process is expected to be in a high efficiency with short processing time because of the small thermal mass involved.

The integrity of the global microstructures of the bonded substrates, as described in the case of GNPs, is expected to be maintained without alteration by the heat as a result of localized heating. Coating thickness of CNTs and exposure time would be the important parameters in the investigation.

3.4 Summary

These two proposed bonding methods, microwave bonding using GNPs and CNTs, share the same features of using biocompatible materials for efficient bonding under localized heating. Nevertheless, only one of the methods will be chosen as the main focus in the downstream investigation due to the limitation of resources. The selection criteria would be based on their response towards microwave irradiation as evaluated in the preliminary experiments in chapter five. In the next chapter, preparation works on the materials and equipments for the experiments will be reported.

Chapter 4: Experimental Preparations

This chapter will be divided into four main sections including experimental preparations overview, mould fabrication, plastic biochip fabrication and material and equipment preparations for microwave bonding.

4.1 Overview of experimental preparations

In order to obtain a plastic biochip, a metal mould is necessary to be fabricated beforehand. Since the micropatterns on the plastic biochips are in micrometers, apparently negligible deviation in millimeter-sized biochips would cause a significant dimensional defect in the plastic micro biochips. Hence, sophisticated fabrication techniques were adopted to fabricate a highly precise metal mould for plastic biochip replication. The sophisticated fabrication technologies included photolithography, deep reactive ion etching (DRIE) and electroforming. The metal mould was later used to replicate plastic biochips through both hot embossing and microinjection moulding techniques. Thus, the fabrication part will be divided into two sections, mould fabrication and plastic biochip fabrication.

Auxiliary materials used in the microwave bonding including gold nanoparticles (GNPs) and carbon nanotubes (CNTs) were synthesized and purchased respectively. The synthesis process of GNPs will be introduced with details in the later section. The equipments used in the microwave bonding will also be mentioned.

4.2 Fabrication of moulds

There are mainly two common replication methods for fabricating plastic biochips including hot embossing and microinjection moulding. A metal mould is required to be fabricated beforehand to act as a replication template. In microfluidic devices, microstructures are in miniaturized dimensions and hence precision is especially important during mould fabrication. MEMS technology offers superior and unique precision in silicon fabrication; however, the silicon itself is very fragile and the thickness of silicon for MEMS processing is restricted to 500 μm which is too thin for acting as a mould. Thus, a silicon master mould was first fabricated using photolithography and DRIE, followed by electroforming for transferring the micropatterns from the silicon master mould to the nickel mould, which is much stronger in strength than silicon.

4.2.1 Photolithography and deep reactive ion etching (DRIE)

Silicon master mould fabrication was done in the Nanoelectronic Fabrication Facility (NFF) in the Hong Kong University of Science and Technology (HKUST). A glass mask patterned with the biochip design, which consisted of microchannels and microchambers, using chromium was prepared by Laser Direct Write System with line uniformity $\pm 0.1 \mu\text{m}$. The chromium-patterned glass masks are shown in Figure 4.1.

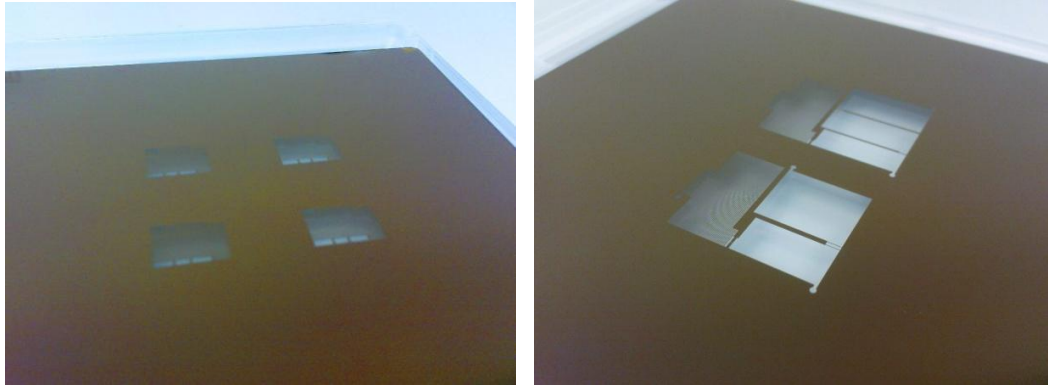


Figure 4.1. Chromium-patterned glass masks for photolithography.

A silicon wafer was first cleaned in sulphuric acid (H_2SO_4) at $120\text{ }^\circ\text{C}$ for 10 min and followed by hydrofluoric acid (HF) at room temperature for 1 min. The wafer was dried by spinning under nitrogen gas before proceeding to photolithography. The schematic diagram for photolithography is presented in Figure 4.2. At the beginning, a protective oxide layer, silicon dioxide, with $1\text{ }\mu\text{m}$ thickness was first grown on the wafer to shield the wafer from being etched in DRIE as shown in (a). The oxide wafer was then coated with photoresist AZ 5214 E as in (b) and prebaked at $110\text{ }^\circ\text{C}$ for 50 sec. The wafer was later exposed to the ultraviolet radiation in low vacuum mode through the chromium-patterned glass mask as shown in (c) and reversal baked at $120\text{ }^\circ\text{C}$ for 2 min. After baking, the wafer was exposed to the ultraviolet radiation in flood exposure mode without the mask as in (d) and the exposed photoresist was later removed, as in (e), by the developer. The oxide region without protective photoresist was etched, as in (f), in an oxide etcher machine and finally a silicon wafer with defined patterns of biochips was ready for silicon etching to define the permanent patterns.

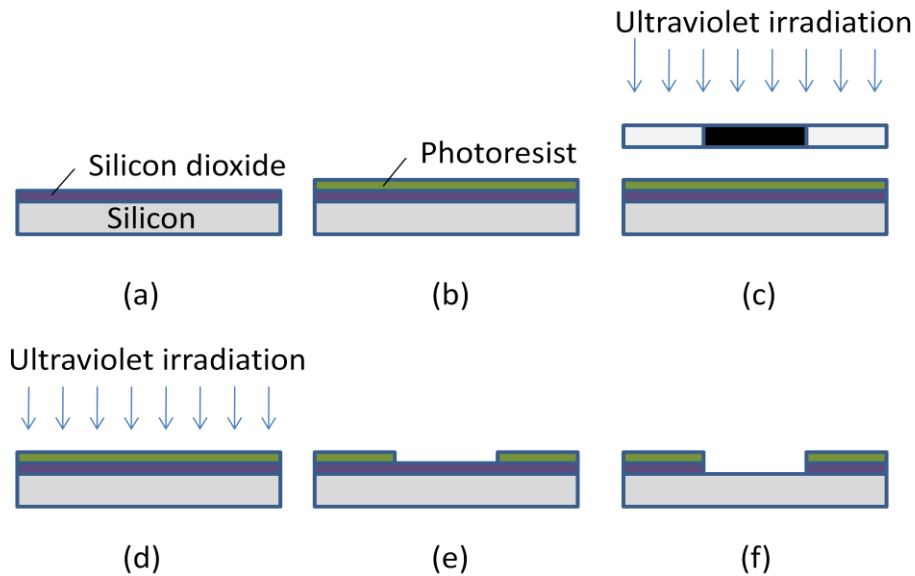


Figure 4.2. Schematic diagrams of photolithography procedures. (a) Oxide growth; (b) photoresist coating; (c) UV exposure through a mask; (d) UV exposure without a mask; (e) photoresist development; (f) oxide etching.

After defining the patterns, the wafer was sent to the DRIE machine. DRIE is a cycling process that alternatively undergoes deposition and etching to produce an anisotropic etch of silicon with high aspect ratio [154]. The working principle of DRIE was shown in Figure 4.3. The patterned substrate was first etched isotropically by chemical etchant to a few microns depth as shown in (a). A chemically inert passivation layer of octafluorocyclobutane (C_4F_8) was then deposited on the wafer as in (b). An anisotropic etching of the passivation layer was followed by bombarding sulfur hexafluoride (SF_6) plasma gas onto the substrate surface. As a result, the walls of the microstructures remained passivated while the bottom parts of them were exposed to the chemical etchant and isotropically etched by a few microns depth as shown in (c). Step (d) repeated the deposition process of the cycle. By repeating the deposition and etching processes, microstructures with smooth walls in high aspect ratios were

fabricated as shown in (e).

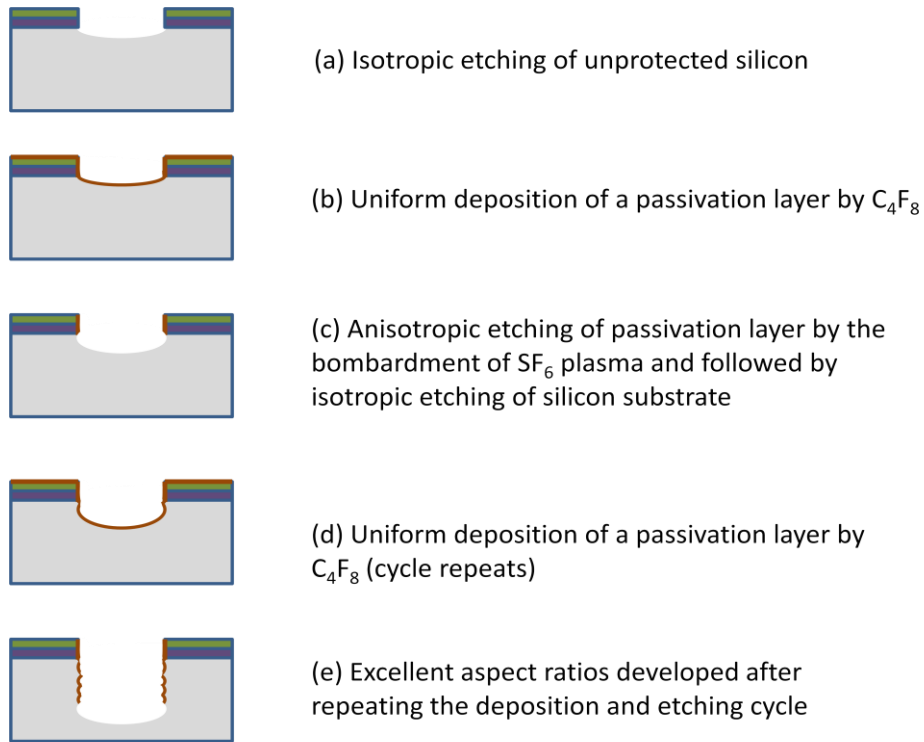


Figure 4.3. Working principle of deep reactive ion etching (DRIE).

After defining the permanent patterns on silicon wafer, the photoresist was stripped away by oxygen plasma and the oxide layer was removed by buffer oxide etch (BOE) solution. The silicon master mould was then dried again by spinning with nitrogen gas and cut into desired shape by diamond saw as shown in Figure 4.4. It presents the finished silicon master mould together with the microscopic images of its microstructures.

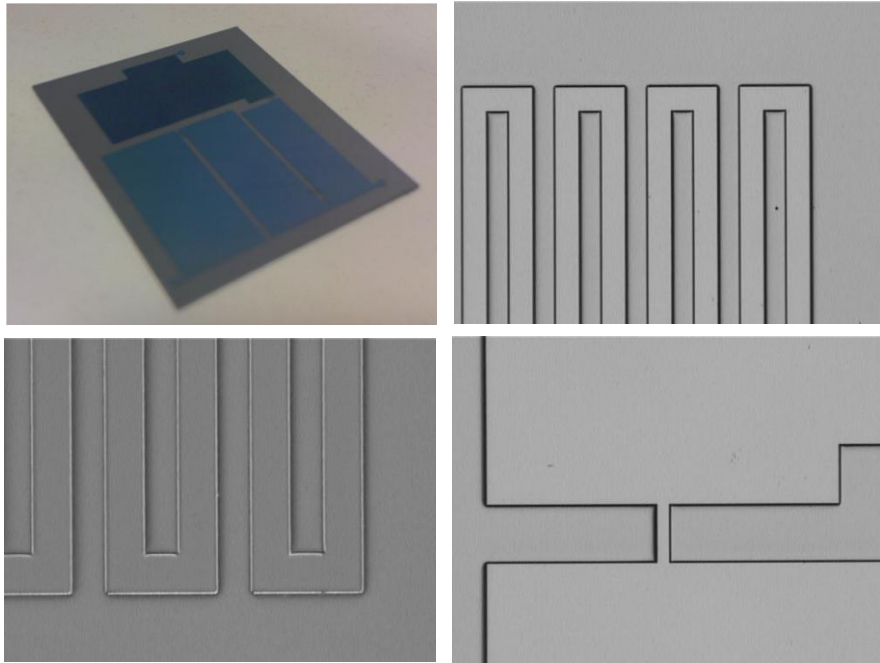


Figure 4.4. Silicon master mould fabricated using DRIE. Left top: silicon master mould; left bottom, right top: microchannels on silicon master mould; right bottom: microvalves on silicon master mould.

Depth of the microchannels was measured using OGP (Optical Gaging Products). The fabricated microchannels gave high uniformity with derivation ± 1 μm which is considered to be in high precision. The microchannels were 45 μm in depth on average. The results are shown in Figure 4.5 and Figure 4.6.

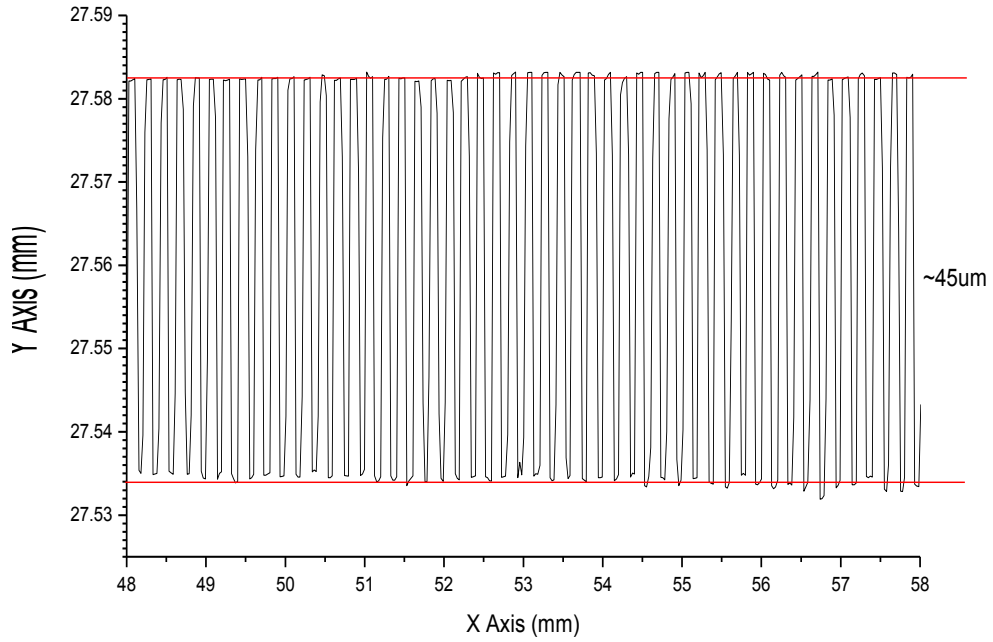


Figure 4.5. Cross-sectional image of a series of microchannels in silicon mould.

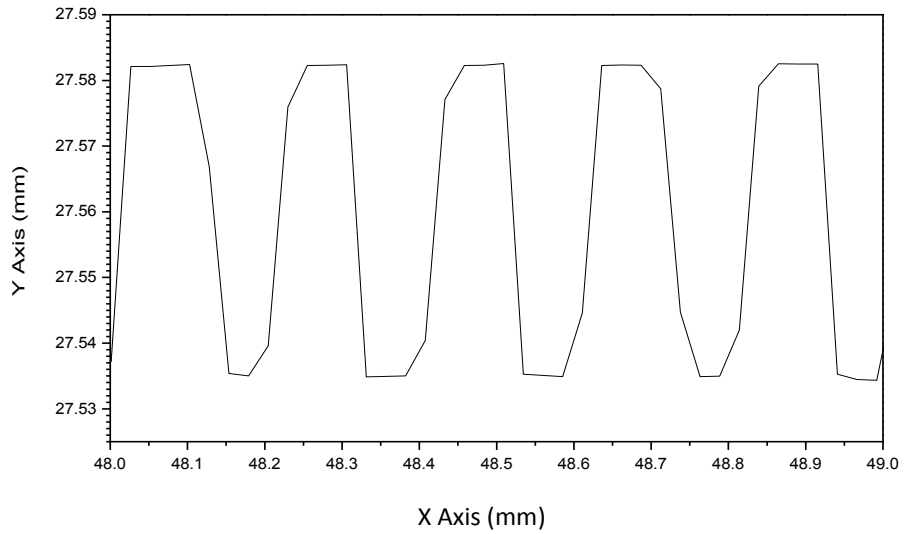


Figure 4.6. Enlarged cross-sectional image of several microchannels in silicon mould.

The fabricated silicon master mould gave an excellent depth and uniformity of the biochip patterns. The finished silicon master mould was then replicated by electroforming to produce a high strength nickel mould.

4.2.2 Electroforming

Electroforming is an electrodeposition process [155] which enables the fabrication of micro and nano scale features from a conductive master mould in high precision. It involves the deposition of metal atoms on conductive master mould through electron transfer in an electrolytic solution. Figure 4.7 shows a simplified working diagram of electroforming and Figure 4.8 shows the electroforming machine used in this experiment.

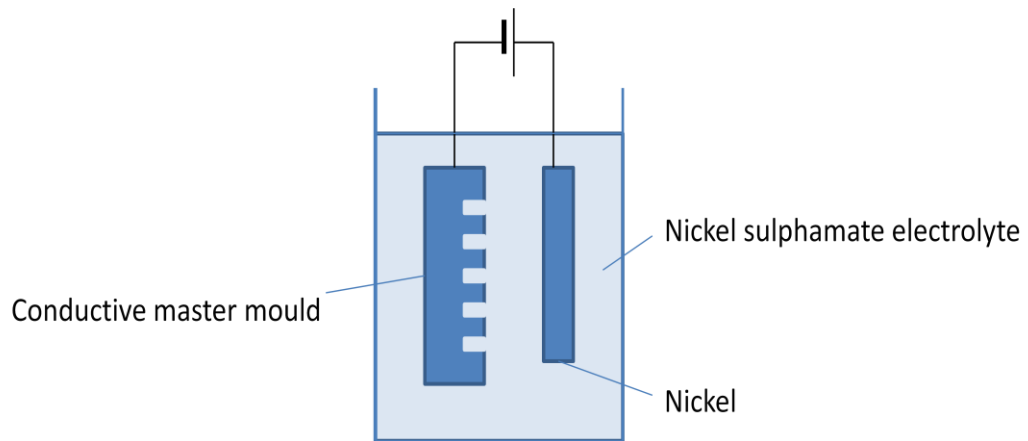


Figure 4.7. Simplified working diagram for electroforming.



Figure 4.8. Electroforming machine.

In the experiment, the fabricated silicon master mould was sputtered with 1000 Å of gold assisted by 500 Å of tungsten–titanium (W/Ti) to form a seed (conductive) layer. Sputtered silicon master mould was then placed at the cathode in a nickel sulfamate electrolyte. Nickel ions were attracted to the cathode and deposited on the silicon master mould in the form of nickel atom because of the electron transfer process: $\text{Ni}^{2+}(\text{aq}) + 2\text{e}^{-} \rightarrow \text{Ni}(\text{s})$. It required at least five days for growing nickel of 2 mm in thickness. The back view of the electroformed nickel mould is shown in Figure 4.9. The silicon master mould on the nickel mould surface was later removed by sodium hydroxide (NaOH) etching at an elevated temperature. The final product, an electroformed nickel mould, is shown in Figure 4.10.

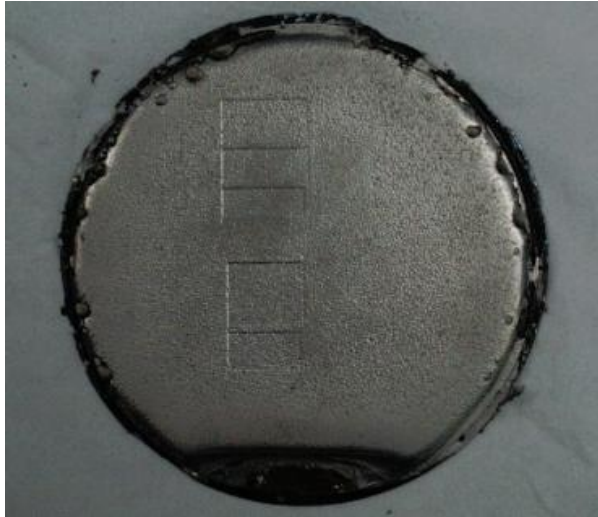


Figure 4.9. Back side view of the nickel mould electroformed from a silicon master mould.

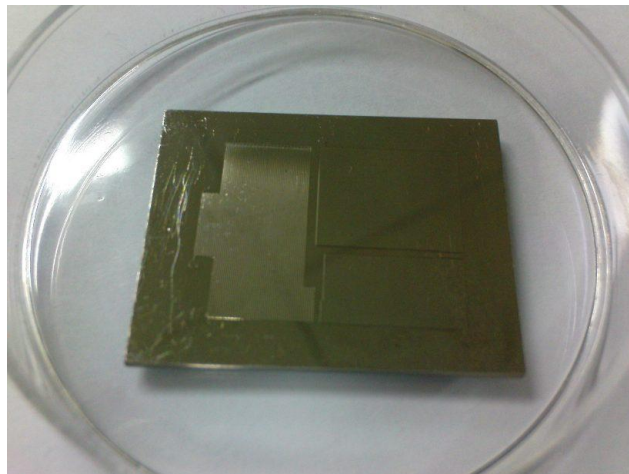


Figure 4.10. Electroformed nickel mould.

The depth of the microchannels in nickel mould was measured by OGP and the cross-sectional image of the microchannels is shown in Figure 4.11.

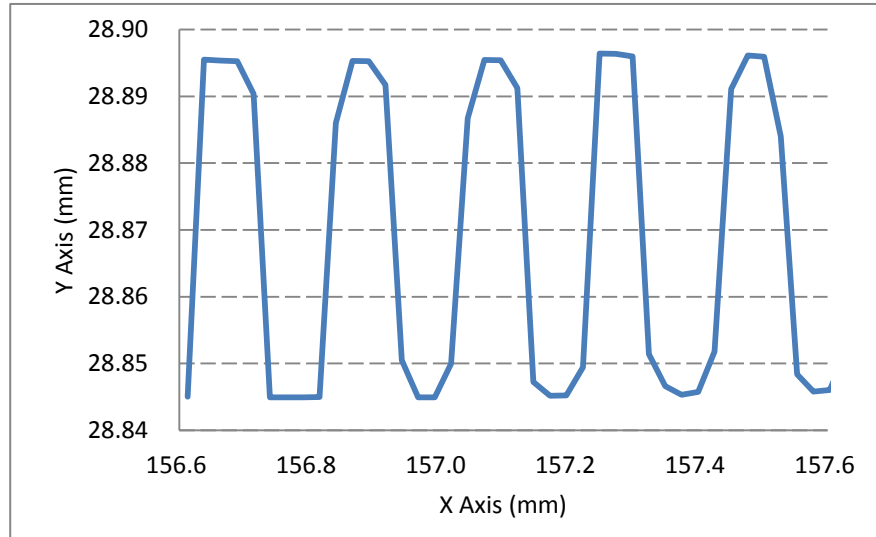


Figure 4.11. Cross-sectional image of microchannels in nickel mould.

The measure depth of the nickel mould was around 50 μm which is different from the previously reported silicon mould (45 μm in depth) because this nickel mould was electroformed from another silicon master mould with 50 μm in depth. The fabricated nickel moulds were later used in both hot embossing and microinjection moulding for plastic biochip fabrication.

4.3 Fabrication of plastic biochips

In the fabrication of plastic biochips, hot embossing is the most common method researchers used in laboratories for research purposes owing to its quick availability, easy accessibility and low setup cost. In the industrial production, however, hot embossing is seldom used because of its low throughput. Instead, injection moulding machine is frequently used for high volume production. In this study, both hot embossing and injection moulding techniques were used to fabricate plastic biochips due to the delayed availability of the microinjection moulding machine. The plastic biochips fabricated using these two methods

showed no observable performance difference on the downstream experiments. The polymer substrate chosen for this study is polycarbonate (PC) which has T_g at 148 °C. Referring to the literature review on polymers in chapter two, PC possesses a relatively high T_g which is suitable for the downstream process like PCR rather than PMMA; and though COC also possesses sufficiently high T_g and high transparency as PC, PC was chosen because of its lower autofluorescence. Temperature, pressure and time of the hot embossing machine and microinjection moulding machine were optimized for the PC biochip fabrication.

4.3.1 Hot embossing

In hot embossing, PC substrate was cut into suitable size and placed between the hotplates together with the nickel mould. The embossing assembly was heated to 170 °C under 3 bars for 10 min. The hotplates and the embossing assembly were allowed to cool down to 80 °C under pressure. The pressure was then removed and then the embossed biochip was separated from the nickel mould. The embossing machine used in this experiment is shown in Figure 4.12 and the embossed plastic biochip is shown in Figure 4.13.



Figure 4.12. Hot embossing machine.

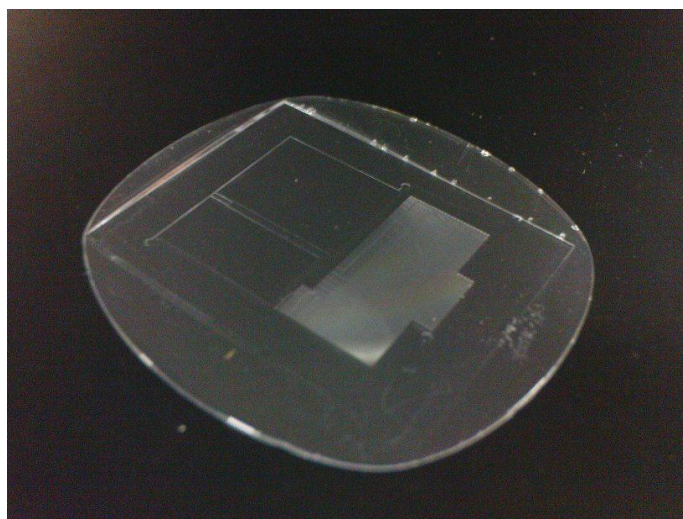


Figure 4.13. Fabricated PC biochip using hot embossing machine.

It can be observed that there is an overflowed edge of the embossed biochip. This edge could be removed easily by cutting or grinding. The embossing quality was examined through the measurement of the embossed microchannel depth by OGP and the result is shown in Figure 4.14.

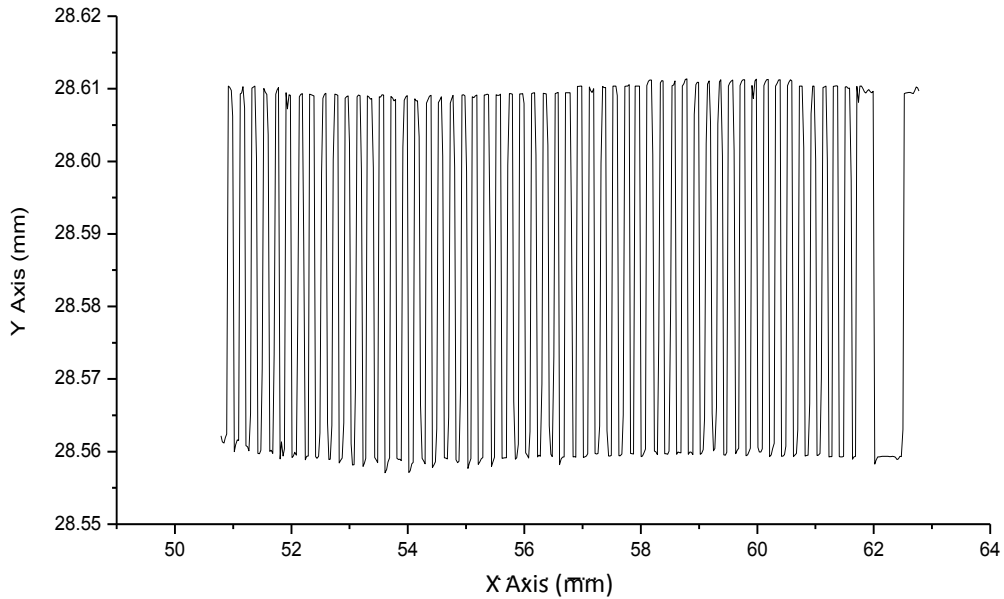


Figure 4.14. Cross-sectional image of a series of microchannels of the embossed PC biochip.

As observed in Figure 4.14, the result from hot embossing is satisfactory as the microchannels on the embossed plastic biochip have fairly the same depth. The average depth of microchannels was around 50 μm .

4.3.2 Microinjection moulding

In microinjection moulding, PC pellets were baked in an oven at 100 $^{\circ}\text{C}$ overnight to remove the moisture inside. After baking, PC pellets were added into a hopper to fill a heated barrel. PC in the barrel was molten and injected through the nozzle to the mould cavity with a speed of 60 mm/s under a clamping force of 2300 kgf. The temperature of the mold and nozzle were 100 $^{\circ}\text{C}$ and 320 $^{\circ}\text{C}$ respectively. The mould cavity was cooled down for 5 s before ejecting the solidified PC biochips. Figure 4.15 shows the microinjection moulding machine used in this experiment. The microinjection moulded PC

biochip is shown in Figure 4.16. Depth of the microchannels of the injection moulded PC biochip was measured using OGP and the results are shown in Figure 4.17.



Figure 4.15. Microinjection moulding machine in Microsystems Technology Center in the Hong Kong Polytechnic University.

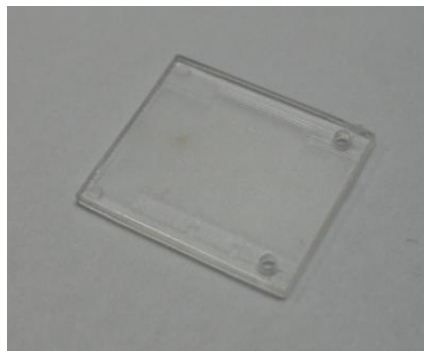


Figure 4.16. Fabricated PC biochip using microinjection moulding machine.

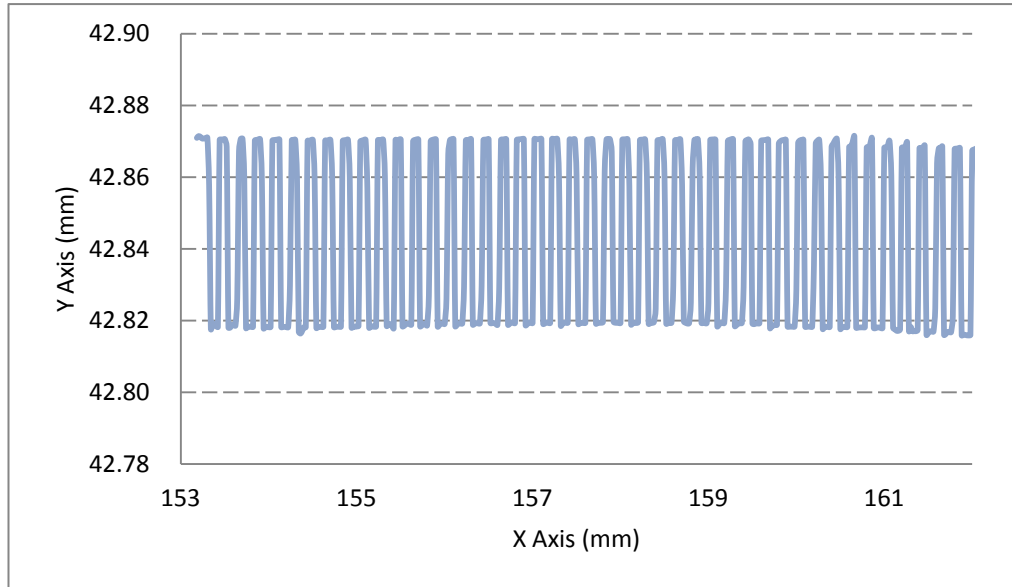


Figure 4.17. Cross-sectional image of a series of microchannels of the microinjection moulded PC biochip.

The average depth of the microchannels was around 50 μm . The microinjection moulded biochip offered a high uniformity on the microchannels. Biochips fabricated by both hot embossing and microinjection moulding were ready to be utilized in the downstream bonding experiments.

4.4 Materials and equipments for microwave bonding

Prior to the bonding experiments, some materials and equipments for microwave bonding are required to be prepared and they will be introduced in this section.

4.4.1 Materials

In microwave bonding, auxiliary materials are the important key to generate heat for triggering bonding occurred in the substrate interface. The two auxiliary materials, GNPs and CNTs, were synthesized and purchased respectively. Synthesis process of GNPs will be first introduced followed by the CNTs.

4.4.1.1 Gold nanoparticles (GNPs)

As reviewed in section 3.2.1, various researches on microfluidic devices using GNPs ranged 10 – 15 nm as detection probes were introduced. Using GNPs within this size range as the auxiliary material thus has unique value where the bonded devices might have future potential development in bioanalytical applications. GNPs within this range should be used as the starting point of the microwave bonding investigation.

GNPs with sizes ranged in 10 – 15 nm were synthesized by citrate reduction [156]. Figure 4.18 and Figure 4.19 show the experimental setup of the process. Equipments included were a condenser, a round-bottom flask, a magnetic stir bar and a heating mantle. All glassware was cleaned with aqua regia (3 parts of hydrochloride (HCl) and 1 part of nitric acid (HNO₃)) thoroughly and followed by washing with deionized water. The cleaned glassware was dried in oven overnight before use. In the synthesis process of GNPs, 20 mL of HAuCl₄ (1 mM) was first boiled and vigorously stirred in the flask under reflux for 30 min. 2 mL of sodium citrate (38.8 mM) was added afterwards and the mixture kept heating and stirring for 10 min before removing the heat. The mixture was then stirred

for further 15 min after heat removal.



Figure 4.18. Experimental setup for GNPs synthesis.

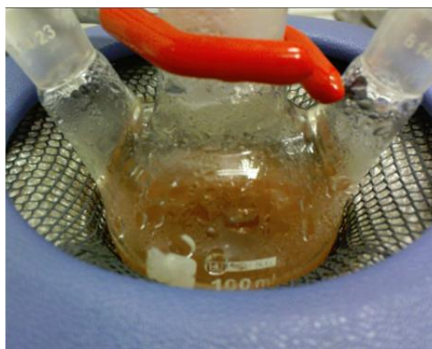


Figure 4.19. Vigorous stirring of solution in the flask.

GNPs synthesized using this standard reagent ratio should have sizes around 13 nm and it was confirmed by its burgundy color as shown in Figure 4.20 because GNPs appear different colors according to their sizes.



Figure 4.20. Burgundy color given by GNPs with 13 nm in diameters.

GNPs were stabilized by the adsorbed negatively charged citrate ion to prevent its natural tendency of self-aggregation. Synthesized GNPs were stored in refrigerator before use.

4.4.1.2 Carbon nanotubes (CNTs)

Since the proposed method of CNTs is developed based on the previously reported work [82], the same type of CNTs would be used in order to achieve the same vigorous response of CNTs upon microwave irradiation in this investigation. Multi-walled carbon nanotubes (MWNTs) with outer diameters ranged 20 – 40 nm and length ranged 5 – 15 μm were purchased from Nanotech Port (NTP). Figure 4.21 shows the SEM image of the purchased CNTs. The thermal conductivity of the purchased CNTs is around $2000 \text{ Wm}^{-1}\text{k}^{-1}$.

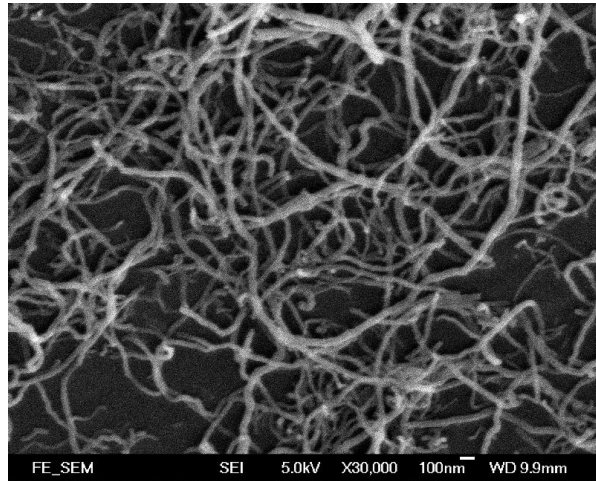


Figure 4.21. SEM image of the purchased CNTs.

The purchased CNTs were in powder form. They were dispersed in propanol with a concentration approximately of 2 mg/mL for use.

4.4.2 Equipments

The equipments for the microwave bonding experiment included a domestic microwave oven, a stack of glasses, a mortar and pestle and a spray gun. Figure 4.22 shows the microwave oven and the stack of glasses while Figure 4.23 shows the mortar and pestle and the spray gun.



Figure 4.22. Equipments for microwave bonding. Left: a domestic microwave oven; right: a stack of glasses.



Figure 4.23. Equipments for sample preparation. Left: a mortar and pestle; right: a spray gun.

The domestic microwave oven was used to generate microwave irradiation for microwave bonding. The glasses were used to exert and equalize pressure on the bonding substrates during microwave irradiation. The mortar and pestle and the spray gun were used for grinding CNTs and spraying CNTs on the PC substrates respectively.

The domestic microwave oven has three power level options including high, medium and low. Experiments have been carried out to estimate the power outputs of the three power levels. In the experiment, a glass with 40 mL water was sent to microwave oven and exposed to microwave irradiation under different power levels for some seconds. The temperature of water was measured before (T_0) and after (T_1 , T_2 , T_3) microwave irradiation using thermometer. Each testing condition was repeated by three times. An average temperature (T_{ave}) was then calculated from T_1 , T_2 and T_3 under each testing condition. The experimental results are presented in Table 2.

Table 2. Measurement of water temperature before and after microwave irradiation under different power levels.

Power level	High	Medium		Low
Time (sec)	30	30	60	60
T ₀ (°C)	23	23	23	23
T ₁ (°C)	78	52	80	36
T ₂ (°C)	76	54	81	38
T ₃ (°C)	80	50	85	37
T _{ave} (°C)	78	52	82	37

The power outputs of the three power levels were estimated from the amount of energy that water absorbed. Herein, assumption is made that the microwave power output is all absorbed by water and the gain in latent heat is negligible.

The energy absorbed by water can be calculated through the equation:

$$\text{Energy absorbed by the water} = E = mC_p \Delta T$$

where m is the mass of water, C_p is the specific heat capacity of water and ΔT is the change of temperature.

Assume energy absorbed by water = energy output by microwave oven,

$$\text{Power output of microwave oven} = P = \frac{E}{t}$$

where t is the time of exposure.

Below are the data used to calculate energy gained by water where the data of thermal properties of water are acquired from the online resources [157]:

$$\text{Volume of water} = V = 40 \text{ mL} = 40 \text{ cm}^3$$

$$\text{Density of water} = \rho = 1,000 \text{ kg/m}^3 = 1 \text{ g/cm}^3$$

$$\text{Mass of water} = m = \rho V = 40 \text{ g}$$

$$\text{Specific heat capacity of water} = C_p = 4.187 \text{ kJ/kg K} = 4.187 \text{ J/g K}$$

$$\text{Change of temperature} = \Delta T = (T_{\text{ave}} - T_o) \text{ } ^\circ\text{C}$$

Table 3. Estimated power outputs of the three power level options.

Power level	High	Medium		Low
Time (sec)	30	30	60	60
T_o (°C)	23	23	23	23
T_{ave} (°C)	78	52	82	37
ΔT (°C)	55	29	59	14
Energy (J)	9211	4857	9881	2345
Power (W)	307	162	165	39

The calculated power outputs of the three power levels were shown in Table 3. Shorter exposure duration, 30 sec, was used for high power level so as to avoid splashing of water resulted from overheating. Longer exposure duration, 60 sec, was used for low power level so as to ensure the heating reaching a measurable level that could increase the accuracy of measurement. Both 30 sec and 60 sec were used in medium power level, the results gained from these two conditions perfectly matched each other with only 3 W in difference. It implies the microwave irradiation is roughly steady within one power level regardless of

the duration of exposure. From the experiment, it was found that the microwave oven is able to operate at three power levels which are 307 W, 163 W and 39 W corresponding to high, medium and low respectively.

The experiment aimed to provide a rough estimation on the power output of the microwave oven. More stringent method on microwave power estimation should be referred to ISO/TR 10305-2:2003 or on temperature estimation inside microwave oven could be referred to the publication titled “Fabrication and characteristics of porous NiTi shape memory alloy synthesized by microwave sintering” by Tang et al. [158].

4.5 Summary

PC biochips were successfully fabricated from the nickel mould using hot embossing and microinjection moulding. Auxiliary materials for microwave bonding such as GNPs and CNTs were synthesized and purchased respectively. The microwave bonding equipments were prepared and the performance of the domestic microwave oven was reviewed. The microwave oven is able to offer steady power output under three power level options including 307 W, 163 W and 39 W. In the next chapter, coating process of the two auxiliary materials and preliminary tests on the microwave bonding will be reported.

Chapter 5: Responses of Gold Nanoparticles and Carbon Nanotubes towards Microwave Irradiation

In this chapter, coating methods of the auxiliary materials onto PC substrates will be investigated. Preliminary experiments on estimating the bonding efficiency of microwave bonding assisted by GNPs and CNTs will also be demonstrated and discussed.

5.1 Gold nanoparticles (GNPs)

GNPs will first be studied for its coating method on PC substrates, followed by a preliminary experiment on estimating its bonding efficiency under microwave irradiation.

5.1.1 Deposition of GNPs

Two coating methods, droplet-based coating and dip-coating, of GNPs will be demonstrated in this section. The aim of this part is to develop a coating method which could achieve a uniform coating of GNPs on PC substrates. The coating method with better performance would be employed in the downstream experiment.

5.1.1.1 Droplet-based coating of GNPs

A simple droplet-based coating method has been conducted. The idea behind this method is to form a uniform GNPs coating on the PC substrate surface by rapid evaporation of the volatile solution. If the evaporation speed is fast enough that GNPs lose the medium to form aggregation, GNPs would be able to be dispersedly coated on the PC substrate.

GNPs used here were previously synthesized and stored in aqueous solution. In order to transfer GNPs into a volatile medium, propanol, Na^+ solution was added to the GNPs solution for deionization and the solution was spinning down 3 times with a speed of 5.8 rpm for 60 min to remove the supernatant. Propanol was later added to resuspend the GNPs. After transferring the medium, several droplets of GNPs solution were added onto the PC substrate surfaces. The substrate was left inside the fume hood for drying. An image of the GNP-coated substrate was captured and the picture is shown in Figure 5.1.

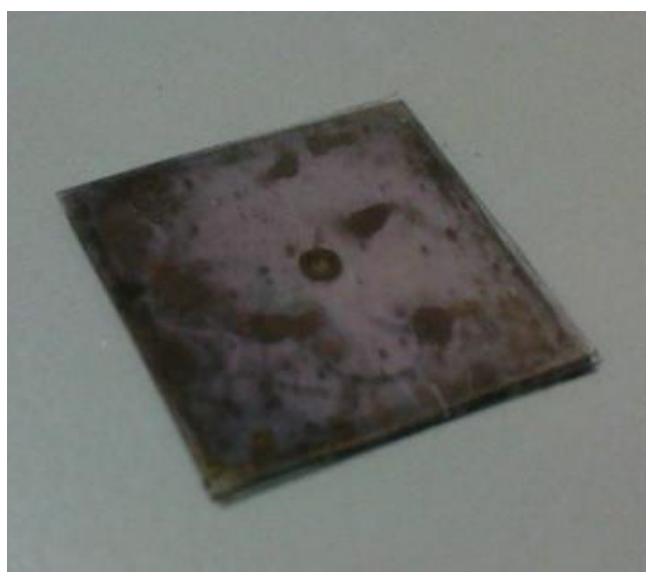


Figure 5.1. Aggregated GNPs upon evaporation of propanol.

In the image, it can be observed that GNPs were aggregated on the substrate surface. Apart from the aggregation nature of GNPs, the main reason accounting for it is the incomplete medium transfer. Though the major portion of solution medium of GNPs has been changed into propanol, there was still small portion of aqueous solution left in GNPs/propanol solution. This small portion of aqueous solution formed tiny droplets, where the GNPs aggregated, upon the evaporation of propanol. As a uniform GNP coating is unable to be achieved by the rapid evaporation of propanol, an alternative approach, dip-coating, would be tested.

5.1.1.2 Dip-coating of GNPs

Another method, dip-coating, was used for depositing GNPs on PC substrates. Before coating, PC substrate was cleaned with ethanol under sonication for 5 min and allowed to dry in fume hood. The substrate was then dipped into GNPs solution (13 nm, 17 nM) and incubated for 10 min. After the incubation, residue solution left on the sample was removed by compressed air. The dip-coated sample appeared pale pink which was expected to be the color of the adsorbed GNPs. The dip-coated sample was delivered to the SEM for further verification and investigation in the coating density. SEM result is shown in Figure 5.2.

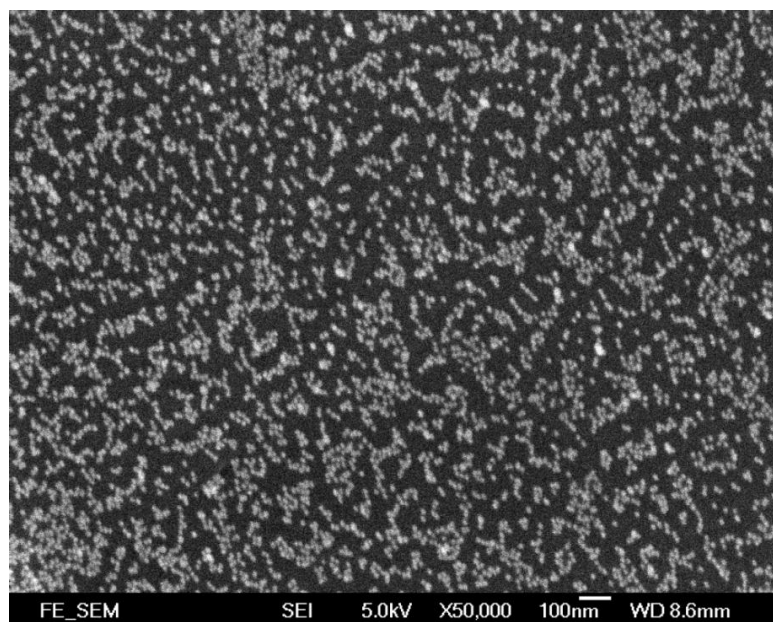


Figure 5.2. SEM image of GNP-coated PC substrate using dip-coating method.

It can be observed that enormous numbers of GNPs were adsorbed on the samples. GNPs were obviously not monodispersed and appeared slight aggregation; however, this result was encouraging as it provided the evidence that the natural interaction between GNPs and PC surface is sufficient to achieve coating of GNPs. Further investigation is required to substantiate if this amount of dispersion density is adequate to generate heat for bonding.

5.1.2 Response towards microwave irradiation

Since there are so far no literature reports on the microwave absorption properties of GNPs, an experiment has been set up to verify if GNPs possess the ability of absorbing microwave energy and converting it into heat; and to estimate if the coating density of the proposed dip-coating method is sufficient for triggering bonding in polymers. This experiment is important to assess the feasibility for using GNPs as the auxiliary material to bond plastic biochips.

In this experiment, three PC substrates with 1.5 mm in thickness were subject to three different conditions. The first substrate was a positive control, which was dip-coated in GNPs solution for 10 min. The second substrate was a negative control, which was dip-coated with GNPs for 10 min and washed with ethanol under sonication for 3 min. The third substrate was the sample, which was dip-coated in GNPs solution for 10 min and subjected to microwave exposure for 5 min under 307 W. The substrate was then washed in ethanol for 3 min under sonication. All PC substrates were cleaned with ethanol before the experiment and dried by compressed air after the experiment. A beaker with 40 mL water was loaded into the microwave oven to prevent magnetron damage during microwave exposure. The coating densities of GNPs on the three substrates were then investigated through SEM. Figure 5.3 to Figure 5.5 show the results obtained from SEM.

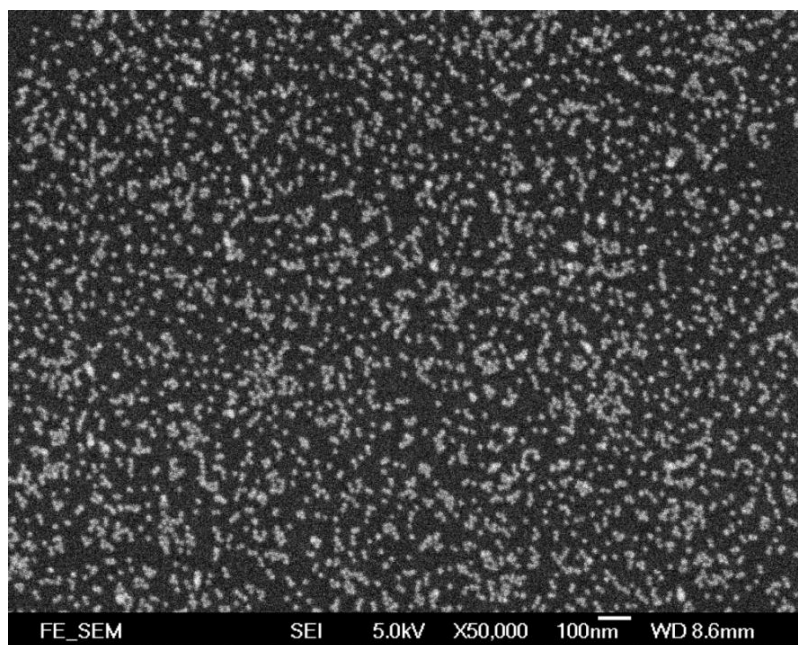


Figure 5.3. Positive control: dip-coating.

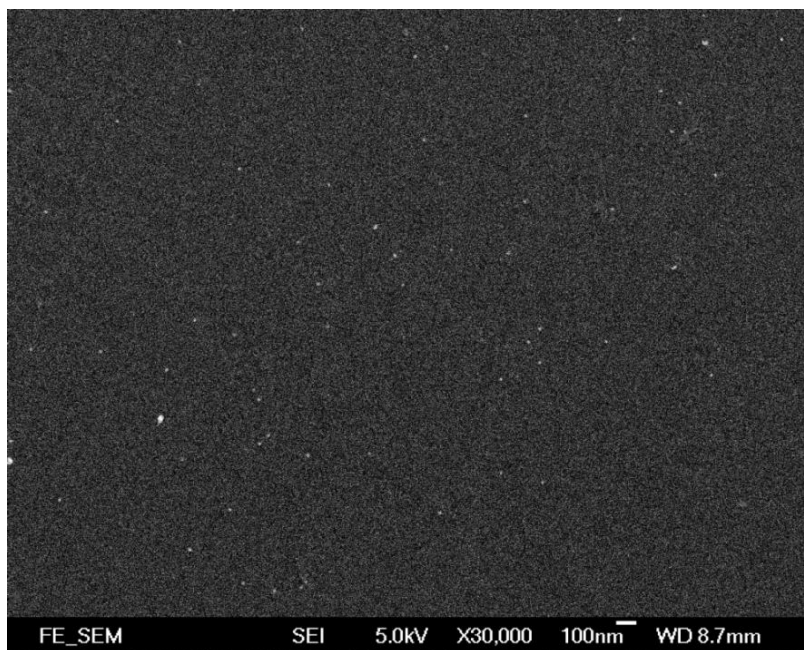


Figure 5.4. Negative control: dip-coating and washing.

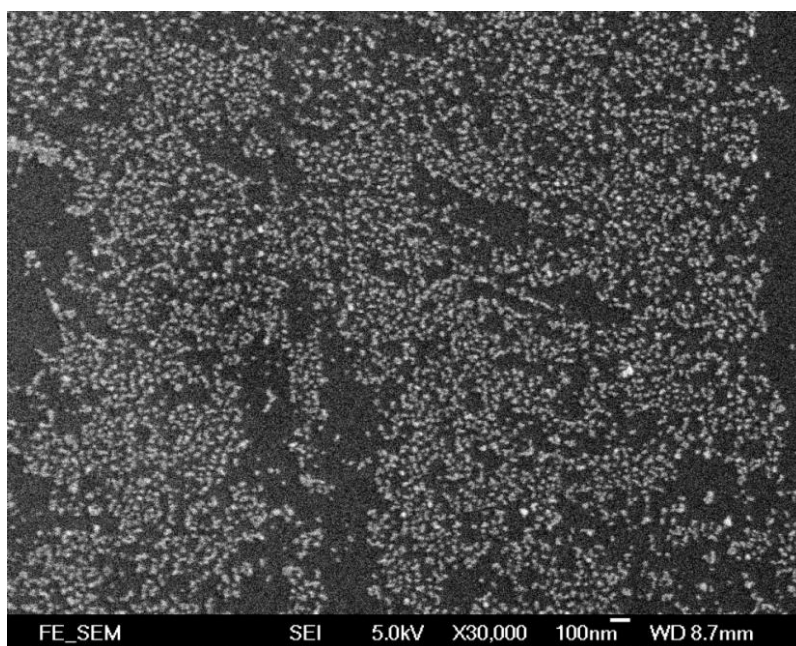


Figure 5.5. Sample: dip-coating, microwave irradiation and washing.

Enormous amount of GNPs was observed in the positive control as previously reported. In negative control, Figure 5.4, there was almost no GNPs existed which suggests that the washing step using ethanol and sonication could

effectively remove the adsorbed GNPs from the substrate surface. In Figure 5.5, GNPs were still observed even after the washing step. This result implies that GNPs were not simply adsorbed on the substrate surface and therefore not be able to be removed by washing with ethanol under sonication. These information is sufficient to support the fact that microwave irradiation has exerted certain effect on the GNPs to alter the interaction between the GNPs and the substrate surface. This effect was probably resulted in the form of an energy transfer from the microwave irradiation into GNPs. The existence of that kind of energy in GNPs, which was at least partially in the form of heat, has raised the temperature surrounding GNPs and strengthened the interaction between GNPs and polymer chains on the substrate surface. This explained why GNPs on substrate surface were not able to be removed after microwave irradiation. In other words, GNPs possess the ability to convert microwave energy into heat energy that is sufficient to soften the polymer surface or to increase the polymer chain interactions towards the GNPs.

Another experiment has been carried out to estimate the effectiveness of GNP-assisted microwave bonding. In the experiment, two dip-coated PC plates were put inside a homemade plastic holder made of PC as shown in Figure 5.6. The clamping pressure of the holder was not determined since a consistent pressure in this stage is not required.

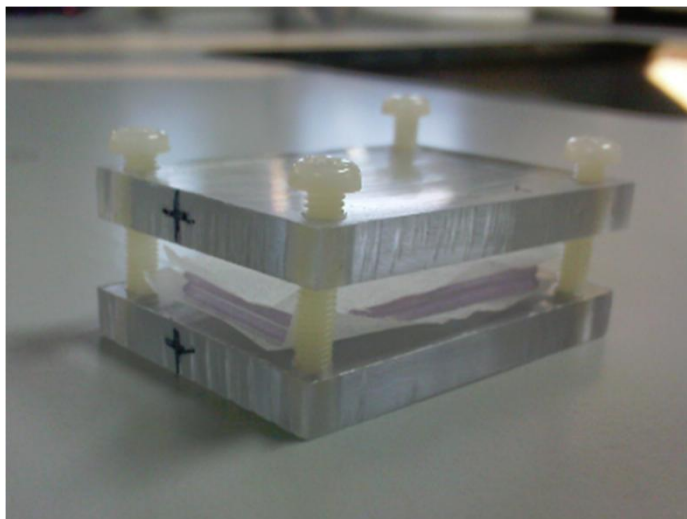


Figure 5.6. Homemade plastic holder made of PC.

The bonding assembly was exposed to microwave irradiation for 5 min under 307 W; however, there was neither sign of heating nor bonding of the assembly. It may be accounted by the fact that GNPs are not able to generate enough heat energy for bonding polymers or the coating density using dip-coating method is not high enough to generate enough heat energy.

To conclude, though GNPs possess the ability of absorbing microwave energy to soften the polymer surface and to increase the polymer chain interactions towards GNPs, it is not able to produce sufficient heat energy to melt the polymer surface or to increase the mobilities of the surface polymer chains to intercalate with the polymer chains in neighboring surface. The possible reasons for the failure in bonding may be due to the limited microwave absorption abilities of GNPs or the insufficient GNP-coating density. Alternative heat source such as IR may also be used to improve the heating effect of GNPs since GNPs can absorb IR energy effectively in a specific IR region.

5.2 Carbon nanotubes (CNTs)

In this section, coating methods of CNTs towards PC substrates will be studied, followed by a preliminary experiment on estimating its bonding efficiency under microwave irradiation.

5.2.1 Deposition of CNTs

Two coating methods, droplet-based coating and spray-coating, will be studied for their coating qualities on PC substrates. The aim of this part is to develop a suitable coating method for CNTs to provide a uniform coating on PC substrates.

5.2.1.1 Droplet-based coating of CNTs

A simple droplet-based coating method was conducted in CNTs as in GNPs. The same idea of this method also applies to CNTs which is to form a uniform CNT coating on the PC substrate through the rapid evaporation of the volatile medium, propanol. If the evaporation of the solution medium is fast enough that CNTs has not yet diffused and aggregated, a uniform layer of CNTs would be retained on the substrate surface.

In this experiment, CNTs were prepared and stored in propanol medium with a concentration of 2 mg/mL. Several droplets of CNTs solution were added onto the PC substrate surface. After a few minutes, the image of the CNT-coated substrate was captured and the picture is shown in Figure 5.7.

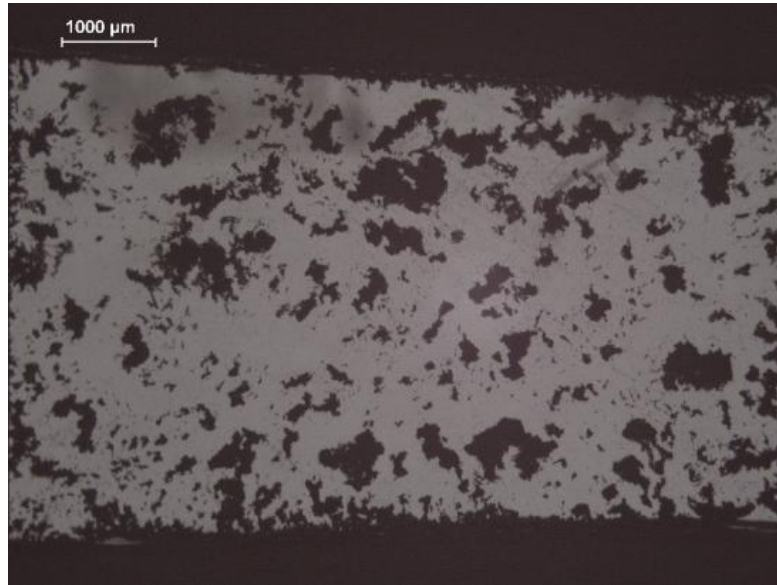


Figure 5.7. Coating of CNTs upon evaporation of propanol.

During the experiment, CNTs started forming tiny clusters before the evaporation of propanol completed. It is obvious that the diffusion rate of CNTs was much faster than the evaporation rate of the solution medium and hence CNT aggregation was observed on the substrate surfaces. From this result, uniform coating of CNTs is unable to be achieved by the rapid evaporation of propanol in droplet form. Alternative approach, spray-coating, would be investigated in the next section in order to achieve a uniform coating of CNTs.

5.2.1.2 Spray-coating of CNTs

From the previous result of droplet-based coating, CNTs diffused and aggregated before evaporation of propanol completed. One of the possible improvements to this issue is to minimize the size of the droplets, so that the evaporation rate of the solution medium could be increased. Spraying was proposed to be a desired method to achieve this aim.

CNTs/propanol solution with a concentration of 2 mg/mL was sprayed on the PC substrate using a spray gun. It was found that, however, the result was not satisfactory as the spraying process was not smooth. The spray nozzle was blocked by the CNT clusters frequently.

In order to eliminate the CNT blockage, CNTs were ground in the propanol solution using mortar and pestle before spraying. The grinding process was around 25 min. The large CNT clusters were broken into smaller pieces during this process. Grinding herein is a critical step that can eliminate the blockage of CNTs in the spray nozzle so as to achieve spraying in a higher uniformity. Figure 5.8 shows mortar and pestle used in this experiment.



Figure 5.8. Mortar and pestle for grinding CNTs.

The completeness of grinding could be indicated by the segregated CNTs of the ground solution. CNTs without grinding remained suspended in the solution for a long time while CNTs with grinding segregated to the bottom after a few minutes. The difference is showed in Figure 5.9.

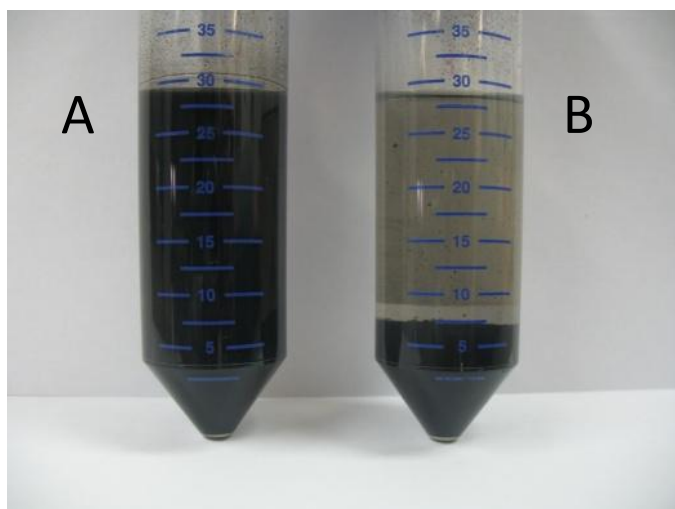


Figure 5.9. CNTs in propanol: (A) before grinding; (B) after grinding.

Ground CNTs solution was loaded to the container on spray gun. The pressure and volume of spraying were optimized. During spraying, there should be a recovery time of 1 min between each spray so as to ensure the previous spray was dried that no unwanted flow of CNTs on the substrate surface; and the angle of spraying should be perpendicular to the sprayed surface. Figure 5.10 is showing the microscopic images of a well-sprayed sample, which followed the proposed directions, and a poor-sprayed sample. The well-sprayed sample offered appealingly uniform coating of CNTs.

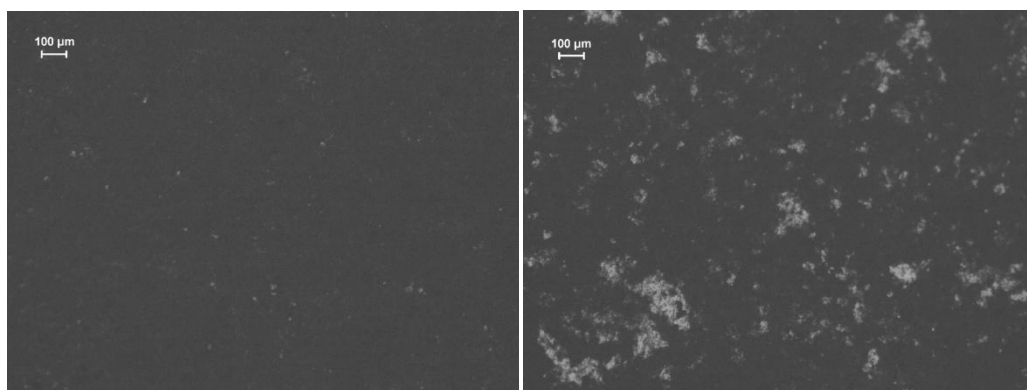


Figure 5.10. Microscopic images of well-sprayed (left) and poor-sprayed (right) of CNTs.

The thicknesses of spray-coated samples were examined using OGP. Figure 5.11 shows the setup of the thickness measurement of CNTs on the spray-coated samples under OGP and Figure 5.12 shows a spray-coated sample.



Figure 5.11. Setup of the thickness measurement of CNTs on the spray-coated PC plates.

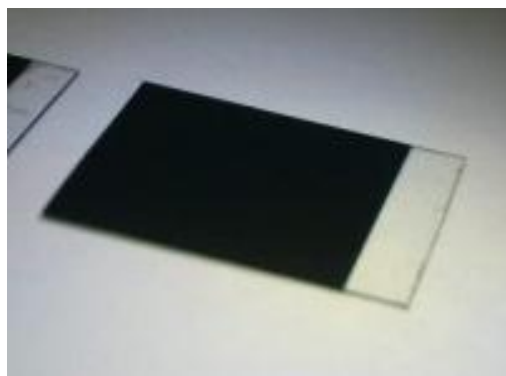


Figure 5.12. CNT-coated PC plate using spray coating.

It was found that the spray-coating result was satisfactory that CNT thickness was controlled within $\pm 5 \mu\text{m}$ ($n = 29$). The thickness table of CNTs of

the spray-coated samples can be found in Appendix A.

5.2.2 Response towards microwave irradiation

After coating the CNTs, a preliminary experiment was conducted to estimate its responsive extent towards microwave irradiation so as to predict its feasibility on bonding polymers.

In the experiment, a PC plate with 0.3 mm in thickness was spray-coated with CNTs and overlapped with another bare PC plate. The assembly was then placed inside the homemade plastic holder made of PC, which was the same one used in GNP experiment. The whole assembly was exposed to microwave irradiation for 30 sec under 307 W. A beaker with 40 mL water was loaded into the microwave oven to prevent magnetron damage. The assembly then removed from the microwave oven for cooling after irradiation.

It was surprising to find that the two PC plates and the plastic holder were all bonded together. The bonded assembly was then pried using a screwdriver. The CNT-coated PC plate was successfully separated from the bare PC plate; however, the back side of the CNT-coated PC plate was still strongly bonded to the PC holder as shown in Figure 5.13 (a). Vigorous force applied on separating the bonded parts led to tear of the CNT-coated PC plate as shown in Figure 5.13 (b).

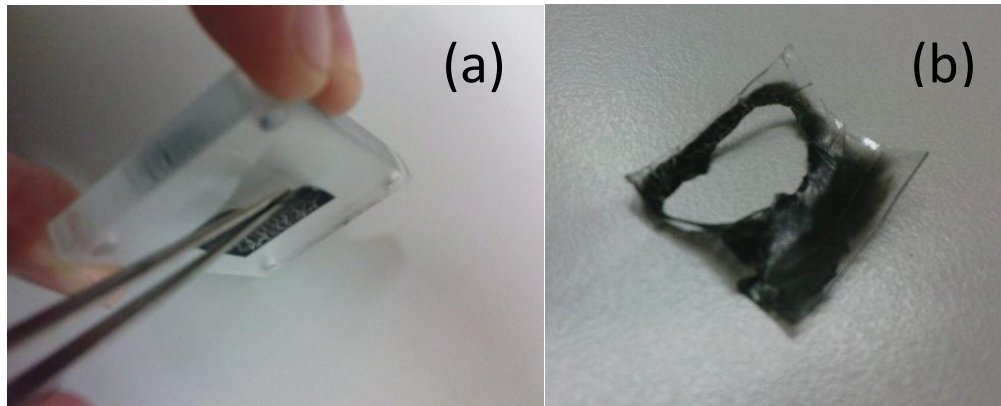


Figure 5.13. Bonded assembly after microwave irradiation for 30 sec under 307 W. (a) Bonded CNT-coated PC and plastic holder; (b) tore part of the assembly.

The tore part implied the fact that bond strength, resulting from microwave irradiation, formed in the bare interface was much stronger than that formed in the CNT interface. This difference could be accounted by the bonding mechanism of polymers. Bonding between polymers requires the intercalation formed between polymer chains from two surfaces. In the bare interface, polymer chains from two surfaces could intercalate with each other easily at an elevated temperature as they were in intimate contact. On the other hand, in the CNT interface, heat energy emitted from CNTs caused surrounding polymer melted and flew; however, CNTs itself acted as obstacles that hindered polymer chains on two surfaces from contacting. Even though there were portions of polymers successfully flew through CNTs and fused with the polymers in another surface, there was still large portion of polymers hedged behind the CNT layer. This resulted in weaker bond strength in the CNT interface compared to the bare interface.

To conclude, owing to the strong bond strength on the interfaces, it is no doubt that CNTs possess strong microwave absorption abilities and are capable

of generating substantial amount of heat energy to trigger bonding occurred. Although the experimental outcome was different from the expectation, it provided an important insight on modifying and improving the current bonding design.

5.3 Summary

GNPs and CNTs have both demonstrated for their microwave absorption abilities towards microwave irradiation. The performance of GNPs in bonding plastic plates, however, was disappointing though it may be due to the insufficient coating density of GNPs or the inappropriate heat source. In any case, GNPs has no doubt to be a potentially applicable auxiliary material in bonding plastic biochips; however, owing to the notable difference in bonding performance between GNPs and CNTs, microwave bonding assisted by GNPs would be temporarily aborted, while microwave bonding assisted by CNTs would become the main focus of investigation starting from the next chapter.

Chapter 6: Carbon Nanotube–Microwave-Assisted Thermal Bonding

This chapter will focus on the investigation of microwave-assisted thermal bonding technology for sealing plastic biochips using CNTs. The chapter will start with a redevelopment of the bonding model for CNTs and an illustration of the heating mechanism of the newly developed method, CNT–microwave-assisted thermal bonding. It will then proceed to the experimental sections including the experimental setup, the investigation on the effective thickness of CNTs and the performance of different CNT thicknesses under microwave irradiation. Evaluation tests such as leakage test, cross-sectional image investigation and tensile test of the bonded biochips will be conducted and examined. This chapter will be ended with a discussion and analysis on the performance of CNT–microwave-assisted thermal bonding with reference to conventional thermal bonding.

6.1 Redevelopment of microwave bonding model for carbon nanotubes (CNTs) – CNT–microwave-assisted thermal bonding

In the previous chapter, it was surprising to find that the microwave bonding assisted by CNTs offered strong bonding on the bare interface rather than the CNT interface. This finding triggered a new idea on the bonding model using CNTs called CNT–microwave-assisted thermal bonding. Figure 6.1 shows the new proposed model.

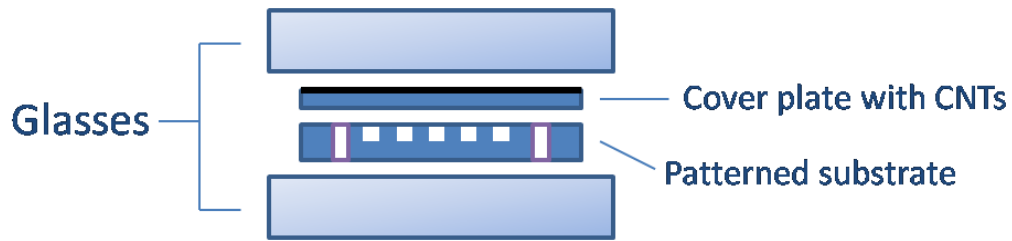


Figure 6.1. Redeveloped bonding model for CNT–microwave-assisted thermal bonding.

In this new model, CNTs are distributed on the exterior surface of the cover plate and the interior surface, which is free of CNTs, is overlapped with the patterned substrate. The assembly is placed between glasses for microwave irradiation. The functions of glasses are to provide a compressive force and a flat platform for CNT–microwave-assisted thermal bonding to occur. According to the result from previous experiment, strong bonding will be formed in the bare interface, which is the interface between the cover plate and the patterned substrate herein, rather than in the CNT interface. This bonding design improves the efficiency of energy utilization that the polymer substrates can be bonded to higher extent upon the same exposure time; or the polymer substrate can be bonded to the same extent with shorter exposure time, compared to the previous design.

Another important improvement of this new design is the material homogeneity that the bonded assembly provided. The CNT heat source is located on the exterior surface to provide thermal energy to the bonding interface while the bonding interface is free of CNTs. The irradiated CNTs can either be removed or left on the exterior surface depending on the requirements of downstream applications. This new design possesses improvements on bonding efficiency and

material homogeneity which are the prerequisite features of industrial scale bonding of plastic biochips. In the following paragraphs, heating mechanism of this new model design will be illustrated.

In the CNT–microwave-assisted thermal bonding model, heat is generated by the CNT layer upon the exposure of microwave irradiation. Heat energy then transfers through the cover plate to reach the bonding interface mainly through thermal conduction. Heat energy increases the mobilities of polymer chains in the bonding interface and further facilitates the intercalation of polymer chains with the neighboring polymer surfaces. Once the microwave irradiation terminates, CNTs cease generating heat and the substrates cool down through transferring heat to the neighboring glasses and patterned substrate which should be in a lower temperature by heat conduction, and losing heat to the surroundings by heat convection. Since the thermal mass involved is relatively small, the cooling process is expected to be completed within minutes.

Before discussing the heat transfer equation, assumption has to be made on the heat source. From the literature and experimental information, it is known that the microwave–conversion process by CNTs is vigorous and the CNTs possess an extremely high thermal conductivity ($2000 \text{ Wm}^{-1}\text{k}^{-1}$). Heat generation and transfer in the CNT layer are thus expected to be extraordinarily quick that the temperature of CNT layer reaches an equilibrium temperature almost simultaneously with the microwave exposure. Under this situation, an equilibrium temperature is reached that the CNT layer is treated as a constant temperature heat source in the system. The heat transfer equation is therefore simplified into one dimensional heat flow as follows.

In the case of one dimensional heat flow in steady state (temperature is not changing with time), heat transfer rate inside the cover plate follows Fourier's law,

$$q_x = -kA \frac{\partial T}{\partial x}$$

where q_x is the heat transfer rate inside the cover plate, k is the thermal conductivity of the polymer (k is assumed to be constant as thermal conductivity in polymer is fairly dependent on temperature [159]), A is the cross-sectional area of the cover plate and $\frac{\partial T}{\partial x}$ is the temperature gradient across the cover plate [160].

Since the system involves CNTs as the heat source, the governing equation becomes more complicated. By considering infinitely small thickness dx , CNTs as an external heat source is considered to be embedded in the defined region [160] as shown in Figure 6.2.

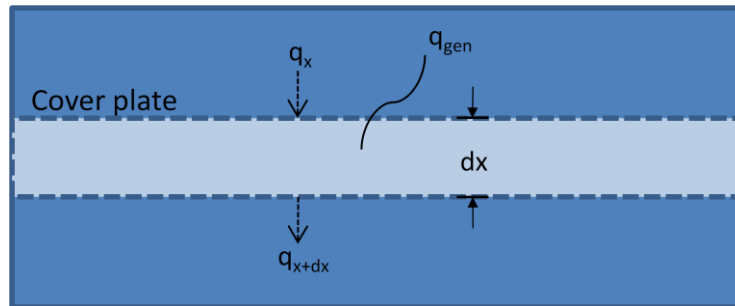


Figure 6.2. Elemental diagram for heat conduction analysis inside the cover plate.

In the defined system with thickness dx , the energy balance is,

$$\begin{aligned} \text{Energy in } (q_x) + \text{energy generated } (q_{gen}) \\ = \text{change in internal energy of polymer} + \text{energy out } (q_{x+dx}) \end{aligned}$$

The energies are given by,

$$\text{Energy in} = q_x = -kA \frac{\partial T}{\partial x}$$

$$\text{Energy generated within the defined system} = q_{gen} = \dot{q}Adx$$

$$\text{Change in internal energy of polymer} = \rho cA \frac{\partial T}{\partial \tau} dx$$

$$\text{Energy out} = q_{x+dx} = -kA \left. \frac{\partial T}{\partial x} \right|_{x+dx} = -A \left[k \frac{\partial T}{\partial x} + \frac{\partial}{\partial x} \left(k \frac{\partial T}{\partial x} \right) dx \right]$$

where \dot{q} = energy generated per unit volume of the cover plate, c = specific heat of polymer and ρ = density of polymer.

The governing equation of the thermal conduction across the cover plate is

$$-kA \frac{\partial T}{\partial x} + \dot{q}Adx = \rho cA \frac{\partial T}{\partial \tau} dx - A \left[k \frac{\partial T}{\partial x} + \frac{\partial}{\partial x} \left(k \frac{\partial T}{\partial x} \right) dx \right]$$

or can be simplified to

$$\frac{\partial}{\partial x} \left(k \frac{\partial T}{\partial x} \right) + \dot{q} = \rho c \frac{\partial T}{\partial \tau}$$

There are two estimations on the CNT–microwave-assisted thermal bonding. Referring to the literature review in chapter 3, microwave absorption abilities of CNTs increase with increasing temperature [144] which means when the temperature increases, the rate of heat energy released or the heat transfer across the cover plate will be increased. The heating process can thus achieve a higher heating rate in a higher temperature. On the other hand, a thicker CNT layer in the bonding system results in a larger amount of energy released, the temperature

in the CNT layer rises with a very high rate at the initial exposure. The heat transfer rate can, as a result, increase to a very great extent at the beginning of the microwave exposure for a thicker CNT layer. Under the mutually double influence by these two factors (i.e. change of heat transfer rate in high temperature and rapid increase in temperature of thicker CNT layer), the required bonding time is expected to be shortened drastically as the CNT thickness increases. It further implies that, during CNT–microwave-assisted thermal bonding model, the bonding time required would not be in a linear relationship with the CNT thickness.

Furthermore, since the thermal conductivity of CNTs is much higher than that in polymers, temperature on the CNTs layer is expected to be relatively uniform as the heat transfer to polymers is relatively slow. Upon controlling the bonding time, it is expected that bonding can be achieved without causing global deformation on the substrate microstructures which is benefited from the single directional heat flow of the designed model and from the short processing time due to the rapid cooling of the small thermal mass in the system. The points listed above are the expected observations during CNT–microwave-assisted thermal bonding based on the physical properties of CNTs and the feature of this new model design.

In the following experiments, the thickness of CNT layer and the exposure time would be the important parameters to study so as to control the expeditiously released heat energy by CNTs. The relationship between CNT thickness and exposure time would be investigated where pressure is kept constant to provide minimum effect on bonding.

6.2 Experimental setup

The embossed plastic biochips used in this experiment had dimensions of 30 mm \times 35 mm containing microstructures of microchannels, microchambers and microvalves with depth in 50 μ m. The microchambers had dimensions ranged from 8 mm \times 15 mm to 13 mm \times 16 mm while the widths of microchannels and microvalves were 100 μ m and 50 μ m respectively.

The cover plates had thickness in 0.3 mm. It was spray-coated with CNTs as described in Chapter 5. The dimensions of the cover plate were 34 mm \times 42 mm with 3 mm \times 34 mm area left uncoated on the right edge for thickness measurement as illustrated in Figure 6.3. The CNT thickness would be averaged from the CNT thickness measurement of the upper part, the middle part and the lower part of the sprayed plate. The actual size of the embossed biochip was 30 mm \times 35 mm only, there was however extra distance of 2 mm from each edge of the cover plate. These extra edges were designed to eliminate potential edging effect during CNT–microwave-assisted thermal bonding.

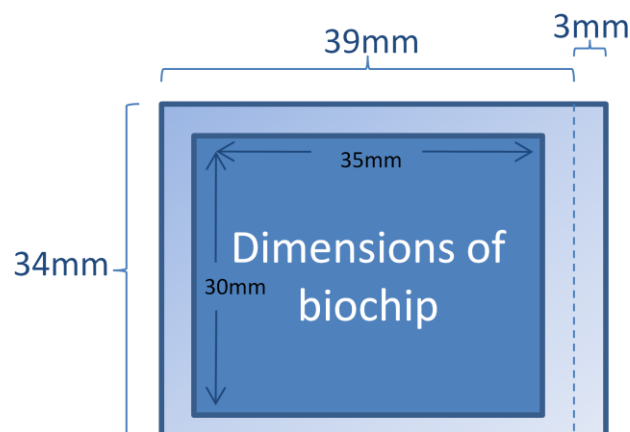


Figure 6.3. Dimensions of cover plate.

Figure 6.4 shows the samples of embossed biochip and CNT-coated cover plate. According to the newly proposed model, embossed biochip was placed at the bottom with microstructures facing up while the cover plate was placed at the top with CNT-coated surface also facing up. In real practice, an additional structured chip was added on top of the CNT-coated surface with structured side facing down. The function of the top structured chip was to eliminate the bubbles formed by the trapped air in the CNT interface. The structured chip in direct contact with CNTs would not bond or just loosely bond to the CNT-coated cover plate, because the CNT layer hindered the intercalation of polymer chains from both surfaces.

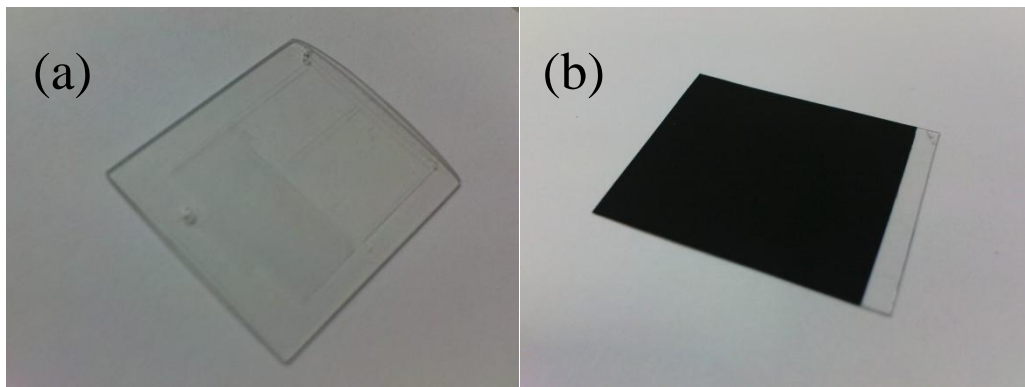


Figure 6.4. (a) Embossed biochip and (b) CNT-coated cover plate.

The bonding assembly was sandwiched between glasses under total applied force of 4.4 N (4.19 kPa). CNT–microwave-assisted thermal bonding was conducted using the equipments and experimental setup shown in Figure 6.5.



Figure 6.5. Bonding equipments. Left: microwave oven; right: bonding setup inside microwave oven with water loading.

As observed from the vigorously released heat generated by CNTs under high power level, 307 W, in the preliminary test, the high power level was considered to be too high for use in this investigation because of the difficulty in controlling the heating rate. Attempt has been made on the low power level, 39 W, to perform CNT–microwave-assisted thermal bonding, however, more than 8 min was required for bonding to occur which was considered to be a long process time. Thus, medium power level, 163 W, was chosen in this investigation owing to its moderate heating rate. In the following section, cover plates coated with different CNTs thickness were studied for the effective thickness in CNT–microwave-assisted thermal bonding.

6.3 Effective thickness of CNT layers

Owing to the non-uniformity of the electric field inside multi-mode microwave oven (which is a common concern in microwave heating system), the variations in CNT thickness measurement, and the limitations on the size of the testing time intervals, an optimal exposure time must not be exclusive to one

average CNT thickness, or an average CNT thickness must not be exclusive to an optimal exposure time. The range of average CNT thicknesses that was capable to achieve over 90% bonded under the same exposure time is defined as the effective thickness.

A set of samples with average CNT thickness ranged between 60 μm and 70 μm were exposed to microwave irradiation under different duration. The successfully bonded biochips, which were examined to exceed 90% bonded through visual check, were plotted with their corresponding microwave exposure time. The effective thickness of CNT layer was estimated through the results shown in Figure 6.6. Experimental data can be found in Appendix B.

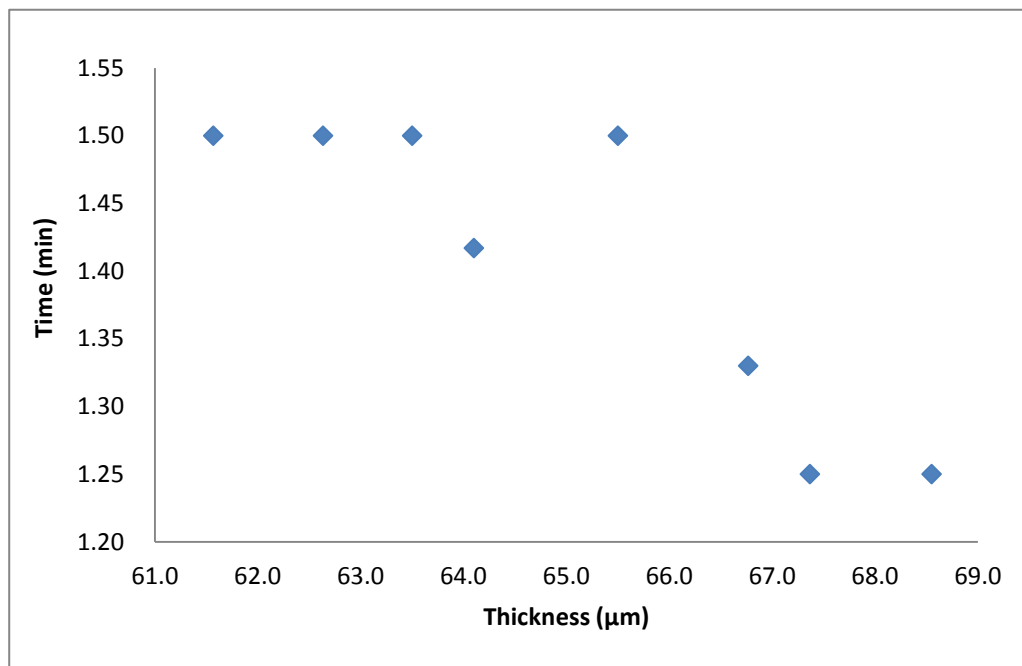


Figure 6.6. Bonding time for over 90% sealed varies with thickness of CNTs.

In the range of 60 μm to 70 μm , the optimal bonding time for each unit thickness was shown. It can be observed that between 61.5 μm to 65.5 μm , most

of the data points lay on 1.50 min. It means that the biochip assemblies required at least 1.50 min (equivalent to 1 min 30 sec) for microwave exposure in order to achieve CNT–microwave-assisted thermal bonding over 90% bonding.

The data point of 64 μm showing a reduced bonding time of 1.42 min (equivalent to 1 min 25 sec) is an experimental design error as 1.42 min was not a testing condition for the time parameter. CNT thickness of 64 μm was able to bond above 1.42 min (i.e. 1.50 min which is equivalent to 1 min 30 sec) while not below 1.42 min (i.e. 1.25 min which is equivalent to 1 min 15 sec). In this case, the data point of 64 μm should be reset to the level of 1.5 min. Hence, the effective thickness of CNTs, according to the previously given definition, was found to be ± 2 μm (i.e. 65.5 μm minus 61.5 μm is 4 μm). The leveling sign starting from data point 67.4 μm may be the beginning of another effective thickness cycle.

6.4 Performance of different CNT thicknesses under optimal exposure time

According to the finding of effective thickness of CNTs in the previous section, cover plates with average CNT thickness within ± 2 μm deviations were classified into a group that are presumed to have the same optimal bonding time. In this section, 9 samples were classified into 3 groups according to the effective thickness of CNTs found in the previous experiment.

6.4.1 Time optimization

Three groups of cover plates coated with different CNT thicknesses were investigated for their optimal bonding time. The three groups of CNT thicknesses included . Each group of cover plates consisted of three samples that the samples were subjected to microwave irradiation on different exposure time. The optimal bonding time would be found from the one being observed to achieve over 90% bonded. The detailed experimental data can be found in Appendix C. Biochips with CNT-coated cover plates from each groups were successfully bonded and their group CNT thicknesses were plotted with their corresponding optimal bonding time in Figure 6.7.

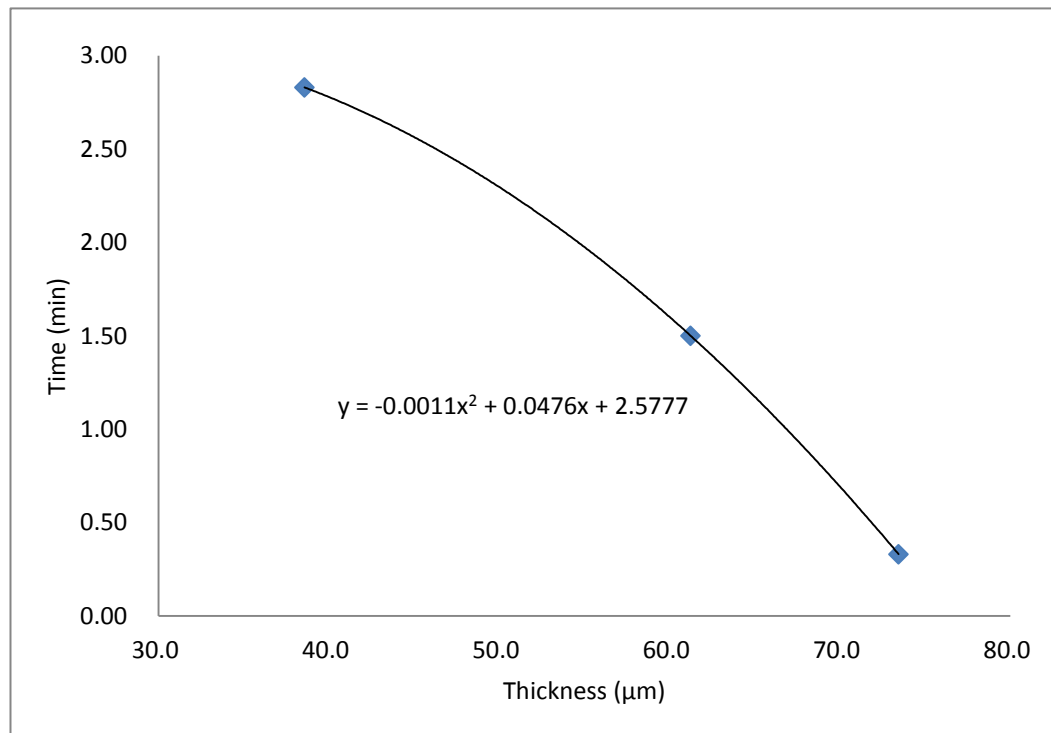


Figure 6.7. Optimal bonding time corresponding to three CNT thicknesses.

The optimal bonding time of the three CNT thickness groups were found to

be 20 sec, 1 min 30 sec and 2 min 50 sec, corresponding to 73.5 μm , 61.2 μm and 38.6 μm respectively. A trend line was established to estimate the relationship of optimal bonding time with different CNT thicknesses ranged between 30 μm and 80 μm .

The polynomial equation in the graph shows a quadratic relationship between the CNT thickness and the optimal bonding time. This quadratic relationship means that slight increase in CNT thickness would cause drastic decrease in bonding time needed. The negative sign of the x^2 coefficient in the equation also indicates an inversely proportional relationship between the CNT thickness and the optimal bonding time. This observation could be accounted by the higher degree of increment in heat transfer rate for a thicker CNT layer, and hence causing the rapid decrease in optimal bonding time. This result met the initial estimation in section 6.1.

6.4.2 Comparison on appearance

During CNT–microwave-assisted thermal bonding, CNTs generated enormous amount of energy that led bonding occurred. The immense energy, in the meantime, also softened or melted the surrounding polymers and as a result CNTs were wet by the polymers. Some CNTs were immersed into the polymer surface and these immersed CNTs were unable to be removed simply by rubbing or washing and hence leaving the appearance of darkening as shown in Figure 6.8; while for the CNTs not immersed, they could be removed easily by rubbing and washing as they just loosely adhered on the polymer surface. The immersed CNTs, however, could be removed by surface polishing because CNTs immersed

only on the surface layer.

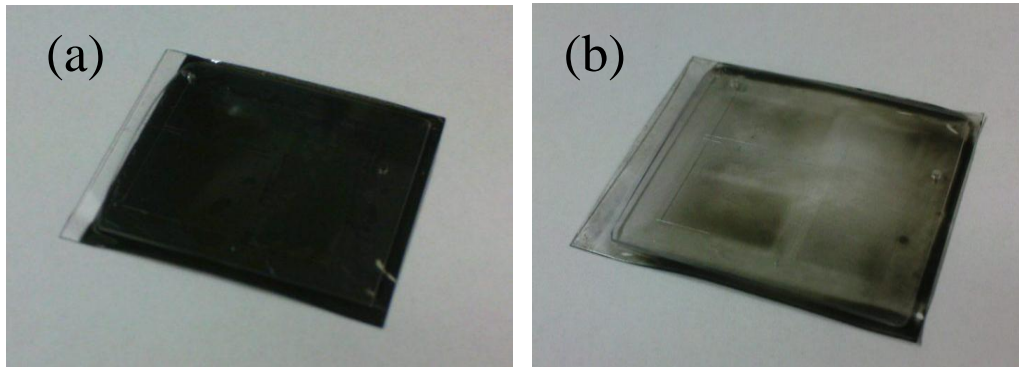


Figure 6.8. Bonded plastic biochip (a) before and (b) after removal of the loosely adhered CNTs.

Figure 6.9 presents the three bonded biochips with their backside views, the CNT-coated surfaces. The bonded biochips using different CNT thicknesses showed different extents of darkening. The extra edges of the bonded biochips were removed.

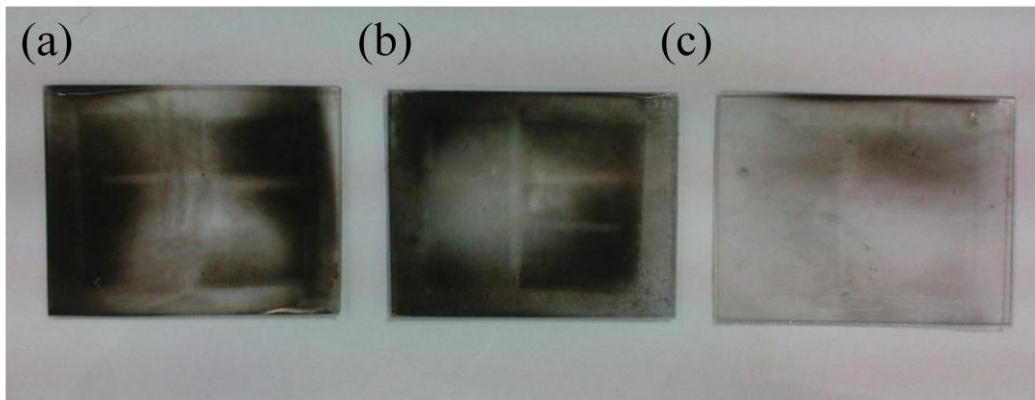


Figure 6.9. Backside views of the bonded biochips with decreasing CNT thickness from left to right: (a) 74.6 μm , (b) 61.7 μm , and (c) 37.5 μm .

As observed in Figure 6.9, biochip with thickest CNTs suffered from the

highest degree of darkening while biochip with thinnest CNTs suffered the least. The occasion of the darkening is obviously determined by the amount of energy released from the CNT layers.

Providing the bonding temperature in the bonding interfaces were the same, thicker CNT layer achieved bonding in a shorter time which meant thicker CNT layer offering a faster heat transfer rate. Upon the same thermal conduction distance, a faster heat transfer rate implied a larger temperature difference across the conduction plate according to the Fourier's law, $q_x = -kA \frac{\partial T}{\partial x}$. It could be further interpreted that the surface temperature of the adjacent polymer of the thick CNT layer was higher than that of the thin CNT layer. The higher surface temperature, acquired from the larger quantities of heat generated from a thicker CNTs heat source, increased the mobilities of the surface polymer chains and the fluidity of the polymer surface, and hence larger quantities of CNTs were wet and submerged into the polymer surface. As a result, cover plate with thicker CNTs coating appeared a higher degree of darkening as shown.

Judging from the appearance of bonded chips, cover plate with thinner CNTs is more appealing while cover plate with thicker CNTs shows less attractive for a system using optical detection method. Nevertheless, thicker CNTs are still preferential for systems with less emphasis on device transparency because of its extremely rapid bonding process within several seconds.

6.4.3 Evaluation test on leakage

Leakage test has been conducted on evaluating the bonding quality of the CNT–microwave-assisted thermal bonded biochip. Blue dye was injected into the bonded biochips through the drilled inlets under an injection pressure of 100 kPa. Dye smoothly passed through the microchannels of the three CNT–microwave-assisted thermal bonded biochips which indicated there was no blockage occurred inside the microchannels. Concerning the ease for observation, microscopic images of the thinnest CNT-coated biochips filled with blue dye are shown below in Figure 6.10.

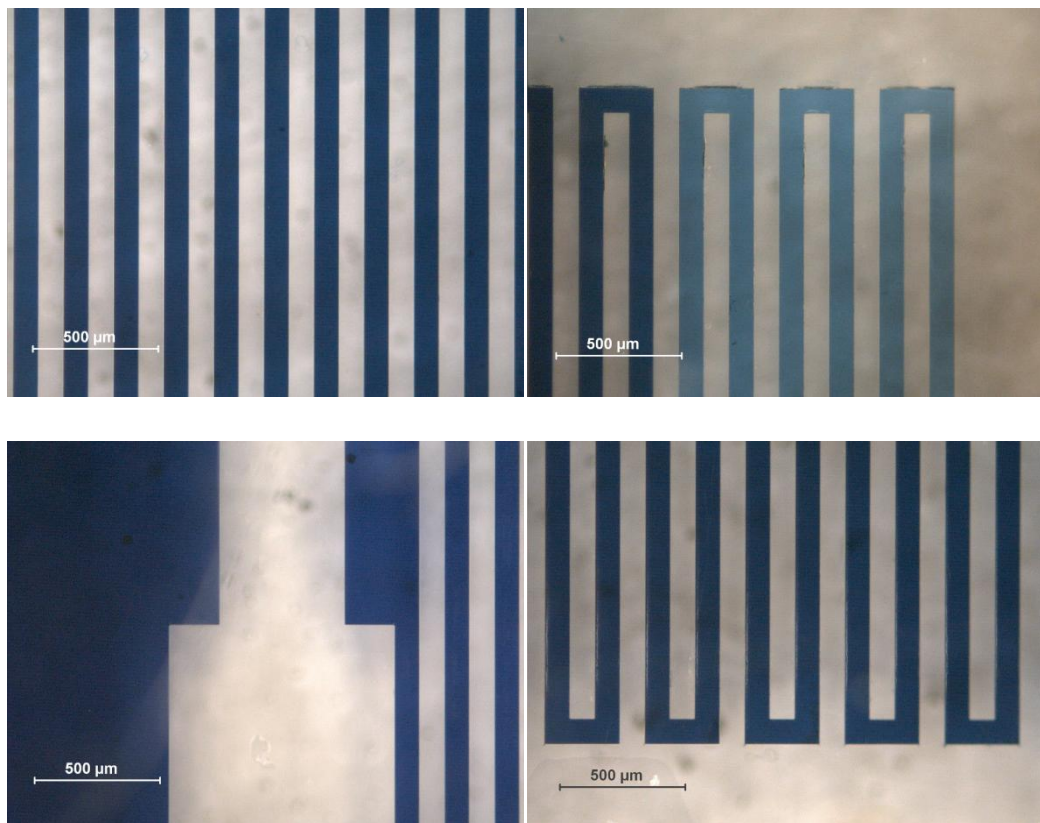


Figure 6.10. Microscopic images of microchannels (left top, right top and right bottom) and microchamber (left bottom) filled with blue dye.

Width of microchannels was 100 μm as observed from the above images. Microvalve with 45 μm in width has also successfully bonded using CNT–microwave-assisted thermal bonding. The microscopic image of the microvalve filled with blue dye is shown in Figure 6.11.

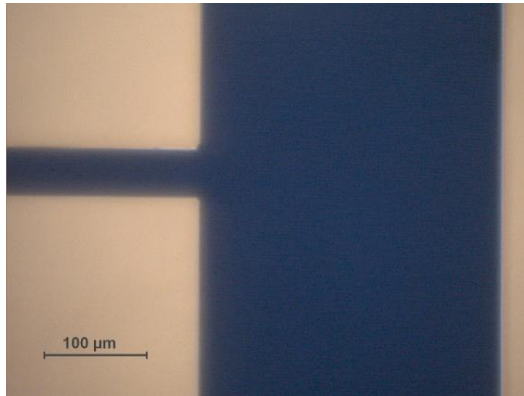


Figure 6.11. Microscopic image of microvalve (the left horizontal blue line) filled with blue dye.

Bonding performance of these three microwave thermal bonded biochips was examined using leakage test. The CNT–microwave-assisted thermal bonded biochips have successfully demonstrated the leakage-free bonding.

6.5 Comparison between CNT–microwave-assisted thermal bonding and conventional thermal bonding

Conventional thermal bonding is a typical method for bonding plastic devices. Successful attempts have been demonstrated in sealing plastic biochips. Thus, in this section, conventional thermal bonding will be used as a comparison with the CNT–microwave-assisted thermal bonding.

6.5.1. Conventional thermal bonding of plastic biochips

From the literature review, the bonding pressure in conventional thermal bonding of PC can be ranged from 0.4 MPa to 20.3 MPa [161-164]. A pressure of 2.5 MPa was chosen from this range and the bonding temperature was studied per 10 °C interval in the range of 90 – 150 °C. A patterned PC substrate with a PC cover plate were first placed in between the hotplates of the hot embossing machine, then the temperature of hotplates would be increased to the bonding temperature and would be maintained for 5 min. The entire system was subjected to heat sink until reaching 40 °C before removing from the pressure load. The whole bonding process required about 45 min.

Table 4. Bonding results of PC biochips using different bonding temperature under 2.5 MPa.

Bonding temperature (°C)	Observations
90	No bonding occurs.
100	No bonding occurs.
110	No bonding occurs.
120	Bonding occurs.
130	Bonding occurs.
140	Bonding occurs.
150	Bonding occurs; bubbles generate.

It was found that bonding would not happen at bonding temperature of 90 – 110 °C; while bonding occurred at a bonding temperature of 120 – 150 °C; however, at 150 °C, bubbles were generated within the bonding pieces which indicated the degradation of polymers in such high temperature. Hence, 120 °C was chosen for bonding the PC substrates to minimize the degree of deformation potentially caused by higher temperature.

A patterned PC substrate was hence thermally bonded to a PC cover plate at 120 °C under 2.5 MPa for 5 min using a hot embossing machine. The conventional thermally bonded biochip, afterwards, was evaluated by the leakage test. The injected fluid was successfully passing through all the microchannels as the CNT–microwave-assisted thermal bonded biochips demonstrated in the previous section.

6.5.2. Cross-sectional images observed under microscope

CNT–microwave-assisted thermal bonded biochip and conventional thermal bonded biochip were sent for cross-sectional cutting to examine the microstructure integrity under microscope. The cross-sectional images of microstructures before bonding are shown in Figure 6.12 as reference.

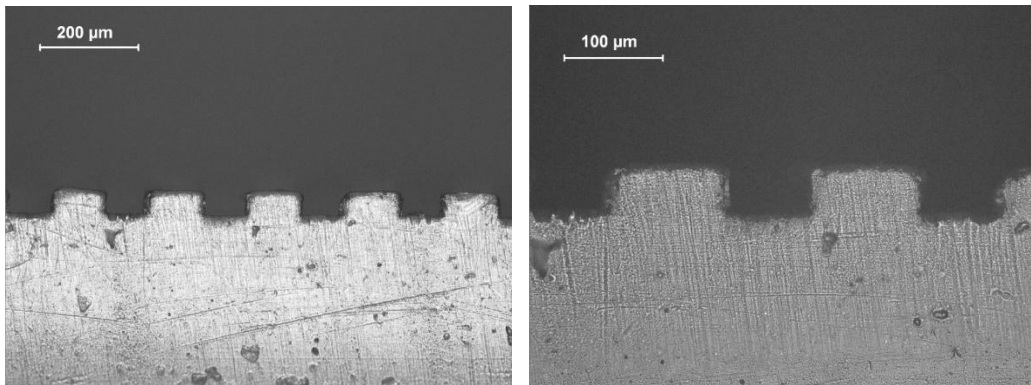


Figure 6.12. Cross-sectional images of the microstructures before bonding.

As mentioned at the beginning of this chapter, the embossed microchannels were 50 μm in depth and 100 μm in width. The cross-sectional images in Figure 6.12 show satisfactory uniformity on the embossed microchannels. The shapes and dimensions of the microchannels are distinct.

The cross-sectional images of CNT–microwave-assisted thermal bonded biochip and conventional thermal bonded biochip are shown in Figure 6.13 and Figure 6.14 respectively.

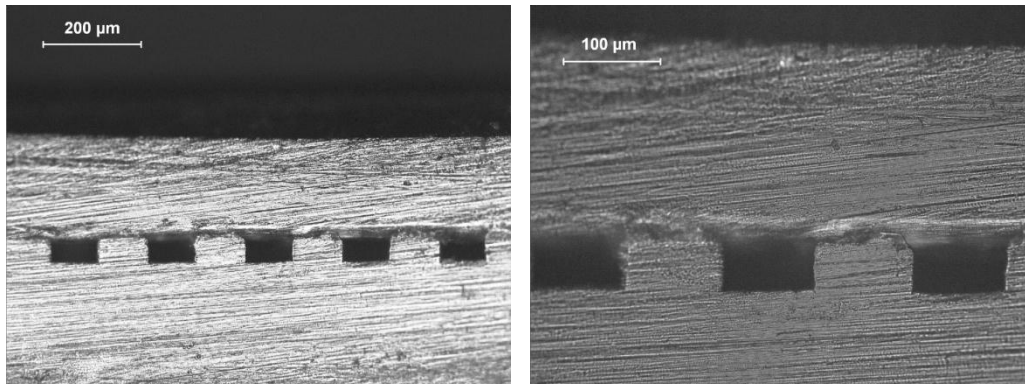


Figure 6.13. Cross-sectional images of the bonded biochip using CNT–microwave-assisted thermal bonding.

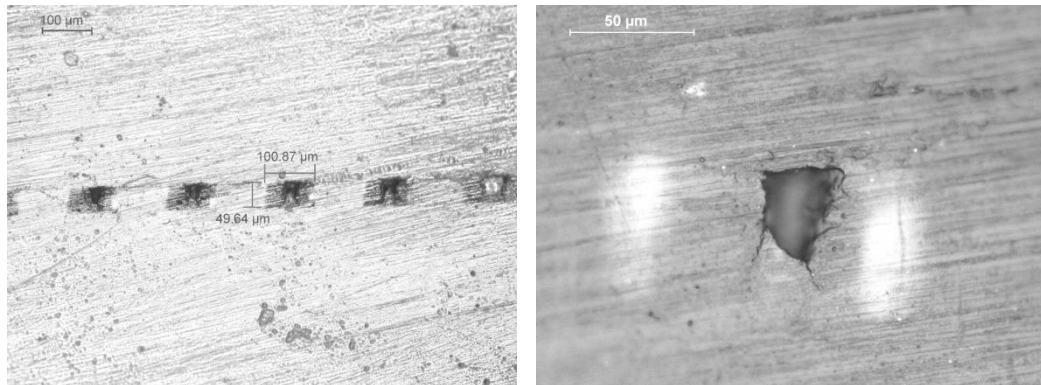


Figure 6.14. Cross-sectional images of the bonded biochip using conventional thermal bonding.

In the CNT–microwave-assisted thermal bonded microchannels shown in Figure 6.13, the integrity of the bonded microchannels was well-maintained; while the conventional thermal bonded microchannels in Figure 6.14, however, show severe deformation.

In the conventional thermal bonded biochip, a portion of polymer diffused and squeezed into the microchannels as observed in the enlarged image of the microchannels. The contributing factors might be the heat burden caused by the large thermal mass (thermal bonding machine) on the substrates, the prolonged

waiting time and/or the overloading pressure. Nevertheless, it still retained diminished microchannels with cross-sectional areas of around $25\ \mu\text{m} \times 30\ \mu\text{m}$ and it explained why the injected fluid could pass through the microchannels smoothly in the leakage test.

On the contrary, the CNT–microwave-assisted thermal bonded microchannels maintained its integrity. The heat influence for polymer fusion was seemed to be confined in the bonding interface and the entire microstructures were away from the heat influence as observed in the enlarged image of the microchannels. This observation in the CNT–microwave-assisted thermal bonded biochip is encouraging. Besides, it is also noticed that the bonding line in the microchannel region was vague, which was not expected to be seen in the bonded interface, especially inside the microchannel region. The vague bonding line could be caused by plastic residues formed during cutting. It could also be melted surface with morphology change caused by rapid heat dissipation in the bonding interface during bonding. These, however, are only some estimation from the observed images. The underlying reason for the vague bonding line requires further investigation to confirm.

6.5.3. Tensile test of the bonded biochips

The bond strength of both CNT–microwave-assisted thermal bonded biochip and conventional thermal bonded biochip were evaluated through tensile test. The bonded biochips were glued to PC blocks ($35\ \text{mm} \times 15\ \text{mm} \times 6\ \text{mm}$) on the top and bottom surfaces. The PC blocks were clamped by the grips and pulled apart in the tensile testing machine (Instron® 3340 Series Single Column Testing

Systems). Figure 6.15 shows the tensile test setup.



Figure 6.15. Setup of the pulling system for the tensile test.

The CNT–microwave-assisted thermal bonded biochip was with CNT thickness of $73.5 \pm 1.8 \mu\text{m}$ exposed for a 20-second microwave irradiation, while the conventional thermal bonded biochip was bonded as described in previous section. The tensile test results are shown in Figure 6.16 and Figure 6.17.

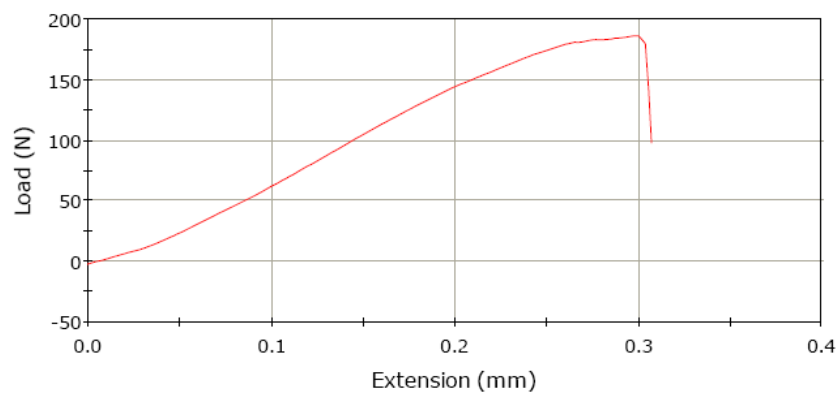


Figure 6.16. Load–Extension graph of the CNT–microwave-assisted thermal bonded biochip.

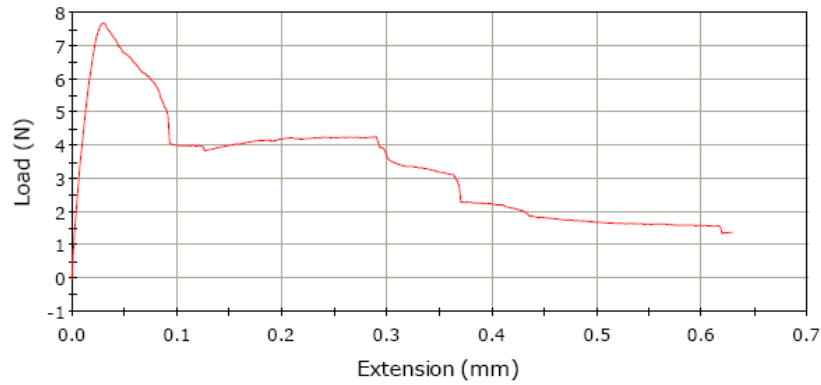


Figure 6.17. Load–Extension graph of the conventional thermal bonded biochip.

Since the actual pulling area was $(15 \times 6) \text{ mm}^2$, the tensile pressure of the CNT–microwave-assisted thermal bonded biochip was found to be as high as 2 MPa. In conventional thermal bonded biochip, the tensile pressure was only 0.08 MPa. The extremely weak tensile strength of the conventional thermal bonded biochip may be due to the cracked patterns of the deformed microstructures. As observed from Figure 6.14, crack patterns are observed inside the diminished microchannels. The crack patterns may result in some weak points that facilitated the separation of the two bonded pieces. The bonded pieces thus experienced a less strong bonding than the bonded pieces with well-maintained integrity. The results from the tensile test are obvious that CNT–microwave-assisted thermal bonded biochip demonstrated a much higher tensile pressure than the conventional thermal bonded biochip.

In some downstream applications such as PCR, since the water vapor generated during the process at $95 \text{ }^\circ\text{C}$ is 12 psi (0.08 MPa) [165], a higher tensile pressure is essential for the bonded biochips in order to increase the reliability of the devices. CNT–microwave-assisted thermal bonding herein is more suitable to offer a reliable sealing of plastic biochips for such downstream application.

6.5.4. Analysis of CNT–microwave-assisted thermal bonding performance

There are three factors to be considered for polymer deformation. The three factors include temperature, time and pressure. These three factors all have proportional relationships with the deformation of polymers, which means when the bonding is conducted at a high temperature or a high pressure for a long time, the deformation becomes more severe. Thus, these factors that may affect the CNT–microwave-assisted thermal bonding performance would be analyzed and discussed with reference to conventional thermal bonding. The analysis and discussion would be divided into three parts: i) temperature distribution, (ii) time duration and (iii) pressure loading.

i) Temperature distribution

In the design of the CNT–microwave-assisted thermal bonding model, heat was generated and transferred from the CNT layer to the bonding interface through the cover plate. The heat thus flew in single directional to the patterned substrate which was in a comparatively low temperature. Upon the optimization of exposure time, the substrate microstructures could be sealed without causing much thermal burden onto the microstructures. Schematic diagram of the heating model for CNT–microwave-assisted thermal bonding is illustrated in Figure 6.18.

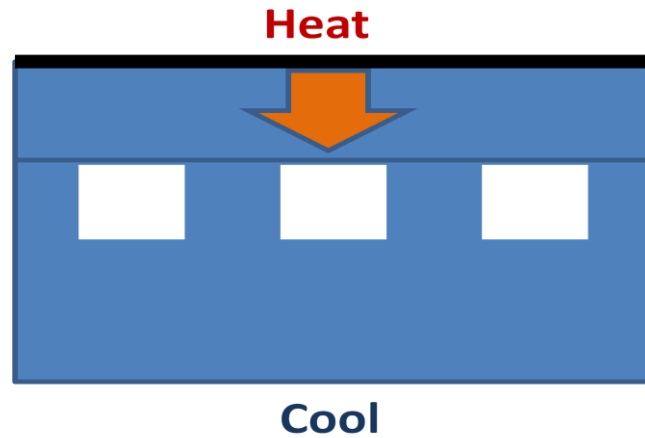


Figure 6.18. Schematic diagram of the heating model of CNT–microwave-assisted thermal bonding.

In conventional thermal bonding, by contrast, the bonding assembly was heated up from both sides as illustrated in Figure 6.19. Thermal energy was thus transferred from hotplates to the bonding interface through both cover plate and patterned substrate. This type of heating system exerted additional thermal burdens on the patterned substrate and thus resulted in a higher chance of deformation in the microstructures.

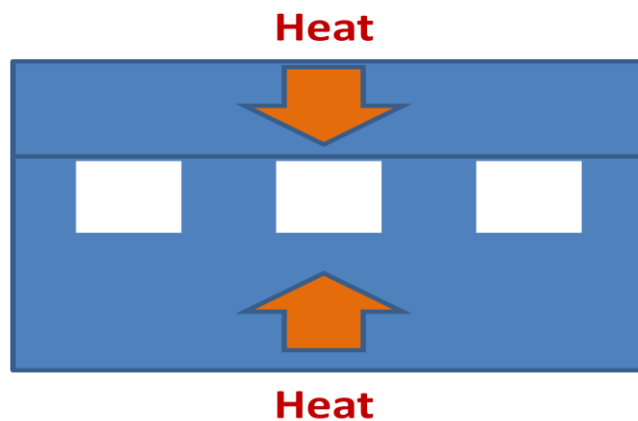


Figure 6.19. Schematic diagram of the heating model of conventional thermal bonding.

ii) Time duration

Concerning the heat transfer, as the cover plate was just 0.3 mm, heat transferred from CNT layer through heat conduction to the bonding interface was expected to be very quick. Another type of heat transfer involved is thermal radiation. Since the heat source, carbon nanotubes, was a black body, it released part of the stored energy in the form of radiation and thereby led to an efficient energy transmission to the relatively rough surface of the embossed microchannel crests resulting in heating. CNT–microwave-assisted thermal bonding could thus be conducted with short processing time, less than three minutes, without imposing a huge thermal burden on the microstructures that may lead to deformation. The integrity of the microchannels, as a result, was maintained.

The appealingly short processing time in CNT–microwave-assisted thermal bonding not only benefited from the efficient heat transfer in heating but also in cooling because of the small thermal mass. In conventional thermal bonding, a prolonged waiting time, which is typically at least 30 min, was necessary to allow the large thermal mass including the hot embossing machine and the bonded biochip to cool down to room temperature, before releasing the solidified assembly. Polymer chains possessing increased mobilities were thus maintained at high energy level during the prolonged cooling time. The cooling process offered sufficient time for these “active” polymer chains diffusing into the microchannels and finally resulted in a severe deformation of the microchannels.

(iii) Pressure loading

As mentioned in section 6.5.2, overloading pressure might be one of the contributing factors of the deformed microchannels in conventional thermal bonded biochip. In conventional thermal bonding, the total applied pressure for bonding PC biochips was 2.5 MPa; while in CNT–microwave-assisted thermal bonding, a total applied pressure for bonding PC biochips was only 4.19 kPa. It is obvious that the high pressure owned part of the reasons for resulting in the severe deformed microchannels.

Nevertheless, it was found that the minimum applied pressure in the conventional thermal bonding machine is 25 kg, which is equivalent to 238.10 kPa. This minimum applied pressure is still almost 57 times of the pressure used in the CNT–microwave-assisted thermal bonding. CNT–microwave-assisted thermal bonding thus offers a new bonding method with the advantage of slight loading in bonding PC biochips that could further minimize the chance of deforming microstructures

6.6 Summary

CNT–microwave-assisted thermal bonding was successfully demonstrated in bonding plastic biochips in this chapter. Various CNT thicknesses were studied for their optimized bonding time. The bonding performance of the CNT–microwave-assisted thermal bonded biochips under the optimized bonding time was evaluated by the leakage test and the results were satisfactory. The studies in microstructure integrity and tensile test showed that

CNT–microwave-assisted thermal bonding offered the bonded assembly with intact microstructures and with high bond strength of 2 MPa as compared to the conventional thermal bonded biochip. CNT–microwave-assisted thermal bonding, which is able to offer homogeneous and leakage-free bonding with negligible deformation, was developed as a promising technique for sealing plastic biochips with short processing time and high bonding efficiency that may further develop into a high throughput process for industrial scale production.

Chapter 7: Conclusions

Conclusions are made in three aspects in this chapter including knowledge contributed to the field of research, limitations of the study and suggestions for future investigation.

7.1 Contribution to knowledge

In the study, the responses of GNPs and CNTs towards microwave irradiation have been evaluated. It was found that both GNPs and CNTs demonstrated abilities in converting microwave energy into heat energy. The microwave absorption abilities of CNTs were, however, found to be much more vigorous than that of GNPs. CNTs was therefore chosen as the efficient microwave absorber for further development of the bonding model.

Regarding the unexpected bonding result of CNTs in the preliminary test, the microwave bonding was redeveloped into CNT–microwave-assisted thermal bonding. The redeveloped model possessed the improvements on bonding efficiency and material homogeneity which are the prerequisite features of industrial scale bonding of plastic biochips.

In the investigation of CNT–microwave-assisted thermal bonding, relationship between the CNT thickness and the duration of microwave exposure of the plastic biochips has been studied and established. Evaluation tests have also been conducted through the leakage test, the examination of microstructure

integrity and the tensile test for the bonded plastic biochips with reference to conventional thermal bonded biochips.

CNT–microwave-assisted thermal bonding was developed to be a novel bonding method for sealing plastic biochips which offers features of material homogeneity, leakage-free and negligible deformation that can be operated with short processing time and high bonding efficiency. The developed method is considered as a promising alternative for bonding plastic biochips in industrial scale production.

7.2 Limitations

The developed method offers the desirable features of bonding plastic biochips. There are, however, still some limitations found during the development. A limitation is found on the size of the plastic biochips. Since the spray gun has a confined spraying diameter, only plastic biochips within the spraying areas are able to have their cover plates coated with CNTs in high uniformity. In this experiment, the variation of CNT coating was controlled within $\pm 5 \mu\text{m}$. In the case of spraying a larger cover plate, more manual movements are involved which means more than one sweep is needed in order to cover the whole plate surface. It would result in a higher variation in coating uniformity. This limitation, however, could be eliminated if the bonding process is industrialized that automatic spraying machine replaces the manual control spraying. The sizes of bonding biochips could thus be more flexible.

Another limitation on CNT–microwave-assisted thermal bonding is the

darkening of the outer surface of the bonded biochips. Though the CNT layer could be removed by polishing after the bonding process, it would increase the manufacturing expense. Hence, for devices involving optical detection, CNT–microwave-assisted thermal bonding may not be the desirable bonding method; while for devices, for example, using electrochemical detection, CNT–microwave-assisted thermal bonding is still a promising alternative choice.

7.3 Suggestions for future investigation

Future investigation in the CNT–microwave–assisted thermal bonding is suggested as follows. It is recommended that future investigation can be conducted on demonstrating the biocompatibility of the CNT–microwave-assisted thermal bonded devices. Though polycarbonate is a well-known biocompatible material, tests on performing PCR or other bioanalytical process such as capillary electrophoresis are recommended. This follow-up work enables a complete investigation on a bonding method development for fulfilling the purpose of sealing biochips for bioapplications.

Further investigation is suggested to explore new applications of the CNTs in the bonded biochips. Since CNTs have broad applications in biological detection, synthesis of new material composites and electronics development, new applications of the incorporated CNTs can be brainstormed so that the adhered or immersed CNTs can be utilized for ultimate use.

Another future investigation is suggested to develop another bonding method using GNPs. As from the preliminary result, GNPs demonstrated an

obvious response to microwave irradiation though it was not strong enough to achieve bonding of polymers in the test. Upon process optimization including the size of GNPs, the deposition method and the exposure condition, the GNP-assisted microwave bonding is possible to be achieved and developed into another promising alternative. An alternative heat source, IR, can also be considered to develop another bonding method that is suitable for bonding plastic biochips through the improvement on the heating effect of GNPs.

APPENDICES

Appendix A. Thickness table of CNTs using spray-coating.

Chip No.	Top (μm)	Middle (μm)	Bottom (μm)	Average (μm)	Deviation (μm)
1	65.0	62.8	65.3	64.4	1.6
2	65.8	62.9	63.7	64.1	1.7
3	64.5	63.6	64.3	64.1	0.5
4	62.1	61.2	59.1	60.8	1.7
5	66.9	62.1	59.4	62.8	4.1
6	67.0	66.4	62.9	65.4	2.5
7	62.9	63.9	61.6	62.8	1.2
8	62.7	62.8	62.4	62.6	0.2
9	66.7	64.5	65.5	65.6	1.1
10	61.8	60.9	61.9	61.5	0.6
11	61.6	64.8	65.9	64.1	2.5
12	66.9	64.6	65.4	65.6	1.3
13	62.1	61.0	67.0	63.4	3.6
14	60.2	62.2	63.1	61.8	1.6
15	64.3	67.2	65.0	65.5	1.7
16	67.5	64.4	58.8	63.6	4.8
17	65.7	61.3	61.5	62.8	2.9
18	68.5	61.6	65.3	65.1	3.5
19	67.1	65.2	62.0	64.8	2.8
20	67.5	66.4	66.4	66.8	0.7
21	67.9	66.5	66.4	66.9	1.0
22	62.0	66.1	62.4	63.5	2.6
23	63.8	61.8	59.1	61.6	2.5
24	63.6	66.3	66.4	65.4	1.8
25	64.7	67.2	65.9	65.9	1.3
26	64.7	61.7	63.9	63.4	1.7
27	63.5	63.5	64.2	63.7	0.5
28	68.0	66.3	67.3	67.2	0.9
29	62.0	60.8	61.9	61.6	0.8

Appendix B. Experimental data for estimating the effective thickness of CNT layers.

Chip No.	Top (μm)	Middle (μm)	Bottom (μm)	Average (μm)	Deviation (μm)	Time (min.sec)	Time (min)	Bonding Status*
1	62.1	61.2	59.1	60.8	1.7	1.30	1.50	N
2	61.8	60.9	61.9	61.5	0.6	1.40	1.67	Y
3	63.8	61.8	59.1	61.6	2.5	1.30	1.50	Y
4	62.0	60.8	61.9	61.6	0.8	1.20	1.33	N
5	62.7	62.8	62.4	62.6	0.2	1.30	1.50	Y
6	66.9	62.1	59.4	62.8	4.1	1.20	1.33	N
7	62.1	61.0	67.0	63.4	3.6	1.20	1.33	N
8	62.0	66.1	62.4	63.5	2.6	1.30	1.50	Y
9	67.5	64.4	58.8	63.6	4.8	1.30	1.50	Y
10	61.6	64.8	65.9	64.1	2.5	1.25	1.42	Y
11	65.8	62.9	63.7	64.1	1.7	1.25	1.42	Y
12	64.5	63.6	64.3	64.1	0.5	1.15	1.25	N
13	65.0	62.8	65.3	64.4	1.6	1.30	1.50	Y
14	63.6	66.3	66.4	65.4	1.8	1.40	1.67	Y
15	64.3	67.2	65.0	65.5	1.7	1.30	1.50	Y
16	66.7	64.5	65.5	65.6	1.1	1.20	1.33	N
17	66.9	64.6	65.4	65.6	1.3	1.20	1.33	N
18	67.5	66.4	66.4	66.8	0.7	1.20	1.33	Y
19	67.9	66.5	66.4	66.9	1.0	1.10	1.17	N
20	68.0	66.3	67.3	67.2	0.9	1.00	1.00	N
21	66.2	67.8	68.1	67.4	1.2	1.15	1.25	Y

22	66.3	68.8	70.0	68.4	2.1	1.05	1.08	N
23	65.8	69.25	70.6	68.6	2.8	1.15	1.25	Y
24	70.0	69.6	69.9	69.8	0.2	1.17	1.28	Y

*Bonding Status: Y – bonded; N – not bonded.

Appendix C. Experimental data for time optimization of three CNT thicknesses.

Group No.	Group thickness (μm)	Chip No.	Top (μm)	Middle (μm)	Bottom (μm)	Average (μm)	Deviation (μm)	Time (min.sec)	Time (min)	Bonding %**
I	73.5 ± 1.8	1	73.7	73.9	78.0	75.2	2.8	0.10	0.17	20
		2	76.0	73.3	74.5	74.6	1.4	0.20	0.33	100
		3	72.9	70.5	71.7	71.7	1.2	0.30	0.50	X
II	61.2 ± 1.9	4	60.4	63.6	65.4	63.1	2.7	1.40	1.67	X
		5	58.4	59.8	59.9	59.3	1.0	1.20	1.33	40
		6	59.7	61.6	63.7	61.7	2.0	1.30	1.50	100
III	38.6 ± 1.9	7	39.4	38.4	43.6	40.4	3.2	2.40	2.67	30
		8	35.6	37.4	37.3	36.7	1.2	3.00	3.00	X
		9	39.2	36.6	36.6	37.5	1.7	2.50	2.83	100

** Bonding %: X – overheated.

REFERENCES

- [1] A. Manz, N. Graber, and H. M. Widmer, "Miniaturized total chemical-analysis systems - A novel concept for chemical sensing," *Sensors and Actuators B-Chemical*, vol. 1, pp. 244-248, Jan 1990.
- [2] S. C. Jakeway, A. J. de Mello, and E. L. Russell, "Miniaturized total analysis systems for biological analysis," *Fresenius' Journal of Analytical Chemistry*, vol. 366, pp. 525-539, 2000.
- [3] E. Verpoorte and N. F. De Rooij, "Microfluidics meets MEMS," *Proceedings of the IEEE*, vol. 91, pp. 930-953, Jun 2003.
- [4] A. Deepu, V. V. R. Sai, and S. Mukherji, "Simple surface modification techniques for immobilization of biomolecules on SU-8," *Journal of Materials Science-Materials in Medicine*, vol. 20, pp. 25-28, Dec 2009.
- [5] A. T. Woolley, D. Hadley, P. Landre, A. J. deMello, R. A. Mathies, and M. A. Northrup, "Functional integration of PCR amplification and capillary electrophoresis in a microfabricated DNA analysis device," *Analytical Chemistry*, vol. 68, pp. 4081-4086, Dec 1996.
- [6] V. P. Pouchkarev, E. F. Shved, and P. I. Novikov, "Sex determination of forensic samples by polymerase chain reaction of the amelogenin gene and analysis by capillary electrophoresis with polymer matrix," *Electrophoresis*, vol. 19, pp. 76-79, Jan 1998.
- [7] J. T. Sprouse, R. Werling, D. Hanke, C. Lakey, L. McDonnel, B. L. Wood, and D. E. Sabath, "T-cell clonality determination using polymerase chain reaction (PCR) amplification of the T-cell receptor gamma-chain gene and capillary electrophoresis of fluorescently labeled PCR products," *American Journal of Clinical Pathology*, vol. 113, pp. 838-850, Jun 2000.
- [8] C. N. Liu, N. M. Toriello, and R. A. Mathies, "Multichannel PCR-CE microdevice for genetic analysis," *Analytical Chemistry*, vol. 78, pp. 5474-5479, Aug 2006.
- [9] Y. J. Wu, Y. Chen, C. X. Zhu, B. Wang, H. R. Yang, F. Yuan, and B. L. Xu, "Multiplex PCR-capillary electrophoresis-SSCP used to identify foodborne pathogens," *European Food Research and Technology*, vol. 228, pp. 511-518, Feb 2009.
- [10] R. T. Zhong, X. Y. Pan, L. Jiang, Z. P. Dai, J. H. Qin, and B. C. Lin, "Simply and reliably integrating micro heaters/sensors in a monolithic PCR-CE microfluidic genetic analysis system," *Electrophoresis*, vol. 30, pp. 1297-1305, Apr 2009.
- [11] J. N. Stuart, J. D. Ebaugh, A. L. Copes, N. G. Hatcher, R. Gillette, and J. V. Sweedler, "Systemic serotonin sulfate in opisthobranch mollusks," *Journal of Neurochemistry*, vol. 90, pp. 734-742, Aug 2004.
- [12] X. Liu, L. Ma, J.-F. Zhang, and Y.-T. Lu, "Determination of single-cell gene expression in Arabidopsis by capillary electrophoresis with laser induced fluorescence detection," *Journal of Chromatography B*, vol. 808, pp. 241-247, 2004.
- [13] J. P. Jakupciak, P. E. Barker, W. Wang, S. Srivastava, and D. H. Atha, "Preparation and Characterization of Candidate Reference Materials for

- Telomerase Assays," *Clinical Chemistry*, vol. 51, pp. 1443-1450, August 1, 2005.
- [14] J. M. Cunliffe, Z. Liu, J. Pawliszyn, and R. T. Kennedy, "Use of a native affinity ligand for the detection of G proteins by capillary isoelectric focusing with laser-induced fluorescence detection," *Electrophoresis*, vol. 25, pp. 2319-2325, Jul 2004.
- [15] R. P. P. Soares, T. Barron, K. McCoy-Simandle, M. Svobodova, A. Warburg, and S. J. Turco, "Leishmania tropica: intraspecific polymorphisms in lipophosphoglycan correlate with transmission by different Phlebotomus species," *Experimental Parasitology*, vol. 107, pp. 105-114, May-Jun 2004.
- [16] K. Mullis, F. Faloona, S. Scharf, R. Saiki, G. Horn, and H. Erlich, "Specific enzymatic amplification of DNA in vitro - the Polymerase Chain-Reaction," *Cold Spring Harbor Symposia on Quantitative Biology*, vol. 51, pp. 263-273, 1986.
- [17] M. A. Northrup, M. T. Ching, R. M. White, and R. T. Wiltson, "DNA amplification with a microfabricated reaction chamber," in *Proceedings of Transducers '93*, Chicago, USA, 1993, pp. 924-926.
- [18] D. S. Lee, S. H. Park, H. S. Yang, K. H. Chung, T. H. Yoon, S. J. Kim, K. Kim, and Y. T. Kim, "Bulk-micromachined submicroliter-volume PCR chip with very rapid thermal response and low power consumption," *Lab on a Chip*, vol. 4, pp. 401-407, 2004.
- [19] M. U. Kopp, A. J. de Mello, and A. Manz, "Chemical Amplification: Continuous-Flow PCR on a Chip," *Science*, vol. 280, pp. 1046-1048, May 15 1998.
- [20] Z. Krivácsya, A. Gelencséra, J. Hlavayb, G. Kissa, and Z. Sárvárib, "Electrokinetic injection in capillary electrophoresis and its application to the analysis of inorganic compounds," *Journal of Chromatography A*, vol. 834, pp. 21-44, 1999.
- [21] D. J. Harrison, A. Manz, Z. H. Fan, H. Ludi, and H. M. Widmer, "Capillary Electrophoresis and Sample Injection Systems Integrated on a Planar Glass Chip," *Analytical Chemistry*, vol. 64, pp. 1926-1932, Sep 1992.
- [22] A. Manz, D. J. Harrison, E. M. J. Verpoorte, J. C. Fettingler, A. Paulus, H. Ludi, and H. M. Widmer, "Planar chips technology for miniaturization and integration of separation techniques into monitoring systems - capillary electrophoresis on a chip," *Journal of Chromatography*, vol. 593, pp. 253-258, Feb 1992.
- [23] V. Tandon, S. K. Bhagavatula, W. C. Nelson, and B. J. Kirby, "Zeta potential and electroosmotic mobility in microfluidic devices fabricated from hydrophobic polymers: 1. The origins of charge," *Electrophoresis*, vol. 29, pp. 1092-1101, Mar 2008.
- [24] H. M. Park, S. M. Hong, and J. S. Lee, "Estimation of zeta potential of electroosmotic flow in a microchannel using a reduced-order model," *Biomedical Microdevices*, vol. 9, pp. 751-760, Oct 2007.
- [25] S. C. Jacobson and J. M. Ramsey, "Integrated microdevice for DNA restriction fragment analysis," *Analytical Chemistry*, vol. 68, pp. 720-723, Mar 1996.

- [26] W. T. Hofgartner, A. F. R. Huhmer, J. P. Landers, and J. A. Kant, "Rapid diagnosis of herpes simplex encephalitis using microchip electrophoresis of PCR products," *Clinical Chemistry*, vol. 45, pp. 2120-2128, Dec 1999.
- [27] Y. Sun and Y. C. Kwok, "Polymeric microfluidic system for DNA analysis," *Analytica Chimica Acta*, vol. 556, pp. 80-96, Jan 18 2006.
- [28] E. Verpoorte, "Microfluidic chips for clinical and forensic analysis," *Electrophoresis*, vol. 23, pp. 677-712, Mar 2002.
- [29] S. I. Fujita, Y. Senda, S. Nakaguchi, and T. Hashimoto, "Multiplex PCR using internal transcribed spacer 1 and 2 regions for rapid detection and identification of yeast strains," *Journal of Clinical Microbiology*, vol. 39, pp. 3617-3622, Oct 2001.
- [30] A. Hatch, A. E. Kamholz, K. R. Hawkins, M. S. Munson, E. A. Schilling, B. H. Weigl, and P. Yager, "A rapid diffusion immunoassay in a T-sensor," *Nature Biotechnology*, vol. 19, pp. 461-465, May 2001.
- [31] J. P. Landers, "Molecular diagnostics on electrophoretic microchips," *Analytical Chemistry*, vol. 75, pp. 2919-2927, Jun 2003.
- [32] I. Medintz, W. W. Wong, G. Sensabaugh, and R. A. Mathies, "High speed single nucleotide polymorphism typing of a hereditary haemochromatosis mutation with capillary array electrophoresis microplates," *Electrophoresis*, vol. 21, pp. 2352-2358, Jul 2000.
- [33] C. C. Hung, S. C. Chien, C. Y. Lin, C. H. Chang, Y. F. Chang, Y. J. Jong, S. T. Hsieh, W. S. Hsieh, M. S. Liu, W. L. Lin, C. N. Lee, and Y. N. Su, "Use of multiplex PCR and CE for gene dosage quantification and its biomedical applications for SMN, PMP22 and alpha-globin genes," *Electrophoresis*, vol. 28, pp. 2826-2834, Aug 2007.
- [34] P. S. Dittrich and A. Manz, "Lab-on-a-chip: microfluidics in drug discovery," *Nature Reviews Drug Discovery*, vol. 5, pp. 210-218, Mar 2006.
- [35] N. M. Cirino, K. A. Musser, and C. Egan, "Multiplex diagnostic platforms for detection of biothreat agents," *Expert Review of Molecular Diagnostics*, vol. 4, pp. 841-857, Nov 2004.
- [36] J. Wang, B. M. Tian, and E. Sahlin, "Micromachined electrophoresis chips with thick-film electrochemical detectors," *Analytical Chemistry*, vol. 71, pp. 5436-5440, Dec 1999.
- [37] S. R. Wallenborg and C. G. Bailey, "Separation and detection of explosives on a microchip using micellar electrokinetic chromatography and indirect laser-induced fluorescence," *Analytical Chemistry*, vol. 72, pp. 1872-1878, Apr 2000.
- [38] J. E. Prest, S. J. Baldock, P. R. Fielden, N. J. Goddard, S. Mohr, and B. J. T. Brown, "Rapid chloride analysis using miniaturised isotachopheresis," *Journal of Chromatography A*, vol. 1119, pp. 183-187, Jun 2006.
- [39] D. Y. He, Z. J. Zhang, Y. Huang, and Y. F. Hu, "Chemiluminescence microflow injection analysis system on a chip for the determination of nitrite in food," *Food Chemistry*, vol. 101, pp. 667-672, 2007.
- [40] Y. Uyama, K. Kato, and Y. Ikada, "Surface modification of polymers by grafting," in *Grafting/Characterization Techniques/Kinetic Modeling*. vol. 137, 1998, pp. 1-39.

- [41] A. Gonzalez, R. Grimes, E. J. Walsh, T. Dalton, and M. Davies, "Interaction of quantitative PCR components with polymeric surfaces," *Biomedical Microdevices*, vol. 9, pp. 261-266, Apr 2007.
- [42] Y. M. Xia, Z. S. Hua, O. Srivannavit, A. B. Ozel, and E. Gulari, "Minimizing the surface effect of PDMS-glass microchip on polymerase chain reaction by dynamic polymer passivation," *Journal of Chemical Technology and Biotechnology*, vol. 82, pp. 33-38, Jan 2007.
- [43] T. B. Christensen, C. M. Pedersen, K. G. Grondhal, T. G. Jensen, A. Sekulovic, D. D. Bang, and A. Wolff, "PCR biocompatibility of lab-on-a-chip and MEMS materials," *Journal of Micromechanics and Microengineering*, vol. 17, pp. 1527-1532, Aug 2007.
- [44] H. G. Choi, P. Boccazzi, A. J. Sinskey, P. E. Laibinis, and K. F. Jensen, "Surface modification of poly(methyl methacrylate) for controlling cell adhesion," in *227th ACS National Meeting*, vol. 227 CA: American Chemical Society, 2004, pp. 57-POLY.
- [45] J. J. Shah, J. Geist, L. E. Locascio, M. Gaitan, M. V. Rao, and W. N. Vreeland, "Surface modification of poly(methyl methacrylate) for improved adsorption of wall coating polymers for microchip electrophoresis," *Electrophoresis*, vol. 27, pp. 3788-3796, Oct 2006.
- [46] S. L. Llopis, J. Osiri, and S. A. Soper, "Surface modification of poly(methyl methacrylate) microfluidic devices for high-resolution separations of single-stranded DNA," *Electrophoresis*, vol. 28, pp. 984-993, Mar 2007.
- [47] A. de Mello, "Plastic fantastic?," *Lab on a Chip*, vol. 2, pp. 31N-36N, 2002.
- [48] F. Bianchi, F. Wagner, P. Hoffmann, and H. H. Girault, "Electroosmotic flow in composite microchannels and implications in microcapillary electrophoresis systems," *Analytical Chemistry*, vol. 73, pp. 829-836, Feb 2001.
- [49] H. Becker and U. Heim, "Hot embossing as a method for the fabrication of polymer high aspect ratio structures," *Sensors and Actuators A: Physical*, vol. 83, pp. 130-135, 2000.
- [50] L. Y. Yu, C. G. Koh, L. J. Lee, K. W. Koelling, and M. J. Madou, "Experimental investigation and numerical simulation of injection molding with micro-features," *Polymer Engineering and Science*, vol. 42, pp. 871-888, May 2002.
- [51] S. Giselbrecht, T. Gietzelt, E. Gottwald, C. Trautmann, R. Truckenmuller, K. F. Weibezahn, and A. Welle, "3D tissue culture substrates produced by microthermoforming of pre-processed polymer films," *Biomedical Microdevices*, vol. 8, pp. 191-199, Sep 2006.
- [52] C. G. K. Malek, "Laser processing for bio-microfluidics applications (part I)," *Analytical and Bioanalytical Chemistry*, vol. 385, pp. 1351-1361, Aug 2006.
- [53] C. G. K. Malek, "Laser processing for bio-microfluidics applications (part II)," *Analytical and Bioanalytical Chemistry*, vol. 385, pp. 1362-1369, Aug 2006.
- [54] Großmaischeid, Deutschland: Kern GmbH, 2008.
- [55] "Cyclic olefin copolymer (COC)," Germany: Topas[®] Advanced Polymers GmbH, 2008.

- [56] "Topas® 6013F-04," Germany: Topas® Advanced Polymers GmbH, 2006.
- [57] "Topas® Cyclic Olefin Copolymer (COC)," Germany: Topas® Advanced Polymers GmbH, 2006.
- [58] "CHEMnetBASE," Chapman & Hall/CRC Press LLC, 2006.
- [59] A. Piruska, I. Nikcevic, S. H. Lee, C. Ahn, W. R. Heineman, P. A. Limbach, and C. J. Seliskar, "The autofluorescence of plastic materials and chips measured under laser irradiation," *Lab on a Chip*, vol. 5, pp. 1348-1354, 2005.
- [60] G. S. Fiorini and D. T. Chiu, "Disposable microfluidic devices: fabrication, function, and application," *Biotechniques*, vol. 38, pp. 429-446, Mar 2005.
- [61] J. Kameoka, H. G. Craighead, H. W. Zhang, and J. Henion, "A polymeric microfluidic chip for CE/MS determination of small molecules," *Analytical Chemistry*, vol. 73, pp. 1935-1941, May 2001.
- [62] R. M. McCormick, R. J. Nelson, M. G. AlonsoAmigo, J. Benvegna, and H. H. Hooper, "Microchannel electrophoretic separations of DNA in injection-molded plastic substrates," *Analytical Chemistry*, vol. 69, pp. 2626-2630, Jul 1997.
- [63] L. Martynova, L. E. Locascio, M. Gaitan, G. W. Kramer, R. G. Christensen, and W. A. MacCrehan, "Fabrication of plastic microfluid channels by imprinting methods," *Analytical Chemistry*, vol. 69, pp. 4783-4789, Dec 1997.
- [64] C. Ageorges, L. Ye, and M. Hou, "Advances in fusion bonding techniques for joining thermoplastic matrix composites: a review," *Composites Part A: Applied Science and Manufacturing*, vol. 32, pp. 839-857, 2001.
- [65] S. Prager and M. Tirrell, "The healing-process at polymer-polymer interfaces," *Journal of Chemical Physics*, vol. 75, pp. 5194-5198, 1981.
- [66] Y. Sun, Y. C. Kwok, and N. T. Nguyen, "Low-pressure, high-temperature thermal bonding of polymeric microfluidic devices and their applications for electrophoretic separation," *Journal of Micromechanics and Microengineering*, vol. 16, pp. 1681-1688, Aug 2006.
- [67] D. S. Kim, H. S. Lee, J. Y. Han, S. H. Lee, C. H. Ahn, and T. H. Kwon, "Collapse-free thermal bonding technique for large area microchambers in plastic lab-on-a-chip applications," *Microsystem Technologies-Micro-and Nanosystems-Information Storage and Processing Systems*, vol. 14, pp. 179-184, Feb 2008.
- [68] Z. Y. Wu, N. Xanthopoulos, F. Reymond, J. S. Rossier, and H. H. Girault, "Polymer microchips bonded by O₂-plasma activation," *Electrophoresis*, vol. 23, pp. 782-790, Mar 2002.
- [69] A. Bhattacharyya and C. M. Klapperich, "Mechanical and chemical analysis of plasma and ultraviolet-ozone surface treatments for thermal bonding of polymeric microfluidic devices," *Lab on a Chip*, vol. 7, pp. 876-882, 2007.
- [70] H. Shinohara, J. Mizuno, and S. Shoji, "Low-temperature direct bonding of poly(methyl methacrylate) for polymer microchips," *IEEJ Transactions on Electrical and Electronic Engineering*, vol. 2, pp. 301-306, May 2007.

- [71] C. W. Tsao, L. Hromada, J. Liu, P. Kumar, and D. L. DeVoe, "Low temperature bonding of PMMA and COC microfluidic substrates using UV/ozone surface treatment," *Lab on a Chip*, vol. 7, pp. 499-505, 2007.
- [72] J. S. Liu, H. C. Qiao, C. Liu, Z. Xu, Y. Q. Li, and L. D. Wang, "Plasma assisted thermal bonding for PMMA microfluidic chips with integrated metal microelectrodes," *Sensors and Actuators B*, vol. 141, pp. 646-651, Sep 2009.
- [73] S. H. Ng, Y. X. Wu, Z. F. Wang, and Z. P. Wang, "Rapid Thermal Bonding of Polymer Microfluidic Devices Assisted by Corona Discharge," in *Symposium on Design, Test, Integration and Packaging of MEMS/MOEMS*, Italy, 2009, pp. 343-348.
- [74] R. Truckenmuller, P. Henzi, D. Herrmann, V. Saile, and W. K. Schomburg, "Bonding of polymer microstructures by UV irradiation and subsequent welding at low temperatures," *Microsystem Technologies*, vol. 10, pp. 372-374, Aug 2004.
- [75] H. S. Lee, D. S. Kim, and T. H. Kwon, "A novel low temperature bonding technique for plastic substrates using x-ray irradiation," in *12th International Conference on Solid-State Sensors, Actuators and Microsystems (Transducers 03)*, Boston, MA, 2003, pp. 1331-1334.
- [76] G. Chen, J. H. Li, S. Qu, D. Chen, and P. Y. Yang, "Low temperature bonding of poly(methylmethacrylate) electrophoresis microchips by in situ polymerisation," *Journal of Chromatography A*, vol. 1094, pp. 138-147, Nov 2005.
- [77] J. H. Li, D. Chen, and G. Chen, "Low-temperature thermal bonding of PMMA microfluidic chips," *Analytical Letters*, vol. 38, pp. 1127-1136, 2005.
- [78] Y. Sun, M. V. D. Satyanarayan, N. T. Nguyen, and Y. C. Kwok, "Continuous flow polymerase chain reaction using a hybrid PMMA-PC microchip with improved heat tolerance," *Sensors and Actuators B*, vol. 130, pp. 836-841, Mar 2008.
- [79] R. T. Kelly and A. T. Woolley, "Thermal bonding of polymeric capillary electrophoresis microdevices in water," *Analytical Chemistry*, vol. 75, pp. 1941-1945, Apr 15 2003.
- [80] Z. F. Chen, Y. H. Gao, J. M. Lin, R. G. Su, and Y. Xie, "Vacuum-assisted thermal bonding of plastic capillary electrophoresis microchip imprinted with stainless steel template," *Journal of Chromatography A*, vol. 1038, pp. 239-245, Jun 4 2004.
- [81] S. W. Li, J. H. Xu, Y. J. Wang, Y. C. Lu, and G. S. Luo, "Low-temperature bonding of poly-(methyl methacrylate) microfluidic devices under an ultrasonic field," *Journal of Micromechanics and Microengineering*, vol. 19, Jan 2009.
- [82] C. Y. Wang, T. G. Chen, S. C. Chang, S. Y. Cheng, and T. S. Chin, "Strong carbon-nanotube-polymer bonding by microwave irradiation," *Advanced Functional Materials*, vol. 17, pp. 1979-1983, Aug 13 2007.
- [83] R. J. Wise and I. D. Froment, "Microwave welding of thermoplastics," *Journal of Materials Science*, vol. 36, pp. 5935-5954, 2001.
- [84] A. C. Metaxas and R. J. Meredith, *Industrial microwave heating*. London,

- United Kingdom: Peter Peregrinus Ltd, 1983.
- [85] H. Potente, O. Karger, and G. Fiegler, "Laser and microwave welding - The applicability of new process principles," *Macromolecular Materials and Engineering*, vol. 287, pp. 734-744, Dec 12 2002.
- [86] K. F. Lei, S. Ahsan, N. Budraa, W. J. Li, and J. D. Mai, "Microwave bonding of polymer-based substrates for potential encapsulated micro/nanofluidic device fabrication," *Sensors and Actuators a-Physical*, vol. 114, pp. 340-346, Sep 1 2004.
- [87] A. A. Yussuf, I. Sbarski, M. Solomon, N. Tran, and J. P. Hayes, "Sealing of polymeric-microfluidic devices by using high frequency electromagnetic field and screen printing technique," *Journal of Materials Processing Technology*, vol. 189, pp. 401-408, Jul 6 2007.
- [88] C. W. Tsao and D. L. DeVoe, "Bonding of thermoplastic polymer microfluidics," *Microfluidics and Nanofluidics*, vol. 6, pp. 1-16, Jan 2009.
- [89] J. Han, S. H. Lee, A. Puntambekar, S. Murugesan, J.-W. Choi, G. Beaucage, and C. H. Ahn, "UV adhesive bonding techniques at room temperature for plastic lab-on-a-chip," in *Proceedings of 7th International Conference Micro Total Analysis Systems*, Squaw Valley, CA, 2003, pp. 1113-1116.
- [90] S. Y. Lai, X. Cao, and L. J. Lee, "A packaging technique for polymer microfluidic platforms," *Analytical Chemistry*, vol. 76, pp. 1175-1183, Feb 2004.
- [91] F. Dang, S. Shinohara, O. Tabata, Y. Yamaoka, M. Kurokawa, Y. Shinohara, M. Ishikawa, and Y. Baba, "Replica multichannel polymer chips with a network of sacrificial channels sealed by adhesive printing method," *Lab on a Chip*, vol. 5, pp. 472-478, 2005.
- [92] C. Lu, L. J. Lee, and Y.-J. Juang, "Packaging of microfluidic chips via interstitial bonding technique.," *Electrophoresis*, vol. 29, pp. 1407-1414, 2008
- [93] J. Kim, H. Kim, and C. Lee, "UV laser bonding of optical devices on polymers," in *Advanced Welding and Micro Joining / Packaging for the 21st Century*, South Korea, 2008, pp. 459-462.
- [94] W. W. Y. Chow, K. F. Lei, G. Y. Shi, W. J. Li, and Q. Huang, "Microfluidic channel fabrication by PDMS-interface bonding," *Smart Materials & Structures*, vol. 15, pp. S112-S116, Feb 2006.
- [95] F. Q. Dang, O. Tabata, M. Kurokawa, A. A. Ewis, L. H. Zhang, Y. Yamaoka, S. Shinohara, Y. Shinohara, M. Ishikawa, and Y. Baba, "High-performance genetic analysis on microfabricated capillary array electrophoresis plastic chips fabricated by injection molding," *Analytical Chemistry*, vol. 77, pp. 2140-2146, Apr 1 2005.
- [96] F. C. Huang, Y. F. Chen, and G. B. Lee, "CE chips fabricated by injection molding and polyethylene/thermoplastic elastomer film packaging methods," *Electrophoresis*, vol. 28, pp. 1130-1137, Apr 2007.
- [97] T. Q. Truong and N. T. Nguyen, "A polymeric piezoelectric micropump based on lamination technology," *Journal of Micromechanics and Microengineering*, vol. 14, pp. 632-638, Apr 2004.
- [98] M. A. Roberts, J. S. Rossier, P. Bercier, and H. Girault, "UV laser machined polymer substrates for the development of microdiagnostic systems,"

- Analytical Chemistry*, vol. 69, pp. 2035-2042, Jun 1997.
- [99] H. Klank, J. P. Kutter, and O. Geschke, "CO₂-laser micromachining and back-end processing for rapid production of PMMA-based microfluidic systems," *Lab on a Chip*, vol. 2, pp. 242-246, 2002.
- [100] D. Paul, A. Pallandre, S. Miserere, J. Weber, and J. L. Viovy, "Lamination-based rapid prototyping of microfluidic devices using flexible thermoplastic substrates," *Electrophoresis*, vol. 28, pp. 1115-1122, Apr 2007.
- [101] C. L. do Lago, H. D. T. da Silva, C. A. Neves, J. G. A. Brito-Neto, and J. A. F. da Silva, "A dry process for production of microfluidic devices based on the lamination of laser-printed polyester films," *Analytical Chemistry*, vol. 75, pp. 3853-3858, Aug 2003.
- [102] H. Y. Chen, A. A. McClelland, Z. Chen, and J. Lahann, "Solventless adhesive bonding using reactive polymer coatings," *Analytical Chemistry*, vol. 80, pp. 4119-4124, Jun 2008.
- [103] P. Abgrall, C. Lattes, V. Conederal, X. Dollat, S. Colin, and A. M. Gue, "A novel fabrication method of flexible and monolithic 3D microfluidic structures using lamination of SU-8 films," *Journal of Micromechanics and Microengineering*, vol. 16, pp. 113-121, Jan 2006.
- [104] J. Perumal, Q. D. Nghiem, D. P. Kim, and J. J. Lee, "Fabrication of inorganic polymer-based microchannel with emphasis on new bonding procedure," *Soft Materials*, vol. 4, pp. 227-235, 2006.
- [105] J. Brydson, *Plastic materials*, 7th ed.: Butterworth Heinemann, Oxford, 1999.
- [106] R. T. Kelly, T. Pan, and A. T. Woolley, "Phase-changing sacrificial materials for solvent bonding of high-performance polymeric capillary electrophoresis microchips," *Analytical Chemistry*, vol. 77, pp. 3536-3541, Jun 2005.
- [107] L. Brown, T. Koerner, J. H. Horton, and R. D. Oleschuk, "Fabrication and characterization of poly(methylmethacrylate) microfluidic devices bonded using surface modifications and solvents," *Lab on a Chip*, vol. 6, pp. 66-73, 2006.
- [108] J. J. Shah, J. Geist, L. E. Locascio, M. Gaitan, M. V. Rao, and W. N. Vreeland, "Capillarity induced solvent-actuated bonding of polymeric microfluidic devices," *Analytical Chemistry*, vol. 78, pp. 3348-3353, May 2006.
- [109] Y. C. Hsu and T. Y. Chen, "Applying Taguchi methods for solvent-assisted PMMA bonding technique for static and dynamic μ -TAS devices," *Biomedical Microdevices*, vol. 9, pp. 513-522, Aug 2007.
- [110] C. H. Lin, C. H. Chao, and C. W. Lan, "Low azeotropic solvent for bonding of PMMA microfluidic devices," *Sensors and Actuators B: Chemical*, vol. 121, pp. 698-705, 2007.
- [111] X. H. Sun, B. A. Peeni, W. Yang, H. A. Becerril, and A. T. Woolley, "Rapid prototyping of poly(methyl methacrylate) microfluidic systems using solvent imprinting and bonding," *Journal of Chromatography A*, vol. 1162, pp. 162-166, Aug 2007.
- [112] M. T. Koesdjojo, Y. H. Tennico, and V. T. Reincho, "Fabrication of a microfluidic system for capillary electrophoresis using a two-stage

- embossing technique and solvent welding on poly(methyl methacrylate) with water as a sacrificial layer," *Analytical Chemistry*, vol. 80, pp. 2311-2318, Apr 2008.
- [113] S. H. Ng, R. T. Tjeung, Z. F. Wang, A. C. W. Lu, I. Rodriguez, and N. F. de Rooij, "Thermally activated solvent bonding of polymers," *Microsystem Technologies-Micro-and Nanosystems-Information Storage and Processing Systems*, vol. 14, pp. 753-759, Jun 2008.
- [114] M. T. Koesdjojo, C. R. Koch, and V. T. Remcho, "Technique for Microfabrication of Polymeric-Based Microchips from an SU-8 Master with Temperature-Assisted Vaporized Organic Solvent Bonding," *Analytical Chemistry*, vol. 81, pp. 1652-1659, Feb 2009.
- [115] K. W. Ro, H. Liu, and D. R. Knapp, "Plastic microchip liquid chromatography-matrix-assisted laser desorption/ionization mass spectrometry using monolithic columns," *Journal of Chromatography A*, vol. 1111, pp. 40-47, Apr 2006.
- [116] J. Liu, K. W. Ro, R. Nayak, and D. R. Knapp, "Monolithic column plastic microfluidic device for peptide analysis using electrospray from a channel opening on the edge of the device," *International Journal of Mass Spectrometry*, vol. 259, pp. 65-72, Jan 2007.
- [117] T. I. Wallow, A. M. Morales, B. A. Simmons, M. C. Hunter, K. L. Krafcik, L. A. Domeier, S. M. Sickafoose, K. D. Patel, and A. Gardea, "Low-distortion, high-strength bonding of thermoplastic microfluidic devices employing case-II diffusion-mediated permeant activation," *Lab on a Chip*, vol. 7, pp. 1825-1831, 2007.
- [118] A. Griebel, S. Rund, F. Schonfeld, W. Dorner, R. Konrad, and S. Hardt, "Integrated polymer chip for two-dimensional capillary gel electrophoresis," *Lab on a Chip*, vol. 4, pp. 18-23, 2004.
- [119] D. A. Mair, M. Rolandi, M. Snauko, R. Noroski, F. Svec, and J. M. J. Frechet, "Room-temperature bonding for plastic high-pressure microfluidic chips," *Analytical Chemistry*, vol. 79, pp. 5097-5102, Jul 2007.
- [120] M. Rahbar, S. Chhina, D. Sameoto, and M. Parameswaran, "Microwave-induced, thermally assisted solvent bonding for low-cost PMMA microfluidic devices," *Journal of Micromechanics and Microengineering*, vol. 20, Jan 2010.
- [121] Z. B. Zhang, Y. Luo, X. D. Wang, Z. Q. Zhang, and L. D. Wang, "Ultrasonic Bonding of Polymer Microfluidic Chips," in *2008 International Conference on Electronic Packaging Technology & High Density Packaging, Vols 1 and 2*, 2008, pp. 34-38.
- [122] R. Truckenmuller, R. Ahrens, Y. Cheng, G. Fischer, and V. Saile, "An ultrasonic welding based process for building up a new class of inert fluidic microsensors and -actuators from polymers," *Sensors and Actuators a-Physical*, vol. 132, pp. 385-392, Nov 2006.
- [123] Z. B. Zhang, Y. Luo, X. D. Wang, Y. S. Zheng, Y. G. Zhang, and L. D. Wang, "Thermal assisted ultrasonic bonding of multilayer polymer microfluidic devices," *Journal of Micromechanics and Microengineering*, vol. 20, Jan 2010.
- [124] M. E. Vlachopoulou, A. Tserepi, P. Pavli, P. Argitis, M. Sanopoulou, and K.

- Misiakos, "A low temperature surface modification assisted method for bonding plastic substrates," *Journal of Micromechanics and Microengineering*, vol. 19, Jan 2009.
- [125] J. Kim and X. F. Xu, "Excimer laser fabrication of polymer microfluidic devices," *Journal of Laser Applications*, vol. 15, pp. 255-260, 2003.
- [126] J. J. Lai, H. Yuan, X. J. Yi, and S. Liu, "Laser bonding of multilayer polymer microfluidic chips," in *Semiconductor Lasers and Applications II*, 2005, pp. 56-62.
- [127] M. Li, Y. C. Lin, C. C. Wu, and H. S. Liu, "Enhancing the efficiency of a PCR using gold nanoparticles," *Nucleic Acids Research*, vol. 33, p. 10, 2005.
- [128] H. Li, J. Huang, J. Lv, H. An, X. Zhang, Z. Zhang, C. Fan, and J. Hu, "Nanoparticle PCR: Nanogold-Assisted PCR with Enhanced Specificity," *Angewandte Chemie International Edition*, vol. 44, pp. 5100-5103, June 8 2005.
- [129] Z. Z. Zhang, C. C. Shen, M. C. Wang, H. Han, and X. H. Cao, "Aqueous suspension of carbon nanotubes enhances the specificity of long PCR," *Biotechniques*, vol. 44, pp. 537-+, Apr 2008.
- [130] P. Stoller, V. Jacobsen, and V. Sandoghdar, "Measurement of the complex dielectric constant of a single gold nanoparticle," *Optics Letters*, vol. 31, pp. 2474-2476, Aug 2006.
- [131] C. E. Rayford II, G. Schatz, and K. Shuford, "Optical Properties of Gold Nanospheres," *Nanoscope*, vol. 2, pp. 27-33, 2005.
- [132] E. Hleb, I. Zastinskaya, I. Ilyukova, I. Koneva, A. Uss, I. Semenenya, J. Hafner, E. Hanna, J. Myers, S. Zhdanok, and D. Lapotko, "Method of LANTCET for cancer diagnostics and treatment at cell level," in *Nanotech 2009 Conference*, Houston, TX, USA, 2009, pp. 48-51.
- [133] C. T. Nguyen, J. T. Nguyen, C. Wang, and G. Walker, "SERS Gold Nanoparticles for Cancer Cell Surface Marker Detection," in *Nanotech 2009 Conference*, Houston, TX, USA, 2009, pp. 259-262.
- [134] D. R. Bhumkar, H. M. Joshi, M. Sastry, and V. B. Pokharkar, "Chitosan reduced gold nanoparticles as novel carriers for transmucosal delivery of insulin," *Pharmaceutical Research*, vol. 24, pp. 1415-1426, Aug 2007.
- [135] J. Yan, D. Pan, C. F. Zhu, L. H. Wang, S. P. Song, and C. H. Fan, "A Gold Nanoparticle-Based Microfluidic Protein Chip for Tumor Markers," *Journal of Nanoscience and Nanotechnology*, vol. 9, pp. 1194-1197, Feb 2009.
- [136] Y. Sato, K. Sato, K. Hosokawa, and M. Maeda, "Surface plasmon resonance imaging on a microchip for detection of DNA-modified gold nanoparticles deposited onto the surface in a non-cross-linking configuration," *Analytical Biochemistry*, vol. 355, pp. 125-131, Aug 2006.
- [137] K. H. Cheong, D. K. Yi, J. G. Lee, J. M. Park, M. J. Kim, J. B. Edel, and C. Ko, "Gold nanoparticles for one step DNA extraction and real-time PCR of pathogens in a single chamber," *Lab on a Chip*, vol. 8, pp. 810-813, 2008.
- [138] T. W. Odom, J. L. Huang, P. Kim, and C. M. Lieber, "Structure and electronic properties of carbon nanotubes," *Journal of Physical Chemistry B*, vol. 104, pp. 2794-2809, Apr 2000.
- [139] C. Dame, L. M. Xie, W. Zagozdzon-Wosik, H. K. Schmidt, and J. Wosik,

- "Complex permittivity measurements of single-walled carbon nanotubes at microwave frequencies," in *Nanotech 2009 Conference*, M. Laudon and B. Romanowicz, Eds. Houston, TX, USA, 2009, pp. 304-307.
- [140] X. L. Liu and D. L. Zhao, "Microwave permittivity of multi-walled carbon nanotubes," in *Asian International Conference on Advanced Materials*, Beijing, China, 2005, pp. 559-562.
- [141] K. R. Paton and A. H. Windle, "Efficient microwave energy absorption by carbon nanotubes," *Carbon*, vol. 46, pp. 1935-1941, 2008.
- [142] X. Liu and Q. Li, "Microwave Dielectric Characteristics of Single-walled Carbon Nanotubes," *Modern Applied Science*, vol. 3, pp. 51-56, Jan 2009.
- [143] A. A. Yussuf, I. Sbarski, J. P. Hayes, M. Solomon, and N. Tran, "Microwave welding of polymeric-microfluidic devices," *Journal of Micromechanics and Microengineering*, vol. 15, pp. 1692-1699, Sep 2005.
- [144] W. L. Song, M. S. Cao, Z. L. Hou, X. Y. Fang, X. L. Shi, and J. Yuan, "High dielectric loss and its monotonic dependence of conducting-dominated multiwalled carbon nanotubes/silica nanocomposite on temperature ranging from 373 to 873 K in X-band," *Applied Physics Letters*, vol. 94, Jun 2009.
- [145] J. H. Wu and L. B. Kong, "High microwave permittivity of multiwalled carbon nanotube composites," *Applied Physics Letters*, vol. 84, pp. 4956-4958, Jun 2004.
- [146] P. Kim, L. Shi, A. Majumdar, and P. L. McEuen, "Thermal Transport Measurements of Individual Multiwalled Nanotubes," *Physical Review Letters*, vol. 87, p. 215502, Nov 2001.
- [147] S. T. Mostafavi, M. R. Mehrnia, and A. M. Rashidi, "Preparation of nanofilter from carbon nanotubes for application in virus removal from water," *Desalination*, vol. 238, pp. 271-280, Mar 2009.
- [148] D. Pantarotto, R. Singh, D. McCarthy, M. Erhardt, J. P. Briand, M. Prato, K. Kostarelos, and A. Bianco, "Functionalized carbon nanotubes for plasmid DNA gene delivery," *Angewandte Chemie-International Edition*, vol. 43, pp. 5242-5246, 2004.
- [149] R. Singh, D. Pantarotto, D. McCarthy, O. Chaloin, J. Hoebeker, C. D. Partidos, J. P. Briand, M. Prato, A. Bianco, and K. Kostarelos, "Binding and condensation of plasmid DNA onto functionalized carbon nanotubes: Toward the construction of nanotube-based gene delivery vectors," *Journal of the American Chemical Society*, vol. 127, pp. 4388-4396, Mar 2005.
- [150] W. Wu, S. Wieckowski, G. Pastorin, M. Benincasa, C. Klumpp, J. P. Briand, R. Gennaro, M. Prato, and A. Bianco, "Targeted delivery of amphotericin B to cells by using functionalized carbon nanotubes," *Angewandte Chemie-International Edition*, vol. 44, pp. 6358-6362, 2005.
- [151] A. A. Shvedova, V. Castranova, E. R. Kisin, D. Schwegler-Berry, A. R. Murray, V. Z. Gandelsman, A. Maynard, and P. Baron, "Exposure to carbon nanotube material: Assessment of nanotube cytotoxicity using human keratinocyte cells," *Journal of Toxicology and Environmental Health-Part A*, vol. 66, pp. 1909-1926, Oct 2003.
- [152] C. W. Lam, J. T. James, R. McCluskey, and R. L. Hunter, "Pulmonary

- toxicity of single-wall carbon nanotubes in mice 7 and 90 days after intratracheal instillation," *Toxicological Sciences*, vol. 77, pp. 126-134, Jan 2004.
- [153] D. X. Cui, F. R. Tian, C. S. Ozkan, M. Wang, and H. J. Gao, "Effect of single wall carbon nanotubes on human HEK293 cells," *Toxicology Letters*, vol. 155, pp. 73-85, Jan 2005.
- [154] S. A. L'armer F, "Method of anisotropically etching silicon," Robert Bosch GmbH, 1996.
- [155] Y. Hirai, S. Harada, S. Isaka, M. Kobayashi, and Y. Tanaka, "Nano-imprint lithography using replicated mold by Ni electroforming," in *International Microprocesses and Nanotechnology Conference*, Kunibiki Messe, Japan, 2001, pp. 4186-4189.
- [156] K. C. Grabar, R. G. Freeman, M. B. Hommer, and M. J. Natan, "Preparation and characterization of Au colloid monolayers," *Analytical Chemistry*, vol. 67, pp. 735-743, Feb 1995.
- [157] "Water - Thermal Properties," The Engineering ToolBox.
- [158] C. Y. Tang, L. N. Zhang, C. T. Wong, K. C. Chan, and T. M. Yue, "Fabrication and characteristics of porous NiTi shape memory alloy synthesized by microwave sintering," *Materials Science and Engineering: A*, vol. 528, pp. 6006-6011, 2011.
- [159] A. B. Bashirov and T. D. Shermergor, "Thermal conductivity of amorphous polymers," *Mechanics of Composite Materials*, vol. 11, pp. 474-476, 1975.
- [160] J. P. Holman, *Heat transfer*, 10th ed. New York: McGraw Hill, 2010.
- [161] Y. J. Liu, D. Ganser, A. Schneider, R. Liu, P. Grodzinski, and N. Kroutchinina, "Microfabricated polycarbonate CE devices for DNA analysis," *Analytical Chemistry*, vol. 73, pp. 4196-4201, Sep 2001.
- [162] J. N. Yang, Y. J. Liu, C. B. Rauch, R. L. Stevens, R. H. Liu, R. Lenigk, and P. Grodzinski, "High sensitivity PCR assay in plastic micro reactors," *Lab on a Chip*, vol. 2, pp. 179-187, Nov 2002.
- [163] L. Klintberg, M. Svedberg, F. Nikolajeff, and G. Thornell, "Fabrication of a paraffin actuator using hot embossing of polycarbonate," *Sensors and Actuators a-Physical*, vol. 103, pp. 307-316, Feb 2003.
- [164] Y. Wang, Q. H. He, Y. Y. Dong, and H. W. Chen, "In-channel modification of biosensor electrodes integrated on a polycarbonate microfluidic chip for micro flow-injection amperometric determination of glucose," *Sensors and Actuators B-Chemical*, vol. 145, pp. 553-560, Mar 2010.
- [165] P. C. H. Li, *Microfluidic Lab-on-a-Chip for Chemical and Biological Analysis and Discovery*, 1st ed.: CRC Press, 2005.